2020-2021

Thermosiphon Research Project

Final Report

Submitted by:
Bradan Bruce
Tyler Coppens
Alek Dunkelberger
Edward Friesel
Justin Fritch
Nick Gibson
Jesse Hagler
Nicole Hemmersbach
Bastian Key
Sam Kluemper
Sanjay Maharjan
Truman Schulz
Jackson Smith

April 19, 2021

Submitted to the
Faculty of the Mechanical Engineering Program
College of Engineering and Computer Science
University of Evansville
Evansville, Indiana 47722

Abstract

A thermosiphon is a passive water heating system and, in its simplest form, comprises a solar collector, a reservoir above the collector, and sets of tubing which connect these components on two sides, forming a loop. System function involves the use of maintained temperature differences in the closed volume of fluid to create density variations and drive flow in a cyclical pattern, resulting in a reservoir of maintained, high temperature fluid for use in heating or energy applications. The goal of the completed research into this system is to systematically vary five key system parameters and to identify settings for each which maximize the energy absorbed by the system. These parameters are (1) the angle of the collector relative to the ground, (2) the power input to the system through the collector, (3) the height of the reservoir above the collector, (4) the total hydraulic resistance of system components, and (5) the temperature of the environment.

Research into these parameters involved base case testing to verify system consistency, followed by variable angle – constant power testing designed to isolate the effect of the collector angle on system performance and variable angel – variable power testing designed to simulate the effect of collector angle on efficiency with associated power losses. Testing in these areas ultimately produced clear trends relating increasing system efficiency with decreasing collector angles both in constant power and variable power contexts, which in the latter case is indicative of the relative insignificance of power loss effects compared to the effects of other system parameters. In both of these cases, a local maximum efficiency at moderate angles is also a potential feature of interest, which in variable power contexts can be shown to be the result of a local maximum in flow rate in this collector angle range. Though limitations in the current data sets make it difficult to ascertain the nature of this local maximum or its relative magnitude to

lower collector angles, further research into these areas of interest is recommended and would be extremely relevant to application contexts.

Similarly, research into the effects of variable hot leg height and variable ambient temperature produce results which align with expectations, with increases in each being associated with improved system efficiency. Due to instrument failures, variable hydraulic resistance testing was not ultimately conducted.

In addition to the completed research, modification to system components and instruments are performed to provide researchers with more precise control and measurement of key parameter. Upgrades to the collector and reservoir supports which make their settings more simply altered, as well as reinforcements to system tubing, are all carried out. Additionally, the addition of an active cooling and ventilation system, designed to rapidly dissipate fluid and ambient heat when desirable, are also installed. Traditional calibration and improvement of system instrumentation for more precise and comprehensive digital measurements, including the addition and manipulation of thermistors and VARIACs, are also pivotal system upgrades.

Acknowledgements

The University of Evansville thermosiphon research team is profoundly grateful for the guidance of project faculty advisor Dr. Douglas Stamps. His technical and logistical insights and investment in project success have shaped the nature and development of thermosiphon research at this institution both in the current academic year and all of those that preceded it. It is his investment in and enthusiasm for the continuation of this work that has ultimately culminated in the reported results and in the strong legacy of this project and team. Additionally, the team is exceptionally grateful for the dedication of Dr. Suresh Immanuel and the entire mechanical engineering department faculty to providing opportunities for continued, substantive project work in these unprecedented times while simultaneously prioritizing the safety of all team members. Coordinating and communicating with students to create an education environment which balances health and productivity is a monumental undertaking but was accomplished with wisdom and consideration. Finally, the team is grateful for the University Evansville institutions that provided funding and made this research possible, including the academic fund board and the CECS dean's department, with special thanks to Dean Ying Shang for her providing of additional and exceptional funding which had a significant impact on the potential scope of the project both for the current team and those that will follow.

Table of Contents

List of Figures

List of Tables

Nomenclature

α	Collector reference angle [°]
C	Specific heat of working fluid [kJ/kg-K]
$\eta_{av\#}$	Average collector efficiency
η_i	Instantaneous collector efficiency
$\eta(t)$	Continuous collector efficiency function
h	Hot-leg height [in.]
K	Hydraulic resistance
N	Number of datum points in test region of interest
P	Power input to collector [W]
$P_{\Delta\theta}$	Power input to collector at deviation from reference angle [W]
P_{max}	Power input to collector at reference angle [W]
R	Heat tape resistance [Ω]
ρ	Density of working fluid [kg/m^3]
$T_{ambient}$	Ambient temperature [°C]
T_{exit}	Temperature of working fluid at collector exit [°C]
T_{inlet}	Temperature of working fluid at collector inlet [°C]
$t_{initial}$	Initial time of test region of interest [s]
t_{final}	Final time of test region of interest [s]
θ	Collector angle [°]
$\Delta\theta$	Difference between collector angle and reference angle [°]
$\forall$	Volumetric flow rate of working fluid [m^3/s]
V_{RMS}	Input VARIAC voltage to heat tape [V]

1 Introduction

1.1 System Overview

A thermosiphon is an apparatus which makes use of maintained temperature gradients in a controlled body of working fluid to induce continuous cyclical flow through an insulated tube system [1]. The necessary temperature differences are created by consistent input of thermal energy to the system at specified locations, and the flow which results from this temperature difference allows the energy to be transferred by the working fluid to a second location and maintained there for use in a desired application [2]. Traditionally, this second position is a reservoir of some type and is held at a higher elevation than the location of energy input, called the collector. In its most simple form, a thermosiphon system consists only of these two fundamental components, a reservoir or tank and collector, which are connected in a closed loop by two sets of tubing, called the hot and cold legs. The relative positions of these components on a representative thermosiphon apparatus are illustrated by the diagram in figure 1.

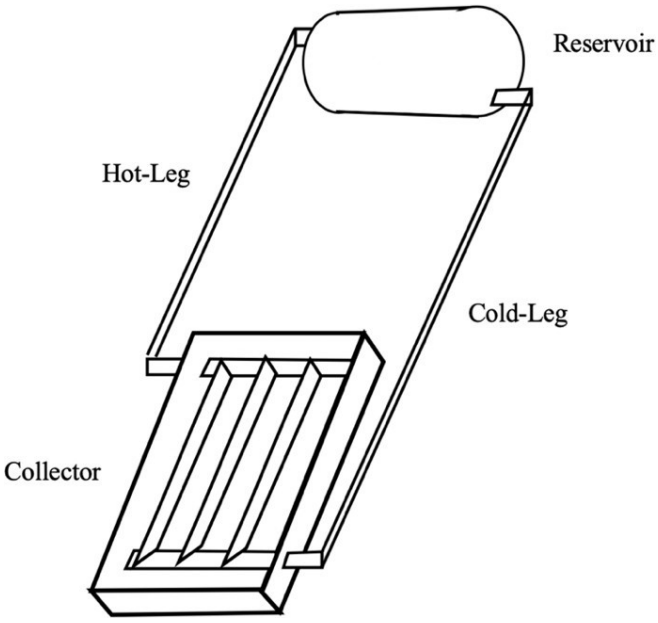

Figure 1: System Components

System function is facilitated by an imposed temperature difference across the collector component. In most applications, fluid in the collector is contained in a series of parallel pipes positioned beneath a glass or plastic layer intended to maximize exposure of the fluid to solar radiation. As a natural, continuous source of thermal energy via radiative heat transfer, the sun causes a temperature gradient to develop across the pipe lengths as the fluid inside absorbs the incoming solar energy. This fluid temperature increases and its associated density decrease causes warmed fluid to buoyantly rise through the collector piping and into the hot leg tubing attached at the top of the collector, ultimately passing into the upper portion of the reservoir. At this point, the cooler fluid which previously filled the tank is forced to the lower portion of the volume by the supply of heated fluid which continues to flow from the hot leg. The movement of this relatively cool fluid into the cold leg through the bottom of the tank and back to the base of the collector completes a single iteration of the working fluid cycle. After a transient period in which the flow rate gradually increases because of initial energy input, the system settles into a steady state characterized by consistent flow through all components. This process continues until the temperatures at all points in the system ultimately equilibrate, eliminating the temperature gradient across the collector and causing the incoming solar energy to simply maintain the fluid temperature in that region until sufficient heat is lost to the environment in the reservoir and tubing to cause a temperature gradient to again develop, again inducing flow. The relative temperature and flow direction of the fluid as it moves through the system during the steady state period are summarized in figure 2.

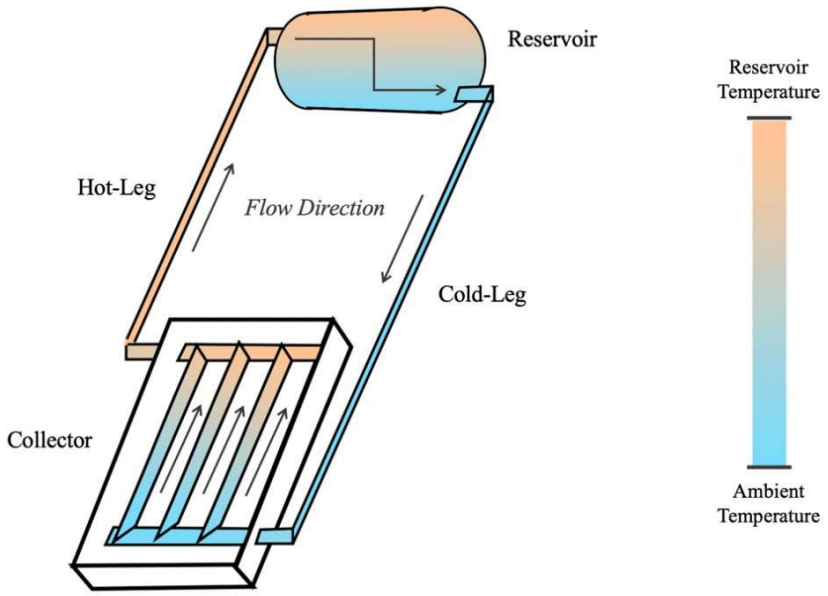

Figure 2: System Temperature Gradients and Flow Direction

Though thermosiphon systems that force flow using pumps exist, they are primarily used in commercial applications [3]. Natural circulation systems, which rely only on convective buoyant forces and temperature differences to drive flow, are the focus of the current study [3]. The two most common applications for this apparatus are as a means of heating water, which is drawn from the reservoir, or radiating heat through the reservoir to an ambient environment [4]. Thermosiphons which are used as water heaters can be further characterized as either direct systems, in which the working fluid serves as potable water and is drawn directly from the reservoir, or indirect systems, in which the heat of the working fluid in the upper portion of the reservoir is used as a means of heating an independent but connected reservoir of potable water [5]. An indirect system is comprised of a closed cycle for the working fluid, while the potable fluid and its connection with a larger network forms an independent open cycle [5]. A direct system is an open cycle which incorporates the larger fluid network directly into the system via connections at the upper and lower portions of the reservoir which draw heated fluid and return cooled fluid to the apparatus, respectively.

The appeal of a system of this type is its relative simplicity: from an initial source of relatively cool fluid, a region of consistently heated fluid at a higher elevation is created for use in energy applications with an apparatus which requires no electrical or mechanical components of any kind [1]. This makes thermosiphon systems particularly applicable for use in maintaining a supply of hot water or thermal energy in developing regions where electrical access and the knowledge or resources required to maintain mechanical components is limited or nonexistent. However, thermosiphon use as an economical and environmental means of heating water is not limited to this context. System can be found attached to buildings and used in solar water heating applications in many parts of the world, making research into their operation and optimization widely applicable [2].

1.2 Background & Literature Review

The current state of thermosiphon system research is largely concerned with two primary objectives: a further understanding of the thermodynamic and fluid mechanical concepts which facilitate system function and an exploration of system performance, as defined by thermal efficiency and affected by key system parameters. The latter category has historically been the focus of research at the University of Evansville. Many years of testing by previous teams and other interested institutions have ultimately led to the identification of five system parameters which have been experimentally observed to significantly impact thermal efficiency during operation and are therefore of interest in system optimization. These parameters include: (1) the angle of the solar collector relative to the ground, (2) the rate and intensity of power input to the solar collector, (3) the ambient temperature of the system environment, (4) the hydraulic resistance of system components, and (5) the height of the reservoir above the collector, called the hot leg. A truly comprehensive study of system function is one that includes precise control,

measurement, and analysis of each of these system features simultaneously. Representations of these five primary parameters are illustrated on the representative system in figure 3.

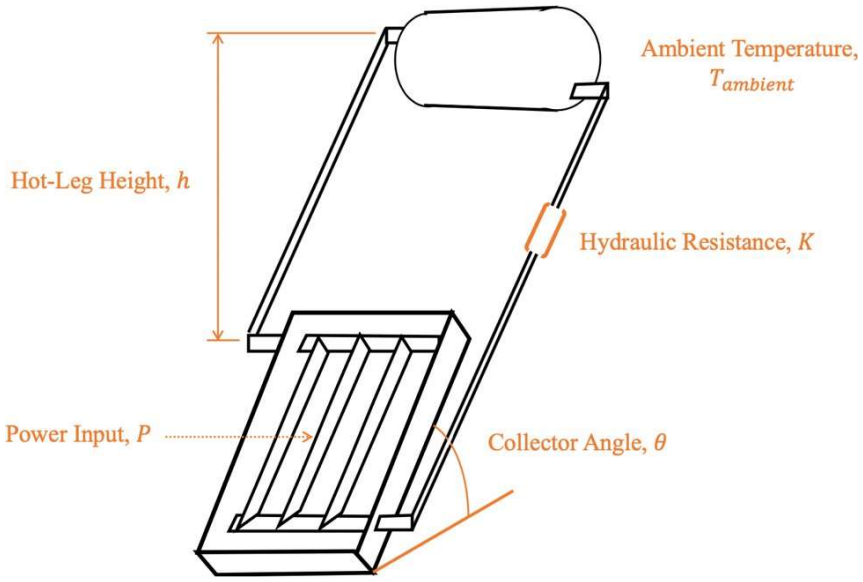

Figure 3: System Parameters of Interest

1.2.1 Collector Angle & Power Input

The findings of the University of Evansville research team in recent years have indicated a relatively clear trend relating the angle of the collector to system efficiency in constant power conditions, though the optimal values associated with these trends are not completely consistent [6] [7]. Results from the two most recent sets of testing from previous years, summarized in figures 4 and 5, each indicate an anticipated increase in collector efficiency with reductions in collector angle up to a limit associated with a moderate angle, at which point a discontinuity traditionally is found to exist indicating a local efficiency maximum. Further angular decreases past this point can be seen to either cause a gain in efficiency similar to the trend observed preceding the discontinuity, albeit with a reduced intercept, or a general decrease in efficiency, making the local maximum functionally the absolute maximum of the data set. The precise nature of the low angle trend and the setting at which this local maximum efficiency occurs,

however, is slightly inconsistent across power levels, environments, and institutions. Based on 2018-2019 research, an angle between 35° and 40° is found to be ideal for both high and low power testing, while research conducted during the 2019-2020 test cycle indicates that this optimal angle is lower for high power testing, between 20° and 30° [6] [7]. Notably, in these cases and those discussed in subsequent sections, high power testing implies testing in which power input has been simulated to be equivalent to that of a sunny day, while low power simulates cloudy conditions.

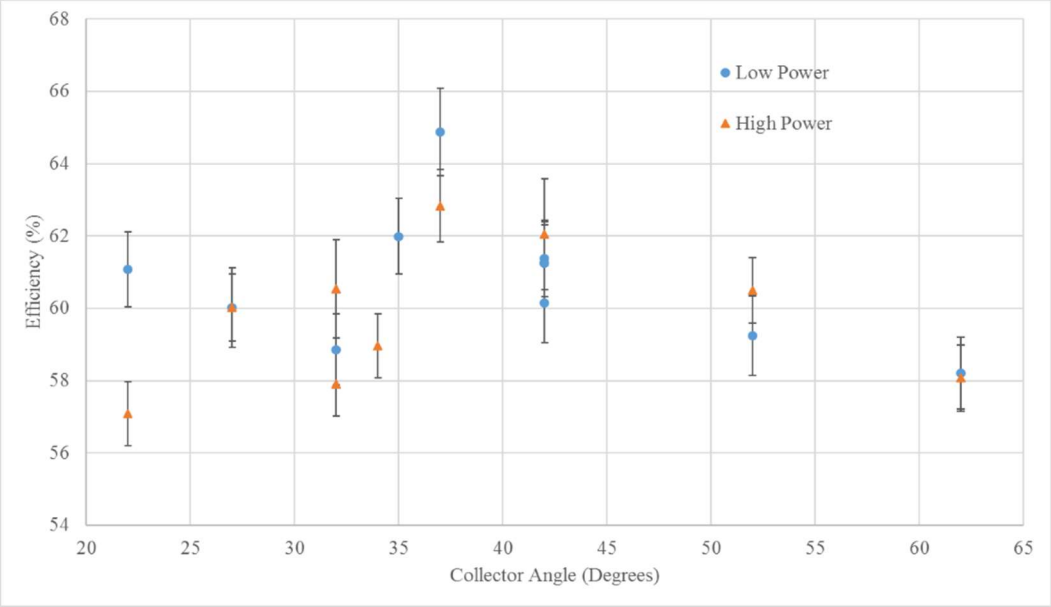

Figure 4: Variable Angle-Constant Power Results, University of Evansville 2018-'19

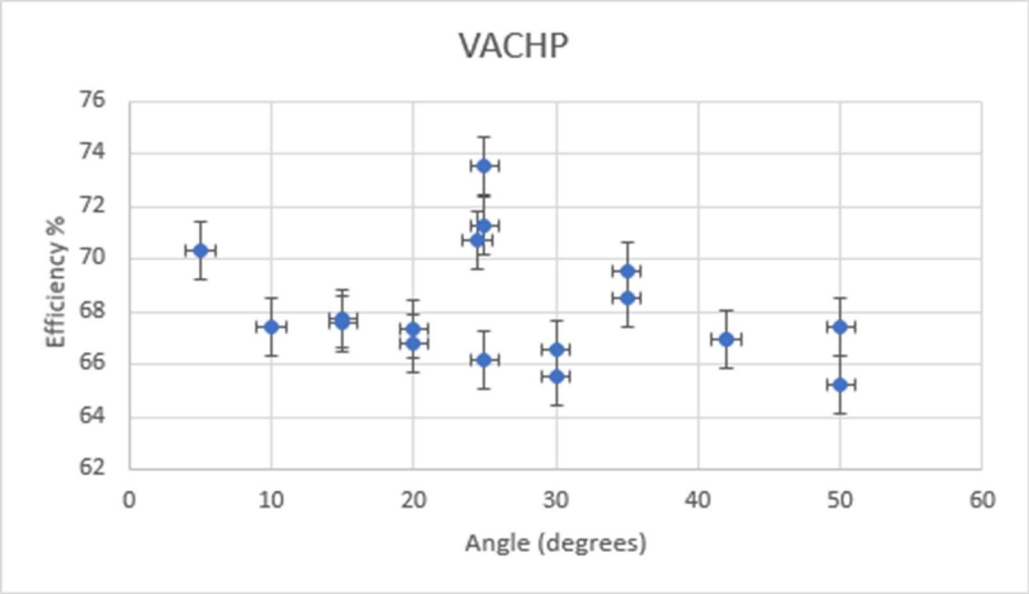

Figure 5: Variable Angle-Constant High-Power Results, University of Evansville 2019-'20

The general state of research into solar collector angle under constant power conditions at other institutions also reveals an inconsistency in both results and theoretical explanations for them. In some cases, high collector angles are found to be associated with higher flow rates and efficiencies, which appears contradictory to the assumed associated increase in frictional forces acting on the fluid as its flow rate increases [8]. The concept that an increase in the magnitude of buoyant forces at lower collector angles has the demonstrable effect of mitigating system flow would also be a consideration in this theory and set of results [9]. In seeming contrast to these findings, other institutions have reported that the angle of the collector, particularly when relatively low, is found to have minimal impact on system efficiency and even have the effect of increasing the thermal effectiveness of the system [10]. In theory, variable angle-constant power testing in which all other parameters are carefully controlled and monitored would produce a conclusive trend which accounts for these seemingly disparate theories.

Unlike systems which are operated in a laboratory setting, the effects of a varied collector angle cannot be divorced from an associated change in power input in application contexts where

the system is dependent on solar radiation intersecting the collector as a power source. Current conventions in thermosiphon installation and operation indicate that a thermosiphon system should be installed with a fixed collector angle equal the latitude of the installation location, called the reference angle. This allows for a maximum solar incident radiation regardless of global position, as indicated by the diagram in figure 6, in which it is geometrically illustrated that maximum solar incidence occurs when collector angle θ is equivalent to latitude α, thereby allowing solar radiation to perpendicularly impact the collector surface [11]. This illustration is a simplification which does not explicitly account for earth's rotational axis or its variability in different seasons but is useful in representing the essential features of the collector angle-latitude relationship and the logic behind conventional thermosiphon installation practices [11].

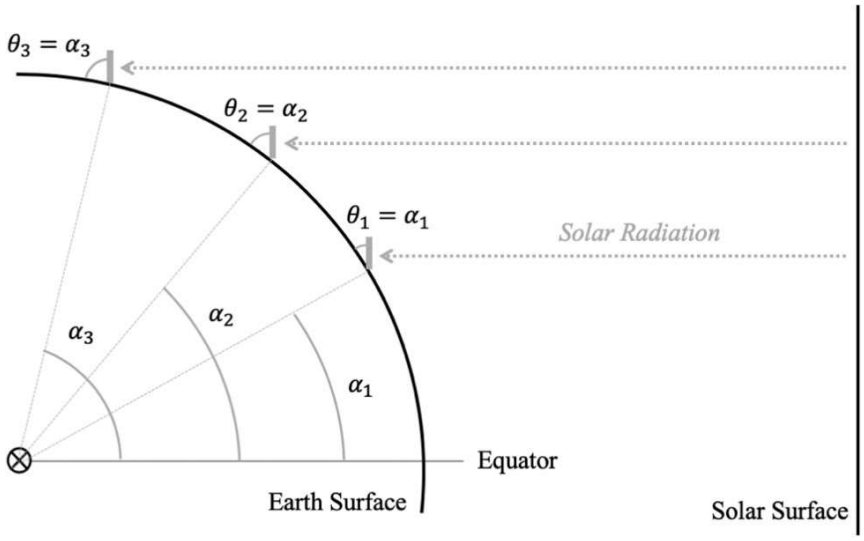

Figure 6: Reference Angle-Latitude Relationship

Notably, this rule of thumb accounts for only power input and not efficiency as a function of collector angle and is guided by formal reporting which indicates that collector angle has minimal effect on efficiency and, therefore, that the optimal angle is driven only by power input considerations [10].

The relationship between collector angle and power input as defined by solar incident radiation is quantified geometrically by equation 1. In this equation, P_{max} symbolizes the maximum solar radiation input, or the magnitude of power input associated with the reference angle. $\Delta\theta$ is the angular deviation from the reference angle, and $P_{\$\theta}$ is the diminished solar radiation associated with this angular deviation.

$$P_{\$\&} = P_{max} cos\,(\Delta\theta) \quad \textbf{(1)}$$

The geometric features of the collector related to this equation are represented by the diagrams in figure 7.

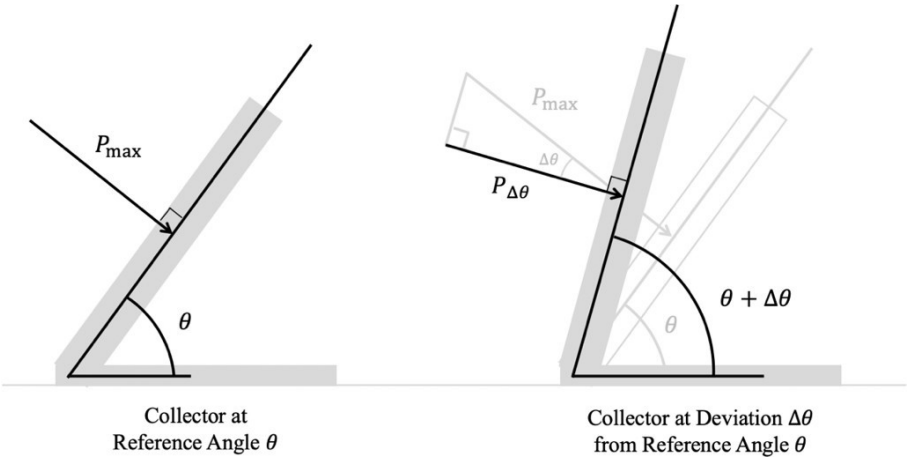

Figure 7: Collector Geometric Features

Because of the nature of the relationship between collector angle and power input, the angle associated with optimal system efficiency and the one associated with maximum power input are only equivalent at very specific latitudes. In all other cases, an optimization of power absorbed by the fluid as it moves through the collector is a function of both power input as solar radiation and collector efficiency based on deviation from the reference angle. Optimization of this set of parameters for application purposes requires testing in which collector angle and input

power are varied in coordination with one another and treated as a single system parameter. Though this potential tradeoff has not been the subject of intense study at the University of Evansville in past years and is not a common area of research in the field of thermosiphon optimization, limited research at other institutions have seemingly confirmed that the angle associated with optimal efficiency is not the angle associated with optimal solar incidence and is actually greater, particularly for systems located near the equator [8].

1.2.2 Ambient Temperature

Ambient temperature can be defined as the temperature of the surroundings in which the thermosiphon system is in operation, be that an experimental laboratory context or its use outdoors in practical applications. As can be clearly seen in figure 8, the collector efficiency has been found to increase with an increase in the ambient temperature in experiments conducted at the University of Evansville between 2018 and 2019, the results of which generally agree with the very limited other literature focusing on this parameter. From these experiments, the maximum efficiency of the collector of approximately 67% was obtained at an ambient temperature around 26°C. The most prominent theory which explains why higher system efficiency corresponds with higher ambient temperatures is due to the smaller temperature difference between the consistently heated collector components and their immediate surroundings [7]. This smaller temperature gradient results in lower heat transfer via convection to the environment and, in reducing this undesirable heat loss, increases the energy transferred directly into the fluid, thereby theoretically increasing the collector efficiency.

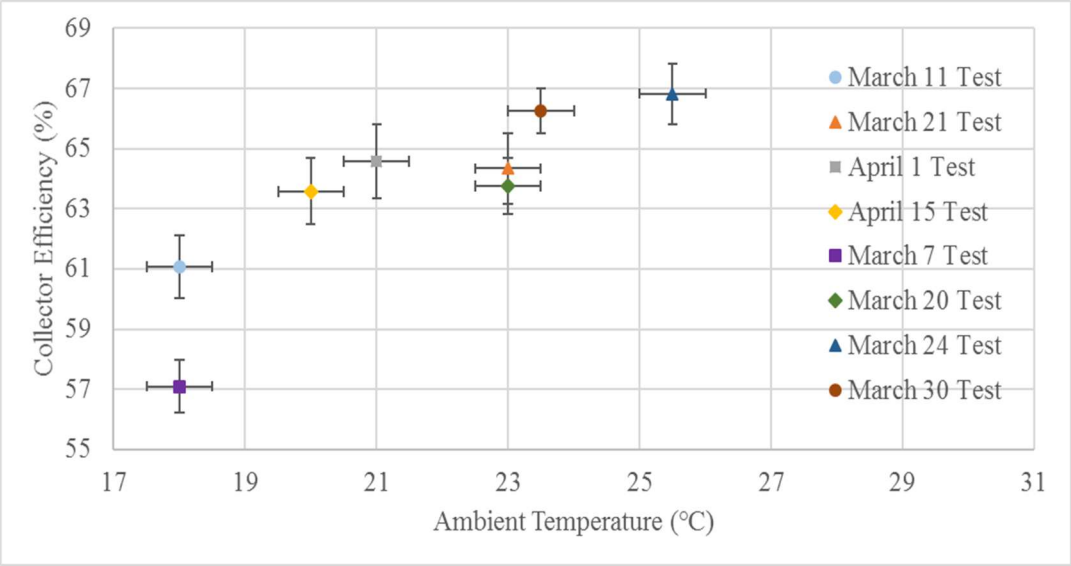

Figure 8: Variable Ambient Temperature Results, University of Evansville 2018-'19

Since the ambient temperature affects the collector efficiency at different combinations of collector angle, tank height, and power input, it is crucial to obtain an accurate understanding and relation between the ambient temperature and collector efficiency to effectively study other system parameters and properly associated observed efficiency changes with the intended geometric variations and not changes in the environment.

1.2.3 Hot Leg-Height

Hot leg height is defined as the elevation difference between the fluid inlet to the tank or reservoir and the fluid outlet of the collector on its upper portion. It is also commonly known as the tank height. Changes in the hot leg height has been observed to cause changes in the collector efficiency because of the effect of this change on buoyant forces within the system fluid [7]. Based on trends from previous year's experiments at the University of Evansville, which are clearly illustrated by the data set in figure 9, the collector efficiency is found to increase with an increase in hot leg height. Current theories associate this positive efficiency impact with the chimney effect, which would indicate that the flow rate increases with increasing hot leg height.

This resulting higher flow rate implies that the collector is capable of absorbing the same amount of power input while developing a lower temperature difference. A lower collector temperature results in less heat loss to the ambient and a higher efficiency for the all of the same reasons that a lower ambient temperature results in higher efficiencies: less heat is transferred via convection due to a lower temperature gradient between system and environment.

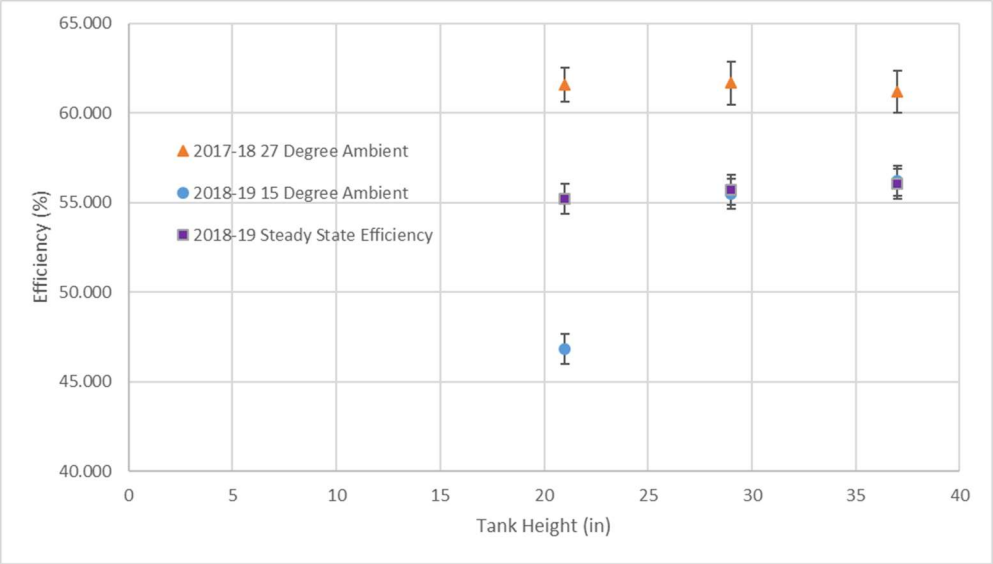

Figure 9: Variable Hot Leg Height Results, University of Evansville 2018-'19

As hot leg height is a design parameter that designers and installers can easily change based on available resources and design requirements, understanding the effects of change in hot leg height to collector efficiency is incredibly relevant. Hence, in the 2020-2021 year, the team conducted tests to verify the trends and results obtained from previous year's experiments and to obtain an accurate working relationship between hot leg height and collector efficiency.

1.2.4 Hydraulic Resistance

The total hydraulic resistance of a flow-based system like a thermosiphon is the result of many contributing factors, including but not limited to the tubing size, surface roughness of the piping and tubing, and the number of valves or tubing geometry used. Based on experiments

conducted in 2018-2019 and presented in figure 10, the solar collector efficiency is found to consistently decrease as the hydraulic resistance is increased [6]. Since hydraulic resistance is a direct function of the materials and geometry used in the design of the solar water heater, determining the effect of hydraulic resistance on collector efficiency is crucial so that designers have a clear idea of what materials and components can be reasonably used to design an effective thermosiphon for any arbitrary context.

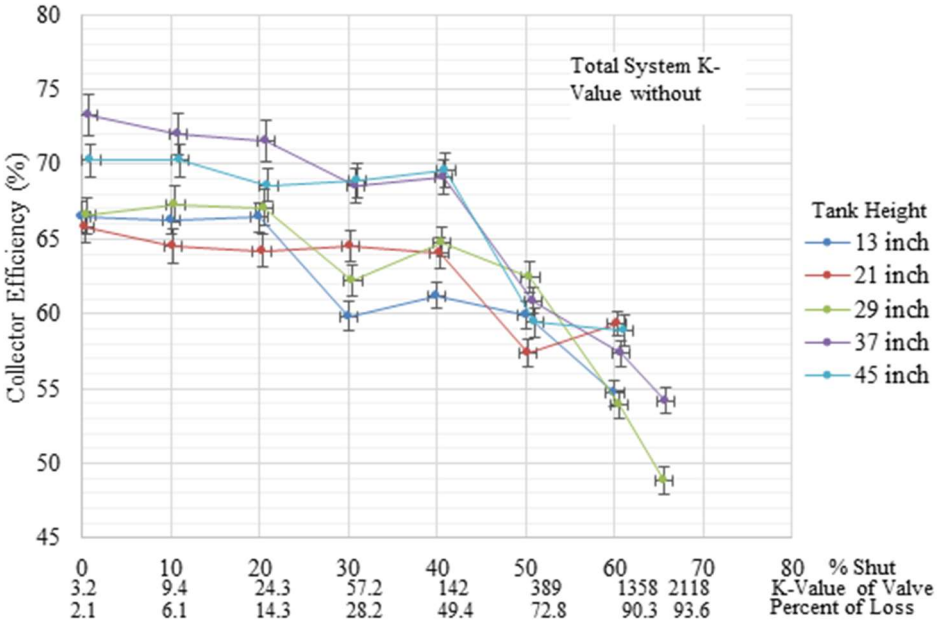

Figure 10: Variable Hydraulic Resistance Results, University of Evansville 2018-'19

1.3 Project Objectives

The primary objective of the team is the collection of a comprehensive set of consistent, defensible data which can be used to both validate previously identified trends in system efficiency based on various system parameters and to establish conclusive trends for parameters that have involved limited testing or inconclusive results in the past. Ultimately, clear trends in system efficiency that result from parameter variations lead to a fuller understanding of system function and to more effective system operation in applications which have the flexibility to use

the indicated optimal parameter settings as guides for installation. The secondary team objective is the presentation of results at the National Conference for Undergraduate Research (N.C.U.R.) and the publication of findings in a scientific publication in coordination with university faculty. This objective was successfully meet through the presentation of all complete research at N.C.U.R. in April of this year. Additionally, maintenance and instrumentation upgrades to the system are of some importance so that testing by future teams can effectively continue with a higher frequency and degree of precision, thereby providing the opportunity for continually evolving research. Finally, the current team placed a significant emphasis on the training of all team members in competency of all project areas, including demonstrable knowledge of system function and research objectives, testing practices, data analysis practices, and troubleshooting techniques. Training checks, testing session in which each student was responsible for performing and analyzing a research test without intervention while simultaneously providing satisfactory answers to questions about system function, were used to measure this training. The form used in this analysis (which also serves as a summary of experimental procedures) is available in appendix A, as of this writing all team members have successfully been trained as indicated by a completed training check.

To accomplish these objectives, the majority of project time and resources were directed toward running tests in which the five key system parameters were strategically varied and the effects of these variations on the efficiency of the system were recorded and analyzed. The parameters of interest as identified by previous research into this type of system are (1) the collector angle, (2) system power input, (3) ambient temperature, (4) hydraulic resistance, and (5) the hot leg height. A phase of testing was dedicated to the study of each of these parameters or, in the case of collector angle and power input, two sets of two related testing phases at

varying power levels and degrees of correlation. Based on these areas of study, there were a total of seven planned phases of research testing and data analysis. Ultimately, the project intent was to conclusively establish an optimal setting or trend for each parameter, and to this end the project objective associated with each test phase is considered successfully met after completion of all planned tests and analysis of data to produce results which are as consistent as possible with the available facility and instrumentation.

1.4 Project Organization

To enforce structure and clearly delineate roles and responsibilities, all project tasks, including all phases of research testing, were grouped into one of seven sections each characterized by a different set of intermediate objectives and each under the direct supervision of one of the five senior team members. The first of these, “Research”, includes all seven phases of research testing and the base case testing which is performed to verify the consistency of results from the system both before and after system modifications are carried out. The seven phases of research testing were further grouped into “Power-Angle Research” (which involves four phases of testing to investigate the unclear relationship between collector angle, power input, and system efficiency) and “Other Research” (which involves three phases intended to confirm seemingly consistent and conclusive trends established in previous years or by other institutions). The most important of these “Other Research” parameters being a study of the effect of ambient temperature variability on result consistency. Because research involves iterative and continuous testing, all team members are associated with its completion in addition to their assignment to another facility modification section or sections. The abbreviations used to differentiate between the seven individual testing phases are defined more elaborately in later sections and are as follows: VACHP, VACLP, VHAVP, and VLAVP are associated with

"Power-Angle Research" and stand for variable angle-constant high power, variable angle-constant low power, variable high angle-variable power, and variable low angle-variable power, respectively. VH, VK, and VT are the "Other Research" phases and stand for variable-hot leg, variable hydraulic resistance, and variable ambient temperature.

The other six main sections consist of the design, maintenance, or modification of the system itself and are divided into categories based on the most relevant system component. The "Collector Modifications" section is tasked with redesigning the frame system used to support the collector and change its angle relative to the ground to make the structure more secure and the collector angle parameter more easily and consistently varied. Replacement of the current power input components (VARIACs and resistance heat tapes) is also included in the "Collector Modifications" section because these elements interface directly with the collector. The "Reservoir Modifications" section tasks similarly involve a redesign of the structure which supports the reservoir above the collector and is used to alter its height, creating increased stability and ease of use in this area. The insulation which surrounds the reservoir also requires redesign to be more effective during testing and simpler to remove and reattach before and after, which also falls under the supervision of the "Reservoir Modifications" section. Unlike the other three facility modification sections, the "Cooling" sections is concerned with the addition of a new set of components to the system in addition to modifications to existing elements. To reduce the time required to cool the system fluid between tests, an active cooling branch, designed and implemented by the "Cooling" section, is designed and fabricated. This section is also concerned with slight modifications to the system environment to aid in ventilation, which would also reduce cooling time. The fourth section, "Tubing Modifications", is tasked with redesign of the hot and cold legs to more effectively protect the instrumentation attached to them and provide

greater access to the system during testing. This section is also associated with the purchase and installation of new data acquisition equipment, including a new DAQ board.

The remaining two sections, both subsets of a larger "Instrumentation" category, are made up of junior and senior team members and are each associated with a unique set of calibration, control, or measurement tasks to improve on the use and results from existing system instrumentation. The first of these two sections is responsible for tasks related to flow control and measurement including the replacement of the current digital flow meter with a new model and coordinating the calibration of the existing model by the manufacturer for use as a backup in future years. Additionally, this section is responsible for the calibration of the existing actuated ball valve. The second "Instrumentation" section is tasked with calibration of thermistors, potentially installation of further thermistors, and investigations into means of wiring VARIAC output, used in the simulation of solar radiation, directly into the data collection interface.

The future of the research project is directly related to the involvement of underclassmen team members. To incorporate these students into the research process, each has been trained in the fundamental aspects of system data analysis by upperclassmen during the first several testing phases. Upon completion of a test, the relevant data file is assigned to a student, who is responsible for performing data analysis and inputting the relevant results into the online data record spreadsheets in addition to the same tasks begin performed by upperclassmen team members. This redundancy is designed to expose all students to the analytical aspects of the project and keep them aware of the current state of the research as well as providing continuous intermediate goals to maintain a sense of progress. Junior team members are also trained in data analysis and are additionally responsible for assisting more directly with facility and instrumentation designs. All team members will assist in the operation of testing during all

research phases as determined by their availability in addition to being assigned to a facility modifications or instrumentation section to perform design and construction work. Figure 11 illustrates this division of tasks among sections and the individuals responsible for each.

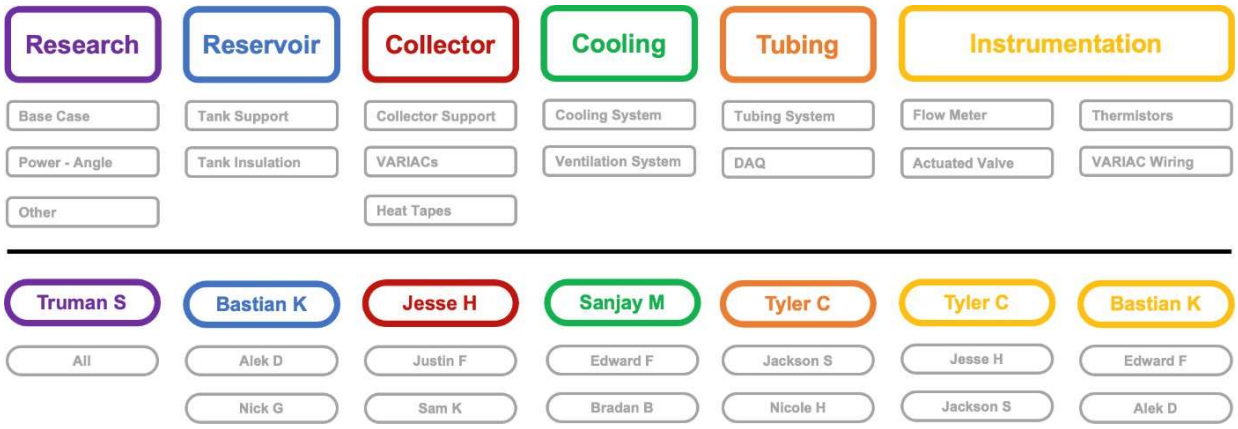

Figure 11: Project Organization

2 Technical Requirements

All experiments must be repeatable and highly precise to use the produced data in publications and for presentation at N.C.U.R, so the technical requirements associated with this research are defined almost entirely by the required precision in testing parameters to make trends clear and data reproducible. As the importance of ambient temperature has been previously discussed, the ambient temperature must be maintained within ±1.0 ℃ to make the collected data useful to determine trends in other parameters. Since ambient temperature can be difficult to maintain at a constant level, the team has insulated the system by establishing an environmental enclosure to create consistent and defensible data. Similarly, the water temperature in the system must be within 1℃ of the ambient temperature at the test start so that the only significant temperature gradient during testing is the one intentionally induced across the collector via input power. Panels in the system's insulation will be removed before and after

testing to cool the system more quickly, and tests are only begun once the water temperature in the system reaches within 1 °C of the ambient temperature. To maintain test validity, power input settings through VARIACs must be monitored during testing to prevent wandering and maintained withing ± 0.2 V (or ± 0.1 V in the case of variable power testing). The indicated technical parameter tolerances and the reference relative to which they are measured to maintain the integrity of experimental results are summarized in table 1 below, and by closely monitoring and controlling these parameters, the produced data is given sufficient credibility for publication and presentation.

Table 1: Experimental Parameter Tolerances and References

Parameter	Tolerance	Reference
Hot Let Height, h [in.]	$\pm$ 0.5 in.	Goal Height
Collector Angle, θ [degrees]	$\pm$ 0.5°	Goal Angle
Collector Inlet Temperature, T_{in} [°C]	$\pm$ 0.5 °C	Ambient Temperature
Other System Temperatures [°C]	$\pm$ 1.0 °C	Ambient Temperature
Ambient Temperature, $T_{ambient}$ [°C]	$\pm$ 1.0 °C	Goal Temperature
Input Power, P [V] *(Variable Power Research)*	$\pm$ 0.2 V	Goal Voltage
Input Power, P [V] *(Other Research)*	$\pm$ 0.1 V	Goal Voltage

3 Technical Approach

3.1 Facility Operations

It is imperative that each year the thermosiphon facility and its associated apparatus are evaluated and upgraded or maintained based on the demand for ever more precise data collection and the life cycle of the components used. Under ideal circumstances, this evaluation would take

place at the earliest opportunity, and any prudent improvements and modifications would be carried out before research testing of any kind. Due to uncertainty surrounding the consistency and duration of facility access in the early stages of this year and the absolute importance of research data to the completion of project objectives, testing commenced at the earliest opportunity and was completed before significant system modifications were implemented. This timeline was determined to be feasible after confirming that, as of the beginning of the current research period, all instruments and components were found to appropriately functioning and so the commencement of research immediately was not detrimental to the legitimacy of results or team member safety.

3.1.1 System Components & Instrumentation

For reference, A visual representation of the thermosiphon system as it existed during research testing (and so before the modifications that followed) and the arrangement of the most relevant pieces of instrumentation across its components is in figure 12 below.

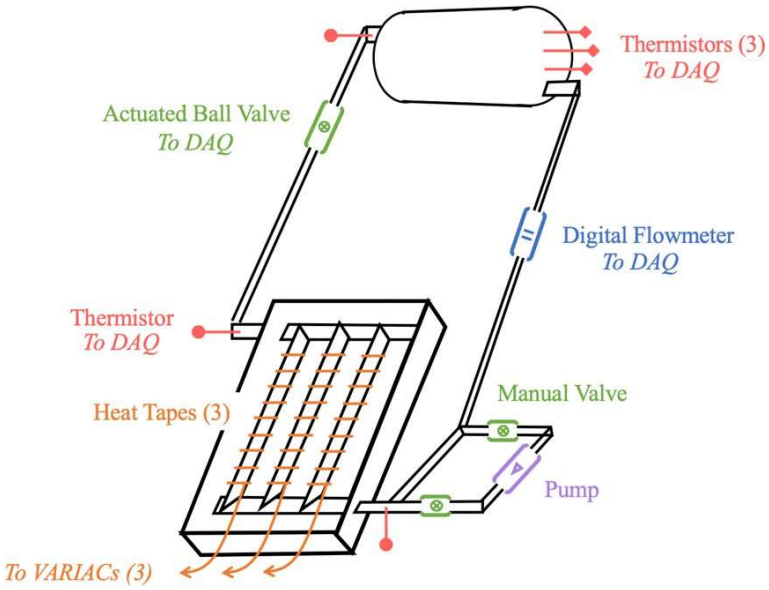

Figure 12: System Instrumentation

The University of Evansville mechanical engineering department houses a controlled research area where the thermosiphon system used in experimental testing is maintained. The thermosiphon resides in an insulated enclosure that includes a set of two mercury thermometers which are used to monitor ambient temperature. The thermosiphon itself also has panels and wrappings of insulation secured closely around all of its components to prevent heat loss to the ambient environment during operation both as a precaution against unreasonably low efficiency data and to prevent the released heat from having a non-negligible impact on environmental conditions. Portions of this insulation can be applied or removed to contain heat or to allow the release of trapped heat in the case of system cooling.

The solar collector of the thermosiphon apparatus consists of a series of parallel metal pipes wrapped with lengths of resistor heat tapes. These heat tapes are the means by which the thermosiphon is supplied with precisely controlled levels of energy to simulate the solar radiation which would provide energy in application contexts. At the exit of the collector, which is an opening at one of its upper corners, tubing interfaces with an outlet pipe and stretches upward, connecting the collector piping outlet to the entrance of the reservoir which is located at the upper portion of one of the two ends of a cylindrical tank. Along that tubing (called the hot leg) is a ball valve which can be used to restrict flow as necessary for variable hydraulic resistance testing.

The tank itself is suspended at a variable height above the collector, and the tubing which connects it to the collector is held at a relatively gradual incline to allow the water to passively flow from one component to the other during system operation. Within the tank on one of the two ends are three thermistors (Omega ON-910-44006) at varying heights. This is to capture the change in temperature across the tank during testing, which due to the nature of the fluid

movement traditionally consists of a gradient perpendicular to the length of the tank. At the exit of the tank, which is on the lower portion of the side opposite the inlet, is tubing that leads to the intake of the collector on the opposite corner from the collector exit. In addition to the three thermistors in the tank, there are three more thermistors located at the collector inlet and exit as well as the tank inlet. Use of this set of six thermistors provides a comprehensive system temperature profile in the form of a series of discrete temperature data points at each thermistor location and for the entire duration of an experimental test.

Between the tank outlet and collector inlet and along the cold leg tubing is an open-bore digital flow meter (INTEK Rheotherm Model 210) that is used to similarly gather discrete volumetric flow rate measurements during research testing. After this instrument a detachable pump is incorporated into the cold leg that can be added to the closed system loop through a by-pass valve and helps circulate fluid during system cooling or mixing without being a source of additional hydraulic resistance during experimental tests. All of these instruments including the six thermistors, the flow meter, and the actuated ball valve are wired to a DAQ board connected to a computer which uses a LabVIEW software interface to collect and analyze the relevant data.

Since this project is based on researching and expanding upon the development of the thermosiphon up to this point, this thermosiphon is an idealized model of a commercial system in that parameters are very closely controlled or, in some cases, simulated. The most relevant example for current research efforts is the replacement of solar energy input with a system consisting of heat tapes and VARIAC transformers. This allows the team to create more controlled and consistent power input situations than would be possible using solar energy. The heat tape is essentially a long resistor which dissipates heat when a current is applied. The power equation 2 below represents the relationship between electrical input and output power. To

monitor and maintain the intake of electricity to the heat tape, VARIACs are connected between the heat tape lengths and the power sources used. This ensures controlled electrical input and therefore more controlled power output, allowing for precise research which is independent of weather conditions or seasonal changes.

$$P = \frac{{V_{RMS}}^2}{R} \quad \textbf{(2)}$$

3.1.2 Instrumentation Modifications

There are several existing components and instruments on the system that had begun to show signs of impending deterioration after prolonged use and which had the potential to be a source of inconsistent or unreliable data during research tests in future years if not addressed. In addition to regular maintenance and instrument replacements, novel modifications to data collection techniques are important to allow further teams to continue to improve on previous research results and thereby draw more definitive conclusions. In each of these instrumentation modification cases; the apparatus are relevant in either the measurement or controlling of system parameters and are grouped in subsequent sections according to this distinction and according to the associated parameter or system location.

3.1.2.1 General Data Collection Techniques

Throughout the research period, the data acquisition system consisted of a N.I. PCI-6221 multifunction I/O device and a N.I. CB-68LP connector block. Both components were borrowed from the Mechanical Engineering department when they were initially installed. All of the more accurate differential input channels were occupied by a number of sensors in the thermosiphon system, with the rest of the sensors relegated to referenced single-ended (RSE) channels.

This semester, with direct funding from the Dean's Account, the team acquired significantly improved emplacements for both of these components. The new multifunction I/O device is a N.I. USB-6218. It features connection terminals built into the device itself, and a USB connector that routes acquired data directly into the CPU for use in LabVIEW. This new device poses several advantages over the previous system. The data acquisition system no longer requires an unwieldy connector block with a thick PCI cable. The USB-6218 features twice the number of differential inputs as the PCI-6221, so the data collected will be more accurate with room to add more sensors to the extra differential channels.

3.1.2.2 Power Control Techniques

For this project some of the most important variables require an understanding of how different amounts of incoming solar radiation to the collector affect the system's performance as quantified by efficiency. To control these variables for research purposes, heat tapes attached to VARIACs are used to create a controllable method to introduce energy into the system. As previously described, heat tapes are essentially very long resistors used to dissipate heat across the lengths of tubing in the collector when current is applied. VARIACs are used to control the voltages fed into the heat tapes from a power source according to the relationship described by equation 2.

At the beginning of this research period the power input system consisted of three VARIACs and three lengths of heat tape. The VARIACs used were very aged and had become slightly inconsistent, requiring constant monitoring and manual adjustments to maintain data credibility. Also, the three lengths of heat tapes, while still highly functional, had become frayed and worn over an extended period of use. To guarantee reliable power input abilities in the future of this project three replacement I.S.E. Staco 3PN1010B VARIACs were planned for purchase

and installation. Additionally, three lengths of ultra-high temperature heating tapes will be purchased and installed to replace the current models. This updates the system with more serviceable instruments and provides more consistent power control techniques which demand lower maintenance during testing, thereby making it easier to control the power input into the system.

3.1.2.3 Power Measurement Techniques

A method of automatically measuring, recording, and displaying the voltage from the VARIACs while tests are being done is a key evolution to the system. This was so that an increasingly accurate measure of the energy that the heat tapes released, which is used to increase the temperature of the system, is digitally recorded instead of requiring iterative manual checks. Since there are limits to the voltage that the connector block and DAQ card could handle, a suitable design for digital power measurement involves a means of stepping down the voltage using a transformer and then converting it to a DC signal and smoothed for measurement by the DAQ card itself. A wiring diagram of the final design for this system is shown in figure 13.

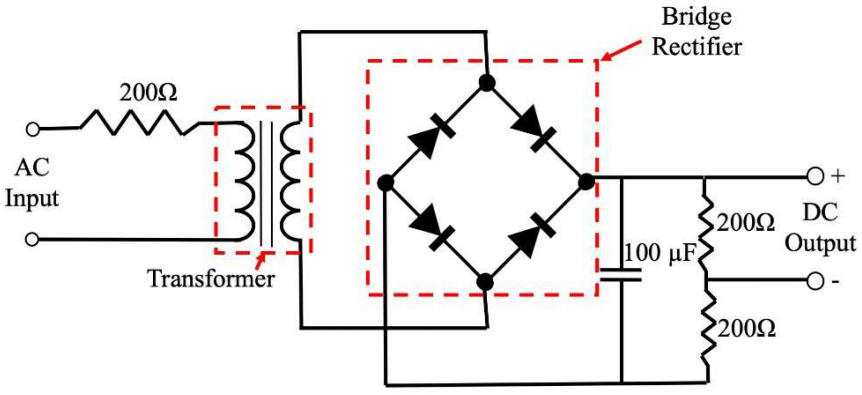

Figure 13: Voltage Measurement Circuit Diagram

The IC chip in this circuit is a bridge rectifier, which converts between AC and DC voltage. Although it removes most of the waves in the output, there are still some remaining

waves, which then are removed by the smoothing capacitor attached across the output of the bridge rectifier. Finally, before the voltage is sent out of the circuit to the connector board for the DAQ, it is split in half by the two resistors attached in series with each other. This is to ensure that no matter what input AC voltage is passed through the circuit, the rest of the circuit will fail before the voltage exceeds ten volts and damages the DAQ. Since three different VARIACs are used in the current thermosiphon system, three of these set-ups are necessary to collect voltages from all the VARIACs. Figure 14 shows the assembled circuit with all three systems attached to a non-conductive board.

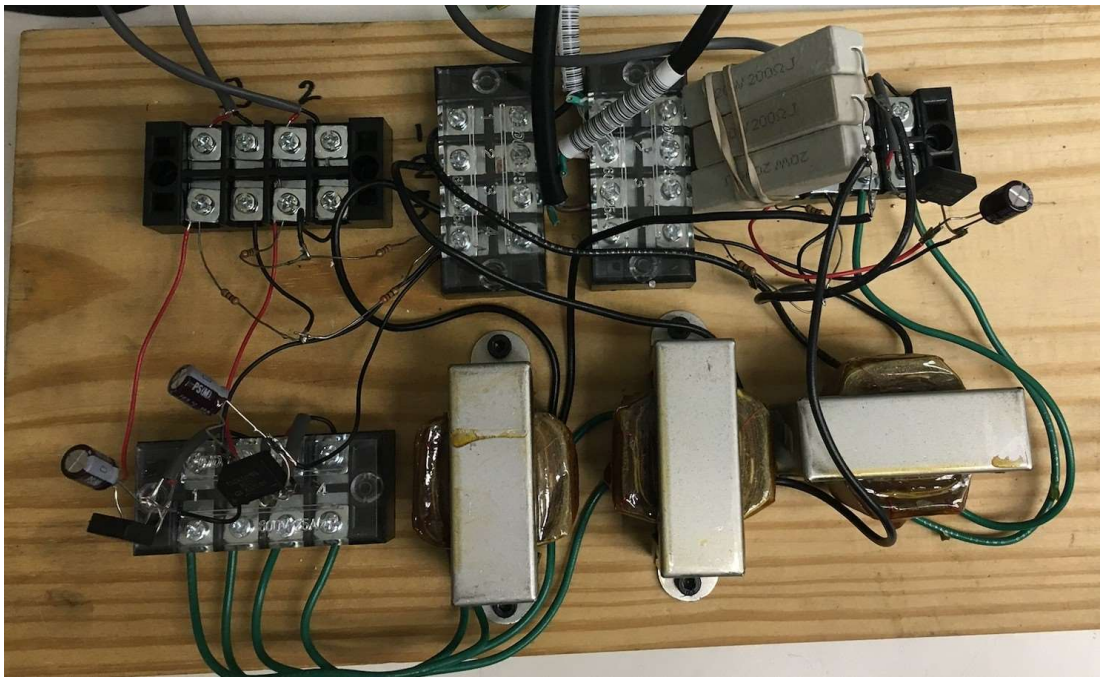

Figure 14: Assembled Circuit

Since the input and output voltages in this system are not the same, it is necessary to develop a relationship between the two through a calibration process. Due to manufacturing errors causing performance errors between each part, each of the three systems, which correspond to the three VARIACs used to energize the heat tapes, need to be calibrated separately to ensure accurate measurements. In order to complete this process, the input and

output voltages are measured and recorded for a variety of different VARIAC settings around the range which is used for the thermosiphon itself. The input voltage from the VARIAC is measured using a Fluke 8808a Digital Multimeter. Since the voltage measured does not remain constant, five measurements are recorded and averaged to represent the input voltage, which is the voltage whose measurement was desired. All three systems are attached into a single VARIAC with a splitting connector to reduce time to complete the calibration. The outputs of the measurement circuit are connected into three separate channels of the CB-68LP Connected Block which is connected into a NI® PCI-6221 DAQ Board. A VI is set up in LabVIEW 2014 to record the voltages coming out of the circuit. The block diagram for this VI is shown in figure 15.

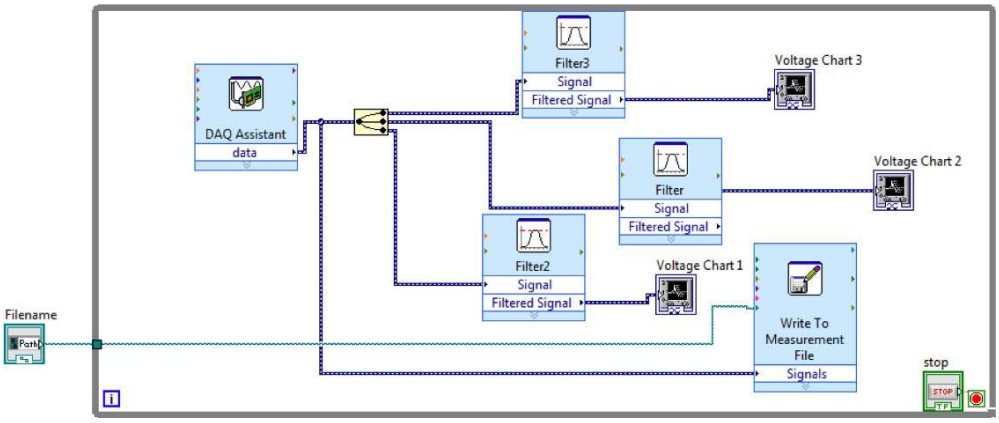

Figure 15: LabVIEW Block Diagram

There are several important settings for this VI to work properly with the circuit to which it is attached. The first two of these settings were in the DAQ assistant block, shown in figure 16.

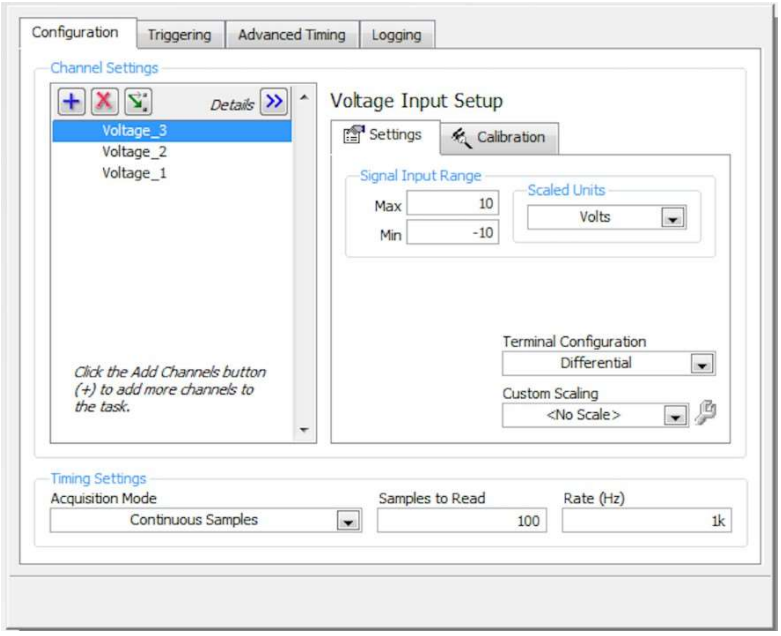

Figure 16: DAQ Assistant

In this settings block, the voltage range is checked and set at ten volts so that it could measure any output within the range of the connector board. The second is that the system is set to record continuous samples after it is started. The frequency was set to 1 kHz to make certain that all points of interest would be recorded and to provide sufficient data points for analysis. The second major grouping of settings is with regards to the filters shown in the block diagram. They are used to reduce the noise from the system, and as such need to remove certain unwanted frequencies. As shown in figure 17, the filter is set to be a low-pass filter with a cutoff frequency of 10 Hz. Waveform charts and a file save block are also added to provide a visual cue to start and stop the program and to record all data between the start and stop times.

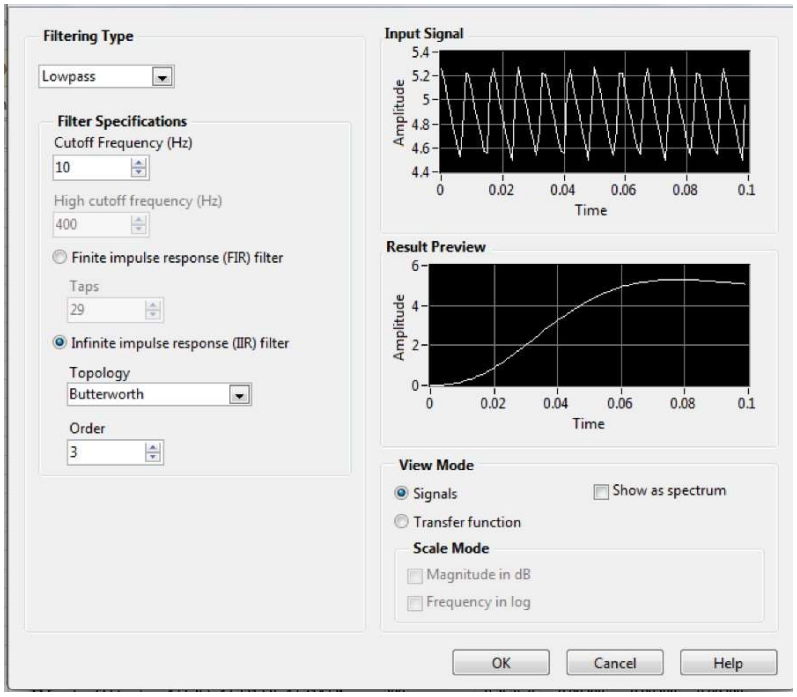

Figure 17: Filter Settings

After completion of these elements, calibration is necessary. Once everything is set up, the VARIAC is set to a given voltage and measurements of the voltage it is inputting are recorded as previously described. Then, the LabVIEW VI is run for approximately four seconds. The VARIAC is then changed to a different setting and the process is repeated. This is ultimately completed for 30 even intervals between and including 5-volts and 77.5-volts. The input and output voltages recorded are then averaged; each of the three measured voltages from the output are averaged separately. Linear regressions of the input voltage with respect to the output voltage are then completed to determine the relationship between the two different voltages. Once these values are input into the thermosiphon project VI and the filters are set up as they were during the calibration, the team will have a functional digital voltage measurement system, providing precise discrete power input data points not limited by manual check frequency.

3.1.2.4 Hydraulic Resistance Control Techniques

The actuated ball valve on the system, also referred to in this report as the K-valve, is a Belimo LRX24-MFT. The valve is supplied with a 24V excitation that drives the actuator and is controlled by a separate voltage source ranging from 0V to approximately 8V. The device provides an output voltage proportional to the angular displacement of the ball relative to its open position. The valve blocks the flow of water well before the ball reaches its maximum 90° displacement; therefore, the percent closure must be related to the point at which flow completely stops, rather than the maximum displacement of the ball.

The most direct way of measuring valve closure is to display the percent closure as a function of the device's output voltage. First, the valve is fully opened by adjusting the control voltage to 0V, and its output voltage is recorded. Next, the control voltage is adjusted so that the valve rotates to its maximum 90° displacement. The valve assembly is oriented vertically, and a short section of pipe is attached to its upwards-facing inlet and filled with water. The control voltage is then gradually lowered until water begins to drip through the valve. The output voltage is recorded at the point of no flow, which serves as the 100% closure state.

Two hundred output voltage samples are recorded in LabVIEW at both points and averaged. A slope-intercept equation is derived based on these two points using linear regression in Excel, as depicted in equation 3.

$$\% \, Valve \, Closure = mV_{out} + b \tag{3}$$

The resulting equation will be inserted into the appropriate function block in LabVIEW with the valve's output voltage as an input. During a test, the control voltage will be adjusted until the desired percent closure is achieved on the front panel display in LabVIEW.

3.1.2.5 Flow Measurement Techniques

Volumetric flow rate is a critical variable in determining collector efficiency. The flow rate is measured using a precision instrument known as a thermal flow meter, also referred to in this report as a Rheotherm, its INTEK proprietary name. Fluid flows through the Rheotherm via an unobstructed, insulated pipe. Along the outside of the pipe are two resistance temperature detectors (RTDs), one measuring the temperature of the incoming fluid, and one measuring the temperature of a constant low-power heater. As flow rate increases, heat is removed more rapidly from the heater via convection, resulting in a decrease in heater temperature. The temperature difference between the RTDs is used in a logarithmic function that supplies an output voltage which can be converted to the flow rate of the fluid in LabVIEW.

Upon completion of research testing, the Rheotherm is shipped to INTEK for calibration as the team is not equipped to perform such precise adjustments. Before its return, further research is required to find the correct voltage-to-GPM conversion formula to be used in the associated LabVIEW function block.

3.1.2.6 Temperature Measurement Techniques

Calibration of system thermistors is vital to continued accuracy, and the opportunities afforded by new data collection instruments are also excellent opportunities to develop greater temperature measurements of the environment. In addition to regular calibration work on the system fluid thermistors, the increased capacity associated with the new DAQ may be immediately utilized through the addition of thermistors to the system enclosure in order to monitor the ambient temperature more precisely and consistently. Three thermistors will potentially be spaced vertically inside the enclosure to study the ambient temperature gradients during a test. The team will have the option to position additional thermistors while the system is being reassembled, and the merits of this possibility will be evaluated at that time.

The thermistors in the system are calibrated using a Fluke 9100S Dry-Well Calibrator Oven shown in figure 14 below. This oven allows for a stable, controlled temperature inside the wells in which thermistors can be placed for measurement.

Figure 14: Fluke 9100S Dry-Well Calibrator Oven

Since the thermistors measure resistance, the Steinhart equation is used to convert resistance to temperature. This equation is shown below in equation 4.

$$T = \frac{1}{A + Bln(R) + Cln^{+}(R)} \quad (4)$$

The coefficients A, B, and C, of this equation are specific to the thermistor model and are provided by the manufacturer. Coefficient values for Omega thermistors (model 44004 to 44008) are shown below in table 2.

Table 2: Omega Thermistor Steinhart Equation Coefficients

Omega Thermistor Model Number	Expected Resistance at 25°C [Ω]	Coefficient A	Coefficient B	Coefficient C
44004	2252	1.468E-03	2.383E-04	1.007E-07
44005	3000	1.403E-03	2.373E-04	9.827E-08
44006	5000	1.032E-03	2.387E-04	1.580E-07
44007	10000	1.285E-03	2.362E-04	9.285E-08

44008	30000	9.376E-04	2.208E-04	1.276E-07

For calibration testing, the dry-well calibration ovens are set to a given temperature. After waiting fifteen minutes for the ovens to reach a steady state, one thermistor is placed inside the oven. After approximately two minutes, the resistance of that thermistor will be measured using a digital multimeter, and the measurement is not be recorded until the tens place reading remains constant for two or more seconds. This measurement method is repeated for each thermistor and for temperatures ranging from 30°C to 70°C in 10°C increments. Another resistance measurement is taken at room temperature with a mercury thermometer as reference.

After all measurements are recorded, the Steinhart equation is used to calculate measured temperature for each thermistor at each reference temperature. The measured temperatures are plotted against the reference temperatures for each thermistor so that a linear regression analysis can be performed. This regression analysis results in a slope and y-intercept from which a linear calibration equation can be obtained.

3.1.3 Component Modifications

In addition to the alteration of data collection techniques, which typically involve modifications to the apparatus which are tangential to thermosiphon system function, significant modifications to the more core thermosiphon components are also implemented for the benefit of future teams. These updates involve the fundamental redesign of the system itself as opposed to the replacement or upgrading of existing components but are similarly designed to allow for more efficient setting of parameters, higher frequency testing, and greater precision.

3.1.3.1 Collector Modifications Design

The original collector support consisted of a rectangular wooden frame hinged at one end. To change settings, the support is lifted by hand and supported with C-clamps tightened onto two

vertical supports on either side of a frame to hold the collector at a desired angle as seen in figure 15. While this process is effective, it does leave room for improvement. The C-clamps tend to settle, resulting in a lower the angle from what was desired and requiring time and multiple operators to manipulate the collector into the desired position before a test can begin.

Figure 15: Existing Collector Support

To fix some of these issues a new support system was initially designed as seen in figure 16. This system consists of two supports at either side of the width of the collector with a hinge at the end of the collector where the cold leg enters. Each support has a roller that rolls along the bottom length of the collector at a constant height which cause the collector to rise as the supports are moved toward the hinged end. These rollers are fixed on their line of movement by guiding rods, and threaded rods run through their centers, which are rotated by an electric motor. Theoretically, a single user could activate the motor and rotate the threaded rods, causing the supports to move along the guides to raise or lower the collector's angle with ease. However, due to manufacturing difficulties and probable binding issues, this idea was abandoned, and the

following secondary design revisited and refined with the intent of implementation. Though this design is ultimately not implemented, the general components of it are presented as reference for future teams who may find use for a more automated system of collector angle adjustments.

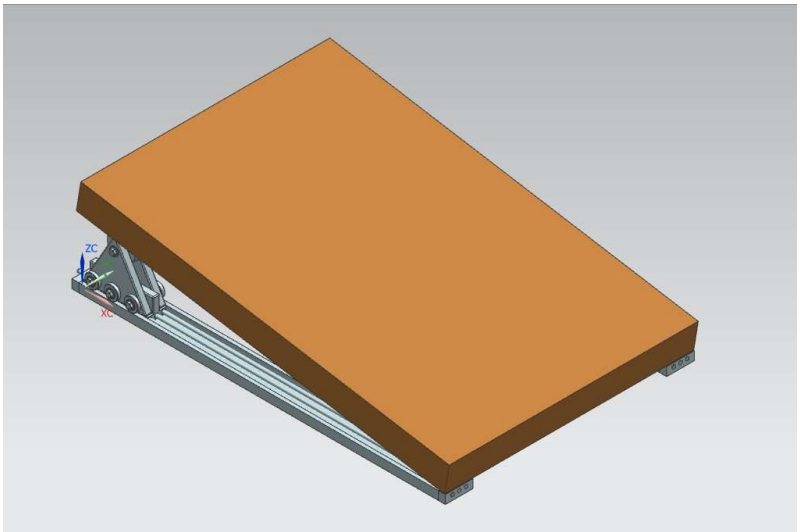

Figure 16: Full Roller and Trolley Assembly

The final design, which addresses the main issues with the current system while pursuing a simplified mechanical idea (and therefore one which is more simply maintained and operated) can be seen in figure 17. In this design, the collector is housed by a frame composed of different lengths of two inch by four inch wooden planks which will reside within the insulated enclosure. Outside the enclosure, another section will feature a mounted winch wound with 3/16 inch steel cable. In the original versions of this design, a standard hand-cranked winch was chosen. This device, however, works primarily in the lifting direction of rotation and is not infinitely variable due to its typical clutch design, meaning it would not be able to make minute adjustments to the collector's angle. To address both of these issues, the winch was replaced with one that utilizes a worm gear. This style of winch is useful for the system's demands in that a worm gear's design allows it to remain locked in place when not actuated, works equally well in both rotational directions, and can convert large rotational inputs into minute rotational outputs. This rotational

conversion allows for minute angle adjustments but also implies that greater angle adjustments require a very large quantity of rotational inputs. Conveniently, the chosen winch features a hex head on its input drive shaft, meaning an electric hand drill could be attached to allow these larger inputs to be set quickly and effortlessly by a single team member.

The steel cable leading out of the winch will be redirected through two pulleys attached to the top of the wooden frame, one outside the enclosure and one inside. This will position the standing end of the cable, which eventually connects with the collector, to come from the top of the enclosure, providing a primarily vertical pulling force for lifting the collector. In the original version of this design, the cable interfaced with the lifting edge of the collector by a single anchor positioned along its center of mass. While this would theoretically achieve the desired function, a thin point of contact with such a broad and heavy load would most likely cause issues when altering the collector angle. Therefore, a final modification was made to the original design in that after passing through the second pulley, a metal ring will be used to convert the single cable into two, allowing for connections on either side of the collector.

This completed design will allow team members to easily raise and lower the collector angle by simply turning the winch with an electric drill. Its simplicity allows for relatively simple and efficient preparation and construction. Additionally, while the cost of its materials is already low, the general nature of necessary materials means that current inventory from previous system modifications will decrease the amount of materials that need to be purchased to construct this design, making it simple, mechanically sound, functional, and efficient to implement.

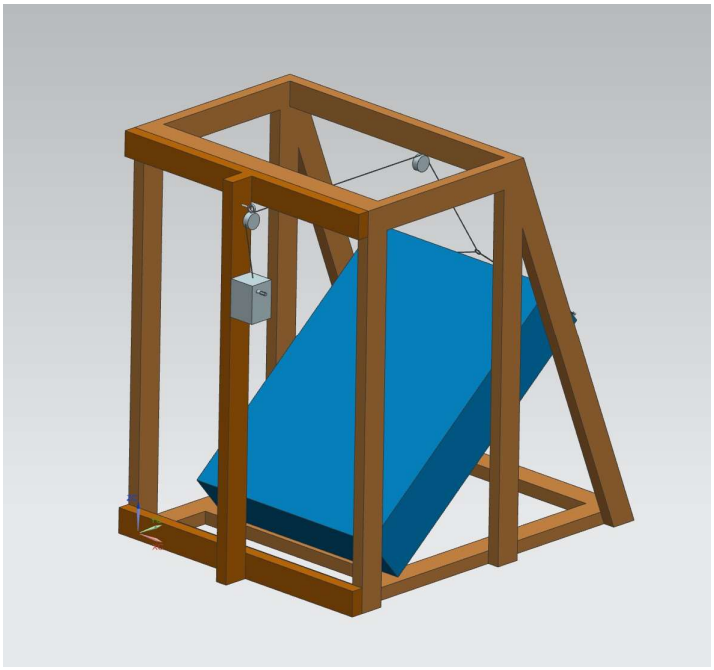

Figure 17: Secondary Collector Support Design

3.1.3.2 Reservoir Modifications Design

The primary motivation for a redesign of the reservoir support system is a desire for more precise control over more discrete differences in hot leg height, something which is limited by the winch and pulley currently used to raise and lower the tank. The new design, which is illustrated in figure 18, features two sets of two six-foot steel metal rods, one set of two on each side of the tank, each of which penetrate through a bearing and act as guides for the reservoir's vertical motion. They also serve to protect the system when uneven loads are applied creating moments around the lengthwise axis of the tank by providing points for the bearing to press back against. On each side of the tank between the two steel rods is an ACME ½-10 threaded rod which acts as a power screw. On the power screw, guided by the two rods, is a steel block that is custom machined to act as a bearing and support. Due to concern that possible out of turn lead screws could cause binding in the lift system, the bearing block is attached to the tank with a slotted hinge. This would allow the tank to rotate slightly if the screw system was broken and to

slide to account for the increased distance between the two attachment points should the bearing blocks be at different heights.

The two rods on either side of the lead screws are supported by blocks of wood which are attached to the frame of the existing insulated enclosure. The two rods are attached into the wood frame for the lift at the top and the bottom, while the threaded rods were set into a bushing at the bottom of the system and a bearing at the top. The bearing at the top only needs to carry transverse loads, so ball bearings are used in this case. At the bottom, both axial and transverse loads are expected, due to this section holding the weight of the tank assembly. To hold this up, a brass plate with a hole in the center will be set into the wooden frame, and a steel plate with a hole in it will be welded around a portion of the threaded rod with the threads removed. The end of the threaded rod will sit in the hole in the brass plate while the top of the brass plate and the bottom of the steel plate are in contact with each other to hold the load of the reservoir assembly. Near the bottoms of the threaded rods are welded bike gears to transmit torque from the motor to the threaded rods. Using bike gears will allow the use of bike chain to attach to the motor which, when activated, will cause both ends of the tank to rise at the same rate. In case of the possibility that the bearings on each side of the tank might become misaligned with each other, two additional sprocket sets will be attached, one to each power screw. Under normal conditions, these sprockets will freely rotate when the tank is raised or lowered; however, in the case that one side of the tank is higher or lower than the other, the chain attached from the motor to that side of the tank will be removed and the secondary sprocket set will be rotated to adjust the tank back into equilibrium. The chain to the motor would then be reattached and the system could return to its normal function.

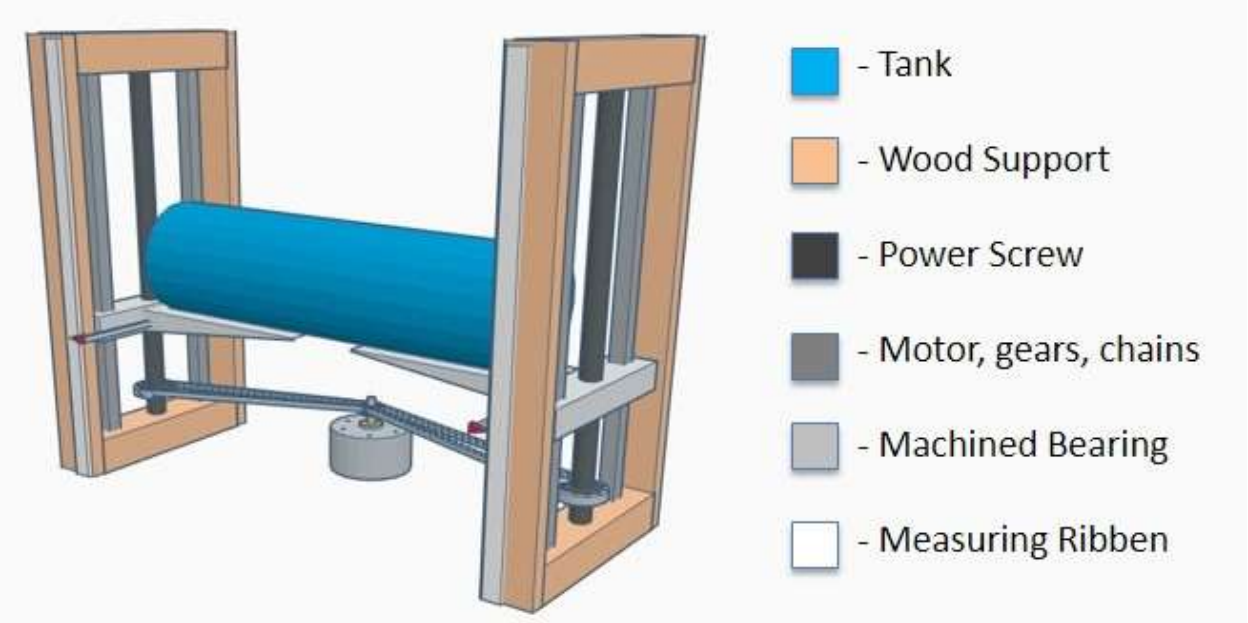

Figure 18: Reservoir Support Modifications

Due to the limited size of the insulated enclosure surrounding the system, the tank is only capable of moving a maximum vertical distance four feet. An extra foot of threads on the power screw will be added to this maximum distance to allow for additional flexibility for future teams.

In addition to a redesigned reservoir support system, the insulation which currently surrounds the reservoir and is beginning to wear has been completely redesigned. The new insulation design involves a sheet comprised of three layers: a thick foil on the outside, fiberglass insulation in the middle, and a sheet of foam insulation on the inside. The layered sheet of insulation remains is arranged in such a way that it can be folded around the surface of the tank. Across the entire middle portion of the tank, the three-layer insulation sheet is cut so that it can fold down like a flap to allow for ventilation during system cooling. During testing, the flap is secured with strips of VELCRO to prevent heat loss to the ambient.

3.1.3.3 Tubing Modifications Design

This year, the team will modify the layout of the hot and cold leg tubing which connect the reservoir and collector. While the current piping layout does serve its purpose, its current state leads to the potential problem of kinking, especially in the hot leg. The main contributor to this issue is the weight of the suspended K-valve combined with the bending of the tubing at the collector outlet. Past teams used sections of PVC pipe which were duct taped to the outside of the insulation in an attempt to remedy the problem of kinking at the K-valve and the collector outlet. The insulation on both legs is deteriorating, and the vinyl tubing has shown signs of soon losing its ability to maintain a constant cross-sectional area after another period of use; at the inlet and outlet of the Rheotherm, this reduction of area could potentially affect the accuracy of flow rate readings.

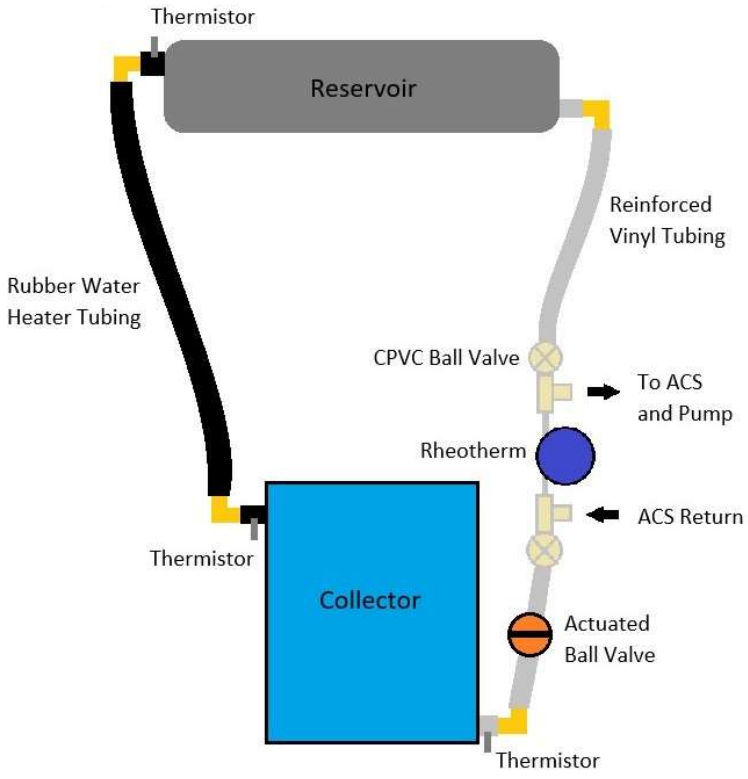

Figure 19: Modified tubing layout with instrumentation

A simplified diagram of the new piping layout is shown in figure 19. The main purpose of modifying the tubing system is to eliminate the possibility of kinking by reducing bending stress on the tubing. The hot leg vinyl tubing is replaced with rubber water heater hose with a temperature rating of 100°C to prevent damage to the tubing even under conditions which cause the water to boil (which traditionally occurs in the hot leg and collector if at all). The cold leg vinyl tubing is replaced with reinforced vinyl tubing which features an internal woven thread mesh. Short lengths of tubing are attached to the barbed hose connectors already present on the collector. Brass elbows are attached to these lengths and angled in the appropriate direction, as opposed to having the piping extend out perpendicularly as before. This method achieves the effect of preventing the hot leg piping from kinking under its own weight. In addition, thermistors are inserted through the tubing wall of these short pipe sections at the inlet and outlet of the collector.

The cold leg layout is modified to accommodate the new active cooling system described in a subsequent section. The new woven vinyl tubing interfaces with the reservoir using brass elbows in the same way as with the collector. As the tubing extends toward the floor of the enclosure, it connects to the inlet junction of the active cooling system. The Rheotherm alone is placed in parallel with the active cooling system, attached with 3/8 inch vinyl tubing and the appropriate CPVC to barbed hose adapters. It is important that the Rheotherm requires adjacent tubing to be largely straight and uninterrupted for the most accurate flow measurement.

The K-valve is moved to a location downstream of the re-entry point of the active cooling system, immediately before the inlet of the collector. It is no longer be suspended on the hot leg, which relieves stress on the hot leg tubing. The pipe section of the K-valve is already connected

to one inch barbed hose connectors, which interfaces nicely with the one inch vinyl tubing to be used in the cold leg.

Lastly, new foam insulation is applied to all tubing and fastened with duct tape where necessary. A simple wooden frame is constructed to elevate the vinyl piping adjacent to the Rheotherm so that it will extend in a straight line from the Rheotherm's inlet and outlet.

3.1.3.4 Enclosure Modifications Design

In order to more precisely control the ambient temperature of the system, the thermosiphon is enclosed in an insulating chamber. This chamber reduces the heat transfer from the system to the environment if environmental conditions are not aligned with research goals. Heating or cooling the entire facility is impractical; therefore, the team designed a ventilation system to aid in cooling the ambient inside the insulated enclosure when necessary. One such situation may occur when the system must be cooled quickly after the completion of a test.

Through the use of a space heater, the ambient system temperature can easily be increased. However, aside from opening the enclosure and using fans, there has not been a method to actively cool the system in previous years. The ambient temperature may need to be rapidly increased or decreased according to the requirement of different tests and to increase the frequency with which tests can be conducted, so having such a cooling system is a critical upgrade. A more intentional ventilation system consisting of strategically placed openings in the enclosure helps cool the ambient temperature when necessary and aids in ease of access to crucial components of the system. There are two main additions to the enclosure which comprise the new ventilation system, each an opening which did not previously exist.

As of the beginning of the research period, only one side of the enclosure was removable. This side is covered by a single large panel when testing is being performed, which can be

removed when access to the system is required. The single opening results in consistent difficulty accessing the components on the opposite side, making the disturbance of instruments or tubing a danger as team members pass through the system components to the other end of the enclosure. The addition of a rear door helps with easy access to the crucial components of the system as well as provide a means of forcing air through the enclosure from one opening and out another. The other primary ventilation system component is a smaller opening supported by a controllable fan on the top of the enclosure. This vent assists in removing warm trapped air. A comparison of closed and opened conditions of the updated ventilation system can be seen in figure 20.

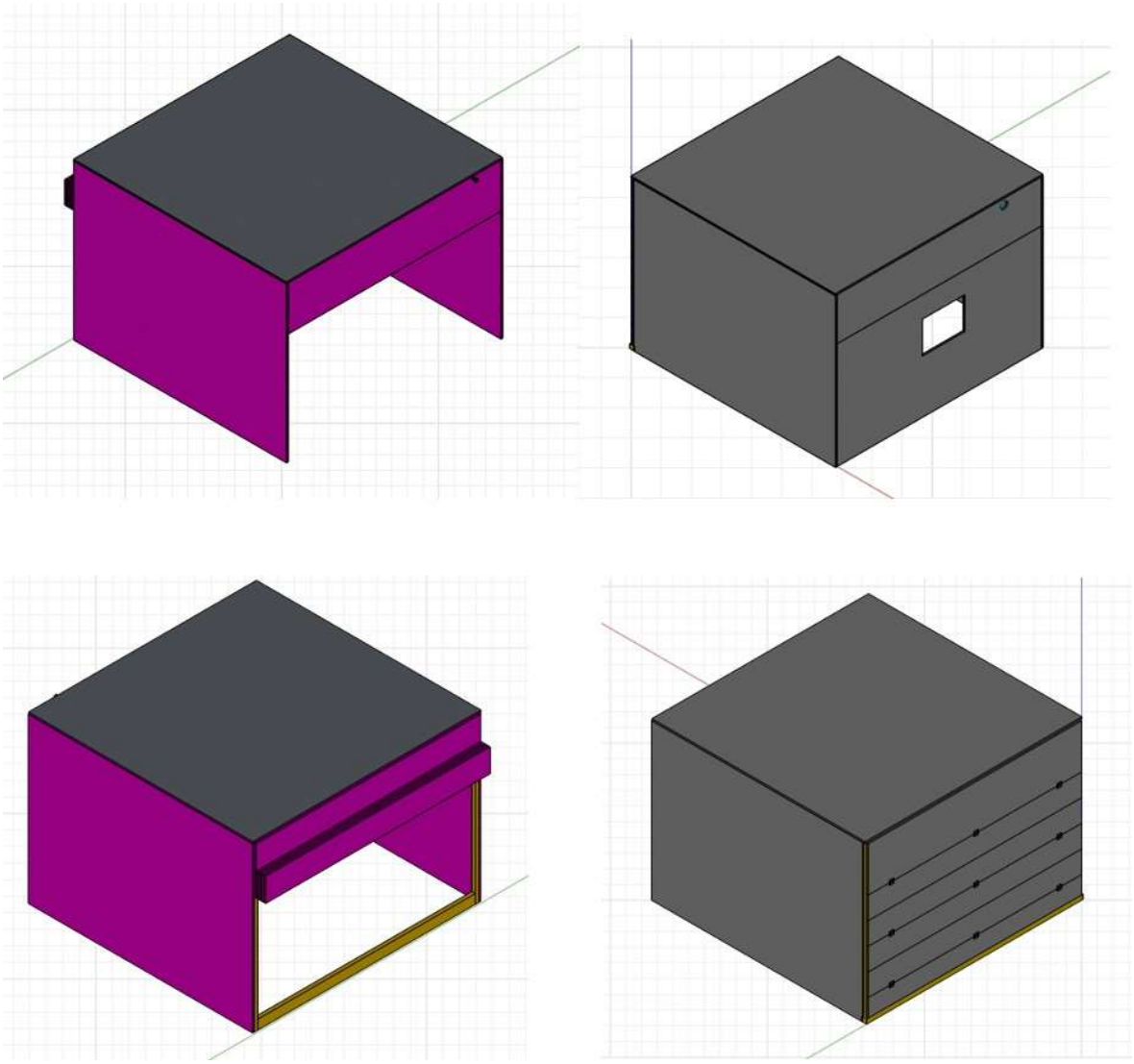

Figure 20: Comparison of Open and Closed enclosure conditions

A foldable hinged door is created to establish an opening that can be easily operated and with minimal space to accommodate the small size of the room. The eight-by-nine-inch polystyrene panel is cut into five twelve inch by nine-foot panels. The sides of the panels are reinforced with aluminum tape to avoid cracks. Five small steel hinges attach two panels with each other. The screws are fastened using a coating of hardener to strengthen the attachment. The fully completed hinged door is attached to the frame using five similar hinges. A two-inch long screw with a long shaft is screwed into the sides of the panels and the frame next to it, as seen in

figure 21. A set of standard rubber bands is used to hold the foldable door in position when both opened and closed by looping around the exposed screws.

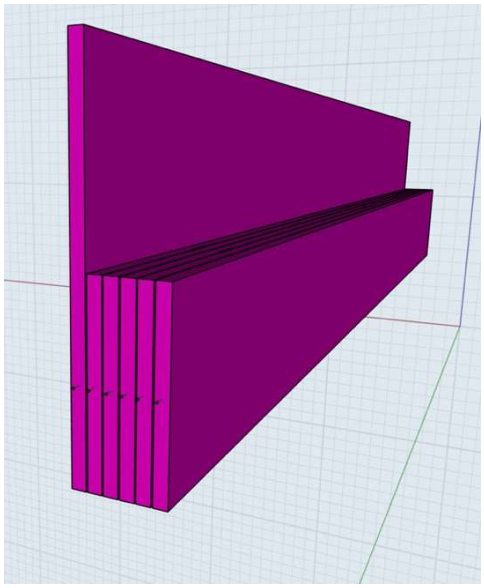

Figure 21: Hinged Door in Folded Position with Screws Attached

For the forced ventilation system, a vent fan is purchased and attached to the corner frame. An opening is created on the insulation, and a duct connects the fan and the opening. A general model fan with respect to the frame can be seen in figure 22.

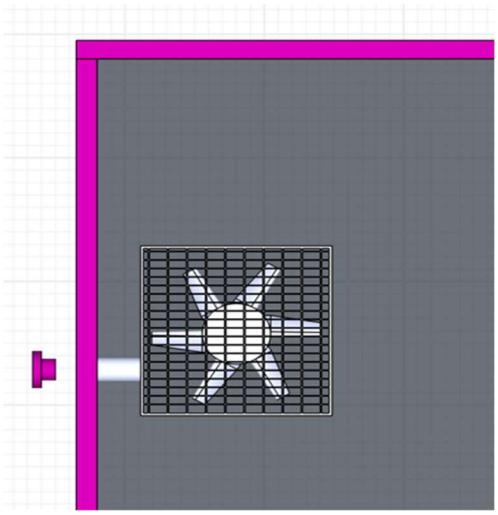

Figure 22: A General Location of the Fan with Respect to the Frame

3.1.3.5 Active Cooling System Design

The ability to change the working fluid temperature in the thermosiphon is crucial for setting up the initial conditions of different tests. The heating of the fluid can be done quickly and with great control by powering the heat tapes in the collector. However, as of the beginning of the research period there is no system established that can cool the working fluid quickly when required. Moreover, since the working fluid inside the thermosiphon system is insulated from the ambient, the cooling process can take hours to cool the fluid temperature by even a few degrees. An example context in which cooling of the system temperature is required is when the test parameter requires a lower temperature than has been reached by the fluid since the previous test was conducted. Also, there is always a temperature gradient present in the thermosiphon system because the warmer water rises to the top of the tank, and the colder water gets collected on the collector. The proper mixing of the system fluid before testing is essential to make all the tests consistent. Hence, a cooling system is developed to cool the working fluid when required or to mix the system fluid without heat transfer. A general design of the cooling system can be seen in figure 23.

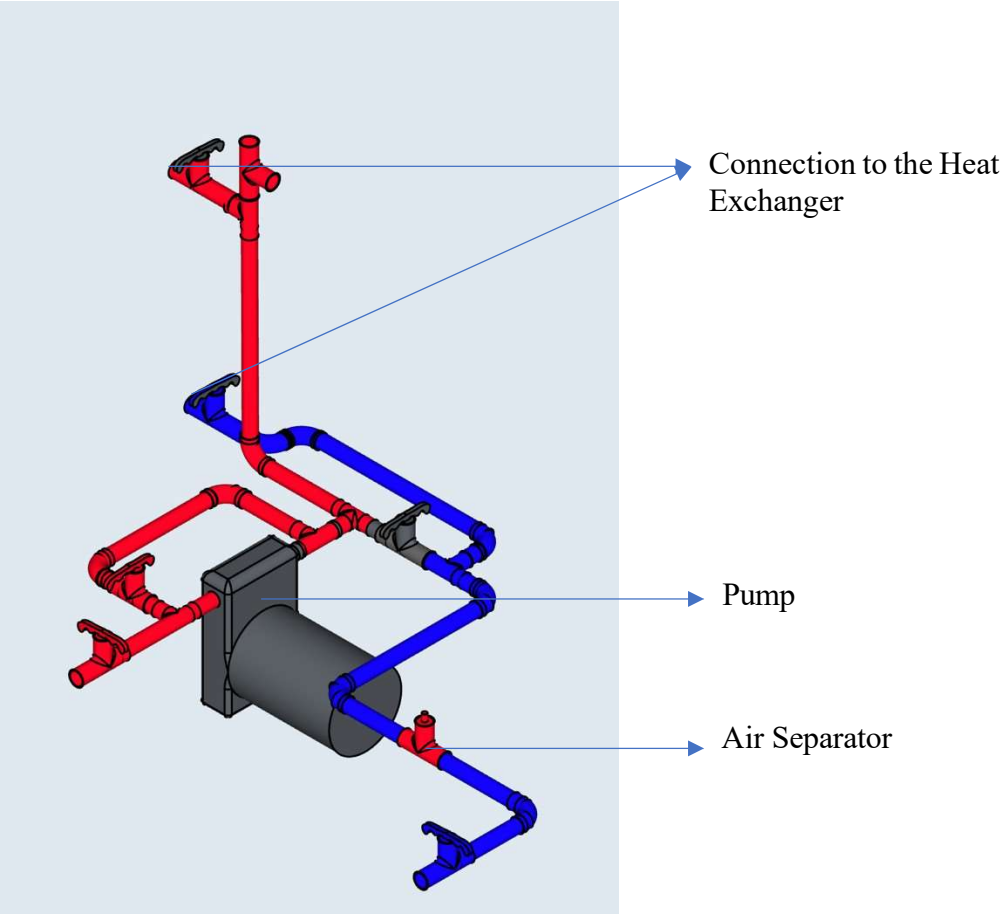

Figure 23: Active cooling system design

There are three modes of operation for the cooling system. The modes of flow can be seen in figure 24. In the first mode of operation, distinguished by pump-driven flow with heat transfer, the fluid flows from the bottom of the tank, circulates through a heat exchanger, and returns to the collector inlet as forced by an activation of a pump. This mode aids in cooling the fluid temperature when needed. In the second mode of operation, a pump-driven flow without heat transfer, the fluid flows from the bottom of the tank, circulates through a straight pipe, and returns directly to the collector inlet. This mode helps to properly mix the system fluid while heating of the system fluid is needed. The third mode of flow is the buoyancy-driven flow which bypasses both the pump and heat exchanger and is used while a test is being conducted.

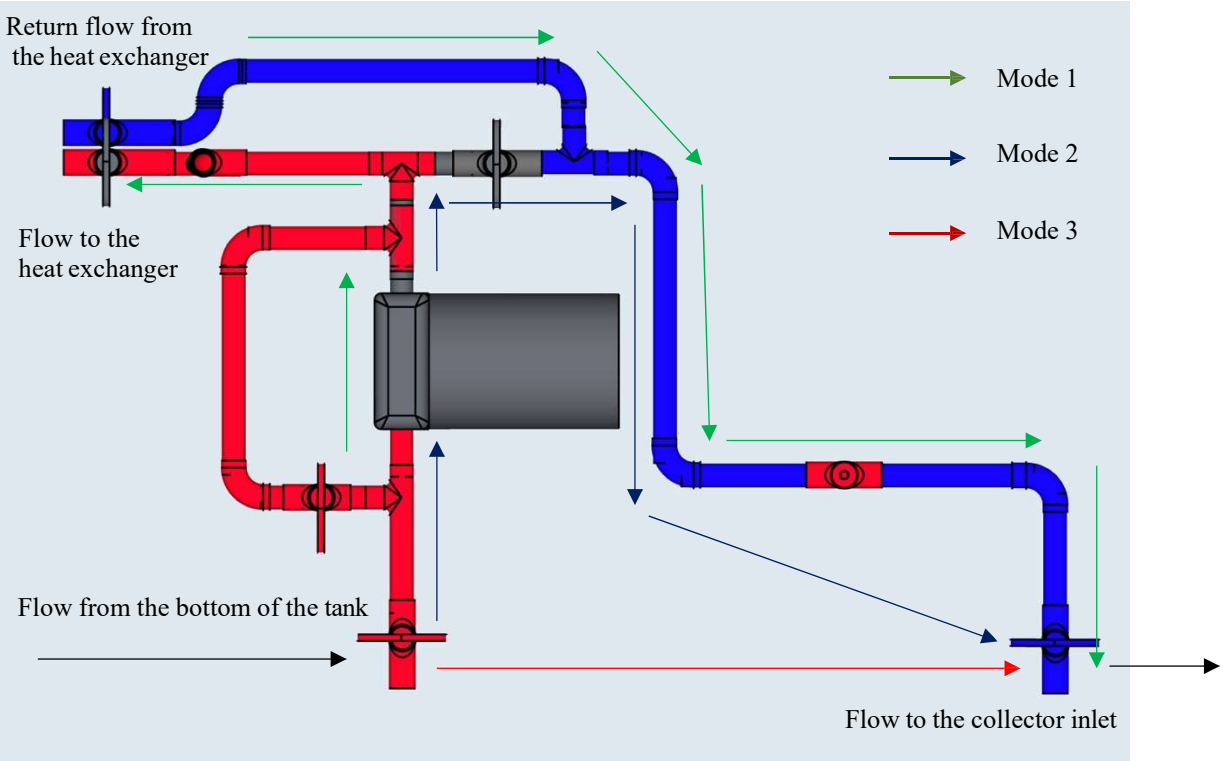

Figure 24: Modes of flow obtained from the pipe network

Since the temperature of fluid in the system can reach high temperatures during testing, it is crucial to have a system that can handle the hot temperature. Therefore, the team will be using CPVC tubing for the cooling system. The thermosiphon system being a closed circuit requires conditions such as complete absence of air bubbles and microbubbles. Therefore, and air eliminator is added to the circuit as seen in figure 24. The pump that was being used before had an issue drawing in air as the pump did not have enough suction power. Hence, new pump with higher capacity will be added to the circuit. The risk of damaging the thermosiphon system components can be mitigated using a recirculating loop in the pipe network.

3.2 Experimental Approach

All research tests are arranged into one of three categories, each comprised of a set of testing phases and characterized by a different set of parameters and priority level within the project based on the results of previous studies and available resources: “Base Case Testing”, “Power-Angle Research”, and “Other Research”.

3.2.1 Base Case Method

A base case test is one of a series of verification tests used collectively to determine that the thermosiphon system results are consistent in the absence of parameter variations and comparable to results from previous experimental phases and institutions. Since significant modifications to the system are traditionally undertaken, performing base case testing after making changes is also important to verify that the modifications did not significantly alter system functionality or consistency. For this reason, two base case testing phases are performed. The first set of base case tests was initially conducted in the beginning of fall 2020 semester, before any modifications were done. The second set will be conducted in the spring semester after all the significant facility modifications are complete. Base case testing is conducted with the same base values as in previous years, as seen in table 3. The power input for the base case tests will be kept constant at 50 V_{RMS}. Because the thermosiphon experiments are conducted in an insulated enclosure, the environment can be heated effectively and with a high degree of control. Still, it cannot be cooled with the same effectiveness based on the current infrastructure of the mezzanine environment. Hence, the ambient temperature of 25℃ was selected so that the tests can theoretically be conducted all year. The collector angle of 38° was chosen because it is the reference angle associated with the latitude of the facility. The hot leg height is kept constant at 21 inches and the hydraulic resistance is maintained at zero percent ball valve closure.

Table 3: Base Case Test Parameters

Parameter	Base Case Value
Collector Angle, θ [degrees]	38°
Power Input, P [V_{RMS}]	50 V
Hot Leg Height, h [inches]	21 in.
Hydraulic Resistance, K [percent valve closure]	0 %
Ambient Temperature, $T_{ambient}$ [°C]	25 °C

3.2.2 Power-Angle Research

The research parameters of highest priority are the collector angle and power input, specifically the relationship between them and the way it relates to system efficiency and global system position. The goal of this set of testing phases is to definitively determine trends which indicate a range in which the collector angle of optimal efficiency exists both as an isolated parameter and in coordination with power input. This is accomplished through variable angle-constant power testing and variable angle-variable power testing, respectively, each of which is comprised of a set of distinct test conditions.

3.2.2.1 Variable Angle-Constant Power Method

Variable angle-constant power tests, abbreviated VACP for convenience, are tests in which all parameters are maintained at their associated base case conditions except the collector angle, which is varied in a range from 14° to 54° at increments of 8°, resulting in six core data points for each testing phase. In response to these points, further testing at intermediate collector angles continues to further clarify trends in data. By varying the collector angle while maintaining a consistent power input, these tests simulate the response of a thermosiphon system constructed at the associated reference angle at a range of latitudes. This period involves two

testing phases, a variable angle-constant high power (VACHP) phase used to simulate clear weather conditions and a variable angle-constant low power (VACLP) phase used to simulate solar radiation obstructed by cloud cover, which are associated with heat tape input voltages of 50 V to 37 V, respectively. In the case of high-power testing, acquisition of the six data points of interest requires only five novel tests because the 38° collector angle data point is identical to previously completed base case tests. Table 4 summarizes experimental conditions for the tests which make up these two key phases of testing. In this table and the similar tables which follow, the test index is comprised of the phase number followed by the test number within that phase. Data points which are of interest in the data analysis of the phase but do not require novel testing are shaded and the reference test index number is indicated. While not relevant to the preliminary research plan, further tests beyond the scope of the initially determined points were indicated by a test index with an alphabetical symbol after the decimal point instead of a number (example: "1.A" indicates the first test in phase one after completion of the initial data set).

Table 4: Variable Angle - Constant Power Test Parameters

Test Index	Collector Angle, θ (Degrees)	Input Power, P (Applied V_{RMS})	Other Parameters h, K, $T_{ambient}$
Phase 1: VACHP			
1.1	14°	50 V	Base Case
1.2	22°	50 V	Base Case
1.3	30°	50 V	Base Case
[Base Case]	38°	50 V	Base Case
1.4	46°	50 V	Base Case
1.5	54°	50 V	Base Case
Phase 2: VACLP			
2.1	14°	37 V	Base Case
2.2	22°	37 V	Base Case

2.3	30°	37 V	Base Case
2.4	38°	37 V	Base Case
2.5	46°	37 V	Base Case
2.6	54°	37 V	Base Case

3.2.2.2 Variable Angle-Variable Power Method

Variable angle-variable power (VAVP) tests are perhaps the tests of most interest to the team and to the current state of thermosiphon research. This set of research phases is designed to simulate a thermosiphon system installed at a specified location, as indicated by a latitude and associated reference angle, and the response of that system to variation in collector angle while accounting for the associated reduction in power input as quantified by equation 1.

Ultimately, it is desirable to identify a clear trend which accounts for the contradictory effects of a more median collector angle, which has been shown to increase efficiency, and the related departure from the reference angle, which causes a decrease in power input. Because this effect would theoretically be most pronounced at angles which vary greatly from the ideal collector angle as indicated by previous VACP testing, this research area involves two testing phases, one based on the relatively low collector angle of 14° and one based on the high angle of 62°. These two phases are called Variable High Angle-Variable Power (VHAVP) and Variable Low Angle-Variable Power (VLAVP), respectively, because in the first case the angles tested are higher than the one which would be conventionally used (the reference angle) and in the latter the test angles are lower than conventional.

For each of these two phases of testing, the angle is varied from the reference angle in a range from 6° to 36° at increments of 6°, which, when combined with previously completed tests of interest from phases one and two, results in sets of seven and six data points resulting from

sets of six novel parameter configurations. Low reference angle testing involves increasing the collector angle by these amounts and high reference angle testing involves angular decreases. For each of these variations, the voltage input to the heat tape is also varied to reflect the anticipated loss in power associated with deviations from the reference angle according to equation 1. By performing a series of tests at reference angles both above and below the moderate angel range associated with a local efficiency maximum, and by including in each of these sets of tests a range of data points which include a moderate angle as a median, trends relating to the relative significance of power loss effects and collector angle effects are made clearer. Table 5 summarizes the data points of interest for this testing phase and the associated angle and power parameter values.

Table 5: Variable Angle – Variable Power Test Parameters

Test Index	**Reference Angle, α (Degrees)**	**Angular Deviation, $\Delta\theta$ (Degrees)**	**Collector Angle, θ (Degrees)**	**Input Power, $P_{\Delta\theta}$ (Applied V_{RMS})**	**Other Parameters $h, K, T_{ambient}$**
Phase 3: VHAVP					
[1.1]	14°	0°	14°	50.0 V	Base Case
3.1	14°	+ 6°	20°	49.8 V	Base Case
3.2	14°	+ 12°	26°	49.5 V	Base Case
3.3	14°	+ 18°	32°	48.8 V	Base Case
3.4	14°	+ 24°	38°	47.8 V	Base Case
3.5	14°	+ 30°	44°	46.5 V	Base Case
3.6	14°	+ 36°	50°	45.0 V	Base Case
Phase 4: VLAVP					
4.1	62°	- 6°	56°	49.8 V	Base Case
4.2	62°	- 12°	50°	49.5 V	Base Case
4.3	62°	- 18°	44°	48.8 V	Base Case
4.4	62°	- 24°	38°	47.8 V	Base Case
4.5	62°	- 30°	32°	46.5 V	Base Case

4.6	62°	- 36°	26°	45.0 V	Base Case

3.2.3 Other Research

Research into the three remaining parameters of interest is planned primarily to replicate and confirm seemingly conclusive results from other teams and institutions which have produced consistent and overt trends in even small data samples. Of these three parameters, research into the effect of variable ambient temperature is of the highest priority because of its relevance in the analysis of other published studies in which ambient temperature is often not carefully controlled or considered a parameter of significance.

3.2.3.1 Variable Hot Leg Height Method

Variable hot leg height testing is represented in this text as VH. The height of the hot leg into the tank of the thermosiphon has been shown to affect the efficiency of the system. In order to quantify this effect, three core data points will be collected from nine inches to 27 inches at six-inch intervals with the exception of the 21-inch height, which is the base case and therefore does not require a novel test. This set of points represents the largest possible hot leg height range using the current facility and the smallest step size which has proven to produce significant result deviations in previous research. This testing phase is designed to determine general trends in the relationship between hot leg height and the efficiency of the system. Table 6 below helps visualize the heights corresponding to the various tests.

Table 6: Variable Hot Leg Height Test Parameters

Test Index	Hot Leg Height, h (inches)	Other Parameters θ, P, $T_{ambient}$, K
Phase 5: VH		
5.1	9	Base Case
5.2	15	Base Case
[Base Case]	21	Base Case
5.3	27	Base Case

3.2.3.2 Variable Ambient Temperature Method

Variable ambient temperature is represented in this text as VT. An enclosure was previously constructed around the thermosiphon to adjust and maintain the ambient temperature in the system's immediate environment. It has been observed in the literature that temperature changes in the ambient have a potentially very significant effect on the system. Because the insulated enclosure is heated efficiently and with precision but not capable or precision cooling, in order to study the lowest ambient temperature, testing took place in the winter. This allows conduction of a wide range of tests to gather information about how the ambient temperature affects the system.

For the 2020-21 academic year, the team gathered information about ambient temperature and six data points will be analyzed. The range begins at 20 °C and terminate at 35 °C. Between 20 °C and 35 °C are six data points, only five of which are novel tests, that differ by approximately 2.5° C. The proposed 20 °C lower limit is a conservative one because testing at lower temperatures is desirable to increase the scope of the overall data range. For this reason, testing at the lowest possible ambient temperature is performed based on weather conditions. The step size between data points in this testing phase is also flexible. Controlling ambient

temperature step sizes as small as 2.5° C traditionally proves difficult and therefore these step sizes serve as guidelines rather than hard-set values. In this set of tests, the number and overall range of points is of greater importance than the differences between individual test iterations. Gathering this information helps determine how the ambient temperature surrounding the thermosiphon affects the efficiency of the system. Table 7 below is to help visualize what test corresponds with what general temperature change based on conservative temperature limits and step sizes.

Table 7: Variable Ambient Temperature Test Parameters

Test Index	Ambient Temperature, $T_{ambient}$ (°C)	Other Parameters θ, P, h, K
Phase 6: VT		
6.1	20	Base Case
6.2	22.5	Base Case
[Base Case]	25	Base Case
6.3	27.5	Base Case
6.4	30	Base Case
6.5	32.5	Base Case
6.6	35	Base Case

3.2.3.3 Variable Hydraulic Resistance Method

The variable hydraulic resistance phase of testing is represented in this text as VK, in which K is used to both because it is the conventional symbolic representation of hydraulic resistance and because it is differentiated from variable hot leg height testing VH. The interface of the actuated ball valve attached to the hot leg of the tank allows for the ability to precisely control percent closure, and thus affect the efficiency of the thermosiphon very strategically. In order to map this information, six data points were planned from 10% closure to 70% closure at

12% intervals. There is not a need to test at 0% closure because base case tests will already be conducted at this level. Doing this was expected to show that the closure of the ball valve decreases the efficiency of the system, which is an extremely prominent trend in the literature and previous experiments. Below is a table to help visualize how the parameter settings associated with this data set.

Table 8: Variable Hydraulic Resistance Test Parameters

Test Index	Hydraulic Resistance, K (% Valve Closure)	Other Parameters θ, P, $T_{ambient}$, h
Phase 7: VK		
[Base Case]	0	Base Case
7.1	10	Base Case
7.2	22	Base Case
7.3	34	Base Case
7.4	46	Base Case
7.5	58	Base Case
7.6	70	Base Case

3.3 Analytical Approach

Upon completion of a research test, the sets of collected discreet VARIAC voltage, collector inlet temperature, collector exit temperature, and flow rate data points are used to calculate a set of instantaneous collector efficiencies η_i by application to equation 5, which represents the ratio between the rate of energy input to the collector to the rate of energy absorbed by the fluid as it passes through the collector. In this equation, the rate of energy absorbed by the fluid is quantified as the product of fluid density ρ (kg/m^3), instantaneous volumetric flow rate $\forall$ (m^3/s), fluid specific heat C (kJ/kgK), and collector inlet and exit temperatures T_{inlet} and T_{exit} (°C). The power input to the collector, which in application would

be solar energy, is in this case a function of the RMS VARIAC voltage V_{RMS} (V) input to heat tape of resistance R (Ω), as previously formalized in equation 2.

$$\eta_i = \frac{\rho \forall C(T_{exit} - T_{inlet})}{\frac{V_{RMS}{}^2}{R}} \quad (5)$$

Determination of the average collector efficiency η for a designated period of steady-state flow would ideally involve calculation of the area under the collector efficiency-time function and division of this value by the study period duration, as indicated by times $t_{initial}$ and t_{final} (s). Equation 6 represents this relationship for a hypothetical continuous efficiency function $\eta(t)$.

$$\eta_{avg} = \frac{1}{t_{final} - t_{initial}} > \int_{t_{initial}}^{t_{final}} \eta(t)\, dt \quad (6)$$

Because the relevant data for this calculation is collected in discreet points, a continuous integral is impossible, and the approximation represented by equation 7 is instead used. This equation represents a relationship which is virtually identical to the previous equation with one exception: the area under the N efficiency-time data points in the period of interest is approximated using the trapezoidal rule. Because the region of interest for an arbitrary test is the steady-state period, which implies a relatively constant efficiency, this approximation is found to be sufficiently accurate and consistent for evaluating system trends based on varied parameters.

$$\eta_{avg} \approx \frac{1}{t_{final} - t_{initial}} \sum_{j=1}^{N-1} \frac{\eta_{j+1} - \eta_j}{2} (t_{j+1} - t_j) \quad (7)$$

The instantaneous efficiency determination and subsequent numerical averaging processes described above are performed by a MATLAB program that uses collected transducer data imported from LabVIEW. This program is also used to plot system data and to perform uncertainty analysis for each test parameter in accordance with ASME PTC 19.1-2013. This

script in its entirely is provided for reference in appendix B. The relevant efficiency result from each test is then recorded in spreadsheets for comparison with other relevant test results in the evaluation of trends in system response.

4 Technical Results

4.1 Facility Operations

As a result of the extended period of base case testing and the unexpectedly anomalous system performance which defined research for many months, many instrumentation and facility modifications are actively being implemented at the time of this writing and are scheduled for completion in the coming days to align with project deadlines. The following sections serve as either detailed updates on the status of planned modifications or as reports of the data and performance changes associated with instrumentation tasks and completed modification work.

4.1.1 Instrumentation Modifications

4.1.1.1 General Data Collection Status

The new USB-6218 I/O device has been assembled, installed, and tested for software compatibility. Thus far, it has been confirmed that, in addition to wiring of previous instruments, the device can accurately measure voltage from a power supply using the previously described apparatus. Once the necessary modifications to the LabVIEW program have been completed, the PCI-6221 I/O device and CB-68LP connector block will be returned to the university.

4.1.1.2 Power Control Status

Because installation of these components is relatively simple and to be implemented only after all other collector modifications are completed, the only tasks associated with this upgrade are the purchasing of replacing components. In response to the failure of two VARIAC in the

middle of research testing, two of the three replacement VARIACs were ordered and immediately installed in the late fall. The remaining pieces of instrumentation, the third VARIAC and the three lengths of heat tape, are currently being acquired for installation as soon as all other collector frame modifications are completed.

4.1.1.3 Power Measurement Status

The voltage measurement system was calibrated through linear regressions showing the relationship between the input and output voltages in the system. Before the linear regressions could be completed, the data points needed to be found for each of the three voltage measurement circuits. A summary of these data points along with their associated uncertainties is shown in appendix C. The uncertainties for the input voltages were found in the user's manual for the multimeter [12]. Sample calculations for the uncertainty are shown in appendix D. The uncertainties for the DAQ card were found in its specifications [13]. Figure 25 is a plot of the input voltages with respect to the output voltages of the first of three voltage measurement circuits. Error bars are included in order to show the uncertainties associated with each of the trials.

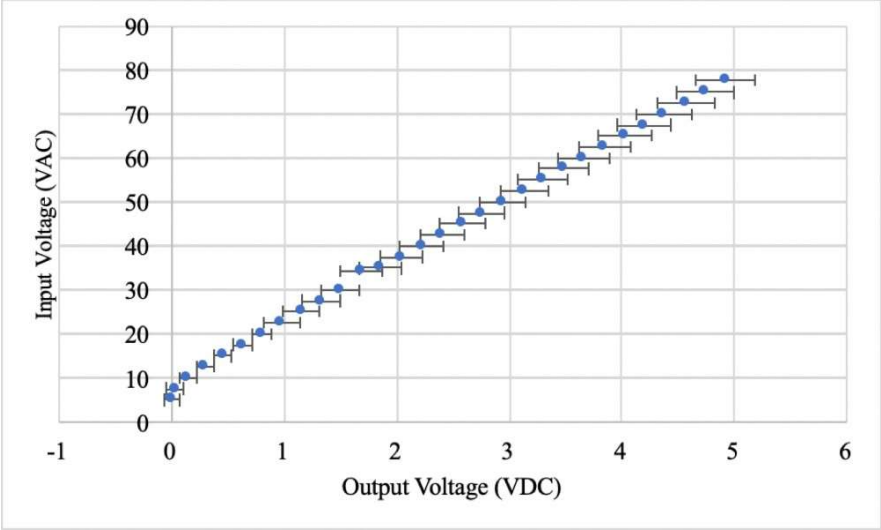

Figure 25: Voltage Measurement Circuit 1 Results

Figure 26 is a plot of the input voltages with respect to the output voltages of the second voltage measurement circuit. Error bars are also included in this case to similarly show the uncertainties associated with each of the trials.

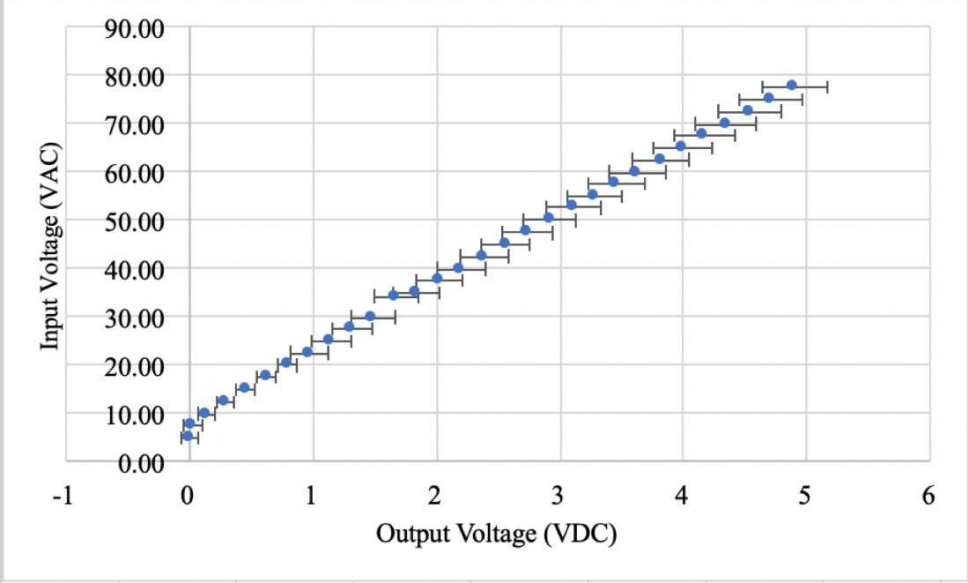

Figure 26: Voltage Measurement Circuit 2 Results

Figure 27 is a plot of the input voltages with respect to the output voltages of the third and final voltage measurement circuit. Error bars are again included.

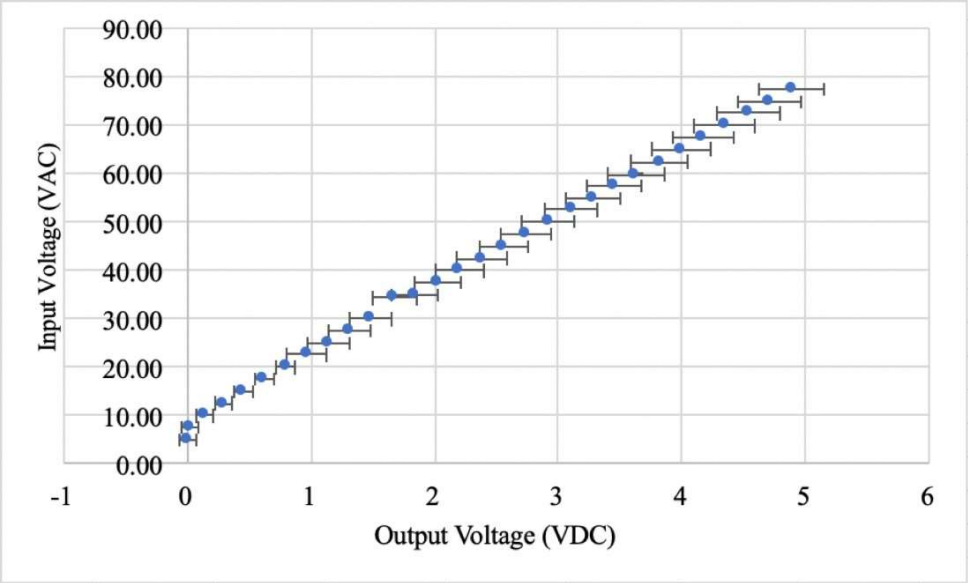

Figure 27: Voltage Measurement Circuit 3 Results

The data points shown on the plots in figures 25, 26, and 27 were then used to complete regression analyses for each of the different voltage circuits. The results of the linear regressions are shown in appendix E. Figure 28 shows the results of the linear regression for the first voltage measurement device as a plot of a theoretical line representing the input voltage for any given output voltage. Two dashed lines are also included on this plot to show the uncertainty at any point along the line.

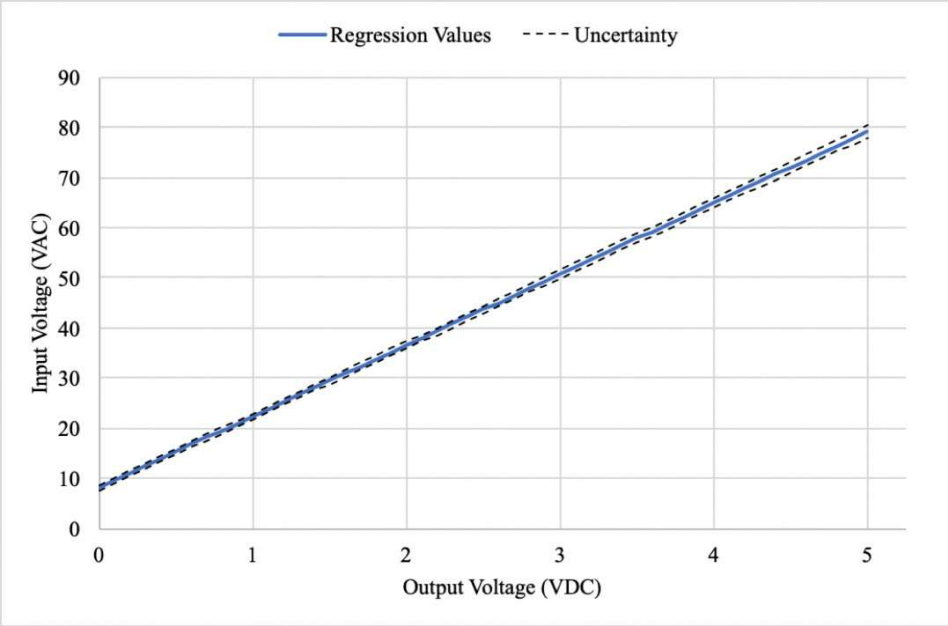

Figure 28: Voltage Measurement Circuit 1 Regression Results

The resulting linear regression equation for the first circuit is shown as equation 8. This is the equation used to develop the line shown in the previous figure and has the uncertainty also shown in that graph.

$$V_{RMS} = 14.1842V_{output} + 8.1983 \quad (8)$$

Figure 25 shows the similar results of the linear regression for the second voltage measurement circuit as a plot of a theoretical line representing the input voltage for any given

output voltage. Two dashed lines are also included on this plot to show the uncertainty at any point along the line.

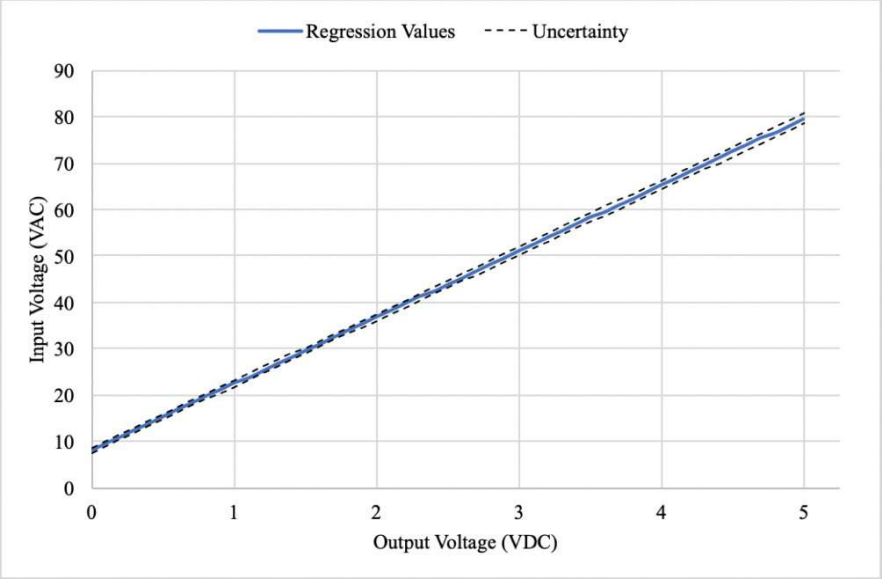

Figure 25: Voltage Measurement Circuit 2 Regression Analysis

The linear regression equation for this second circuit is shown as equation 9. As in the previous case, this is the equation used to develop the line shown in the previous figure and has the uncertainty also shown in that graph.

$$V_{RMS} = 14.2747V_{output} + 8.2445 \quad \textbf{(9)}$$

Figure 26 shows the results of the linear regression for the third and final voltage measurement circuit as a plot of a theoretical line representing the input voltage for any given output voltage. Two dashed lines are also included on this plot to show the uncertainty at any point along the line.

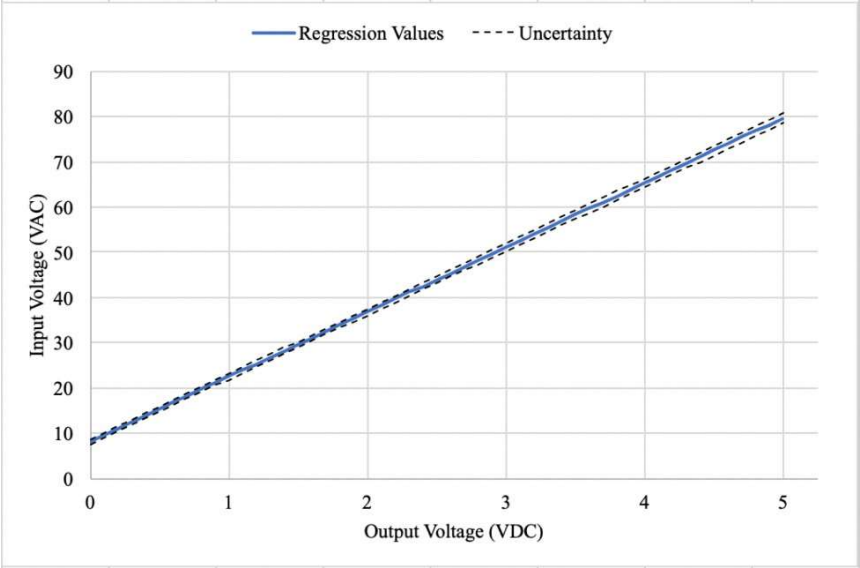

Figure 26: Voltage Measurement Circuit 3 Regression Results

The linear regression equation for this final circuit is shown as equation 10. This is the equation used to develop the line shown in the previous figure and has the uncertainty also shown in that graph.

$$V_{RMS} = 14.2752V_{output} + 8.2555 \quad \textbf{(10)}$$

Each of the linear regression equations are the calibration equations which will be used in the LabVIEW VI to produce an accurate voltage reading for each of the VARIACs attached to the thermosiphon apparatus, producing discrete and precise power input data points associated with each test.

4.1.1.4 Hydraulic Resistance Control Status

Following the procedure outlined in the technical approach section, the following data points were collected:

Table 9: Valve calibration data points

Valve Closure [%]	Average Device Output Signal [V]
0	2.01531669

100	8.76764879

Using these points, equation 11 was developed using linear regression in Excel that relates the K-valve's output signal to percent valve closure.

$$\% \text{ Valve Closure} = 14.8096981189654V_{out} - 29.8462317930127 \quad (11)$$

This equation is valid for the range of V_{out} values listed in the above table. The equation will be copied into the K-valve function block once the existing LabVIEW block diagram is adapted for use with the new I/O device.

4.1.1.5 Flow Measurement Status

For most of the year, the team has relied on the INTEK Rheotherm Model 210 with ½ inch inch line sizes for precise flow rate measurement (henceforth referred to as the ½ inch model). In mid-February, the ½ inch model began giving erroneous readings. Before this time, it would relay steady-state flow rates around 0.07 gal./min. during base case tests. After this time, the flowmeter began giving steady-state flow rates upwards of 0.08 gal./min. on base case tests. This change in flow measurement increased the base case collector efficiencies to around 85%, whereas before the change, base case efficiencies were closer to 75%. This change in efficiency calculations meant that our subsequent tests would no longer be comparable to previous tests performed in the fall semester, as has been detailed in previous sections.

By mid-March, the decision was made to remove the ½ inch model and replace it with the smaller Model 210 with ¼ inch line sizes that was used by a previous team. The hope was that it would allow the team to complete the remainder of the planned research after failed attempts to resolve the issue. The ½ inch model was shipped to INTEK for assessment and recalibration. The necessary pipe adapters were purchased to integrate the ¼ inch model into the existing tubing, and it was successfully installed. The ¼ inch model used the same excitation

voltage and the same data connection cable as the ½ inch model and featured a live flow rate reading on the integrated LCD screen. After adjusting the calibration function in LabVIEW, the device appeared to give accurate flow rate measurements when compared to the LCD screen reading. Results of this swap in flow meters looked promising after running a base case test. Efficiency levels were back to those of previous tests. The steady-state flow rate was about half of what the previous flow meter measured, but the increased temperature difference across the collector presumably made up for it in the efficiency calculation.

Upon resuming variable hot leg research testing, the temperatures in the collector increased enough to cause the water inside to very briefly boil. The team deduced that the reduced cross-sectional area inside the ¼ inch model caused a spike in hydraulic resistance of the fluid circuit, thereby causing the reduction of flow rate. As a result, more heat was able to be transferred into the water as it traversed the pipe network inside the collector. At this point, the remainder of scheduled testing was cancelled in deference to the original flow measurement apparatus, which would shortly be calibrated and returned for installation on the modified system.

On April 12th, a technician at INTEK noted that there was a rust-like powdery coating on the inside of the pipes of the flow meter which was likely the source of the erroneous readings. When the system was drained and disassembled on the 14th, it was discovered that the drainage valve previously on the cold leg had severely rusted on the inside. This component was identified as the culprit of the rust coating and the resulting flow meter errors.

Currently, the team is awaiting the return of the ½ inch model from the INTEK technicians, and it is anticipated that the flow meter will be returned before April 23rd. When it

arrives, its installation will be a top priority as it is crucial to conduct verification tests before completion of the project.

4.1.1.6 Temperature Measurement Status

The thermistors were removed from the system and had their ambient temperature resistances measured in order to experimentally determine the thermistor model. This was done by comparing the measured resistance to the expected resistance shown in table 2. Once this was completed, resistance measurements were recorded for all thermistors at all planned temperatures. The recorded resistances were then put through the Steinhart equation using the coefficients specific to each thermistor model in order to calculate measured temperature. These temperature values are shown below in table 10. Thermistor three (Hot Leg Top) failed earlier in the year and a replacement was not found. Because of this, only thermistors one, two, four, five, and six were properly calibrated.

Table 10: Measured Thermistor Temperatures [°C]

Reference Temperature	Thermistor 1 (Collector In)	Thermistor 2 (Collector Out)	Thermistor 4 (Tank Top)	Thermistor 5 (Tank Middle)	Thermistor 6 (Tank Bottom)
24.25	24.55707863	24.20772465	24.81913016	25.67910456	24.84477864
30.0	29.86162279	29.83269052	30.05027118	30.08918672	30.17980835
40.0	39.35885576	39.5868041	39.84585518	39.80474148	40.00718781
50.0	49.69414713	49.60780285	49.71805894	49.7501044	49.80682535
60.0	59.28121456	59.1298592	59.38404584	59.48091888	59.65109756
70.0	69.33428312	68.91391993	69.47214285	69.47214285	69.66261239

Figures 27 through 31 below show the plot between measured temperature vs reference temperature for thermistors calibrated. Uncertainty bars are shown and the full data analysis can be found in appendix F.

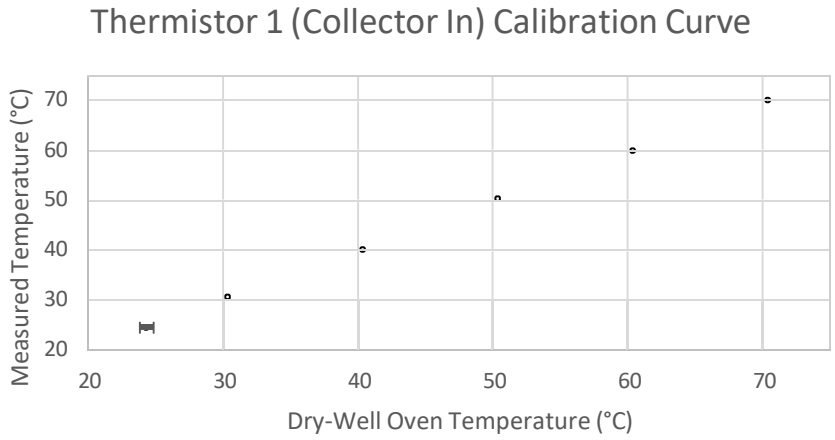

Figure 27: Thermistor 1 (Collector In) Calibration Curve

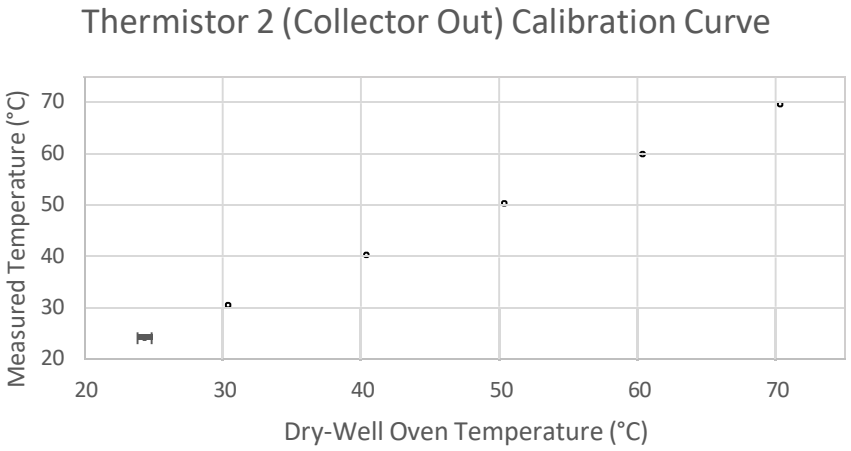

Figure 28: Thermistor 2 (Collector Out) Calibration Curve

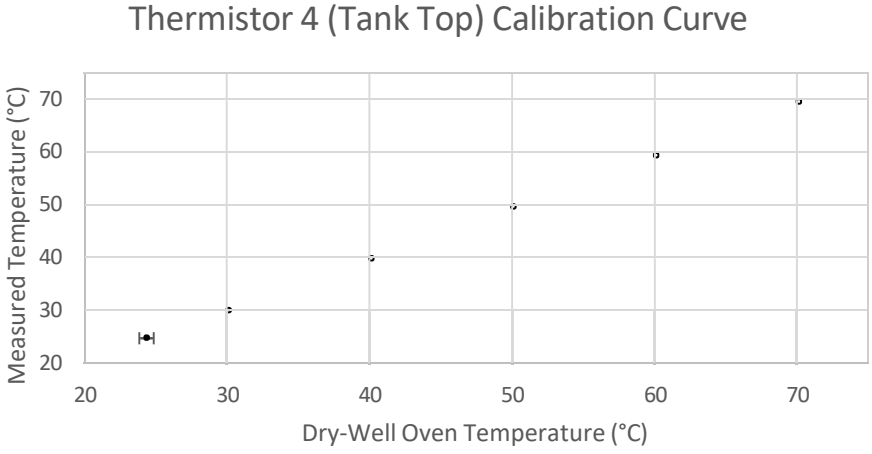

Figure 29: Thermistor 4 (Tank Top) Calibration Curve

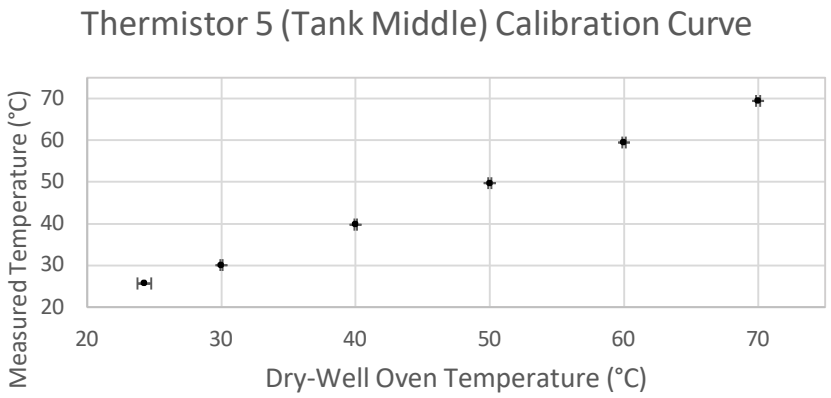

Figure 30: Thermistor 5 (Tank Middle) Calibration Curve

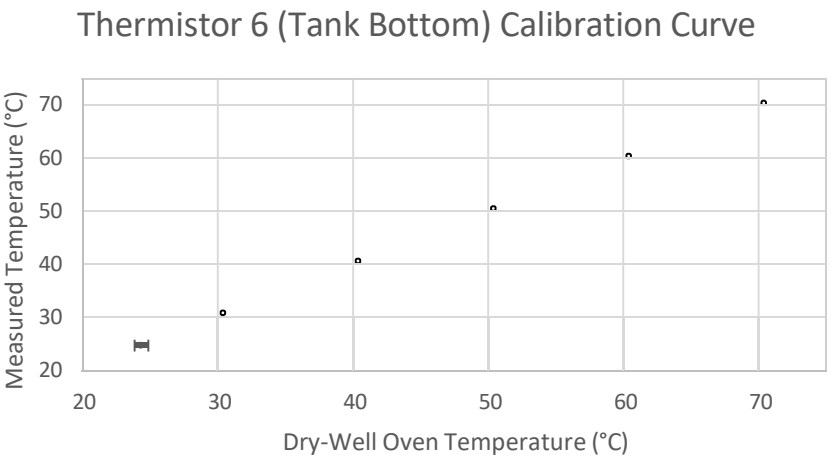

Figure 31: Thermistor 6 (Tank Bottom) Calibration Curve

Linear regression analyses were performed on each of the curves in figures 27 through 31. These regressions which were used to form the calibration equations are shown in appendix G. Equations 12 through 16 show the resulting calibration equations.

$$T_1 = 1.01852151659803 * T_{1,meas} - 0.479444934477073 \quad (12)$$

$$T_2 = 1.02276576564882 * T_{2,meas} - 0.534111809266257 \quad (13)$$

$$T_4 = 1.02293381633847 * T_{4,meas} - 0.884512575333467 \quad (14)$$

$$T_5 = 1.03416739392677 * T_{5,meas} - 1.56625030426223 \quad (15)$$

$$T_6 = 1.01939996222434 * T_{6,meas} - 0.870142423967955 \quad (16)$$

The calibration techniques in this section were performed on the Omega thermistors that were in use throughout this year's research. New thermistors, manufactured by EI Sensor Technologies, were purchased, shipped, and arrived shortly after the old thermistors had been recalibrated. The team plans to apply these exact same calibration techniques to the new thermistors before installing them on the system after all facility modifications are complete.

4.1.2 Component Modifications

4.1.2.1 Collector Modifications Status

Because the tubing and other instruments are most easily installed with the collector in its modified state, installation of the relatively straightforward collector frame is being implemented as soon as possible. Dimensions and material requirements have been determined for construction of the support, and all other components, such as the winch, pulleys, cable, drill, and other miscellaneous hardware pieces have been purchased. Because the current collector frame is functional and because the proposed new one can be installed quickly and simply, construction and implementation will commence upon completion of some other more complex modification work and before the final project deadline.

4.1.2.2 Reservoir Modifications Status

At the time of this report, the final design has been determined for the reservoir lift as has been previously described. Along with this, all the materials necessary to complete the fabrication and assembly of this section have also been chosen. A budget for these materials has been developed and approved for purchases to be made. The modifications are projected to take several days of fabrication before the final assembly can be introduced into the system for integration with other components. Once the parts outlined in the budget have arrived, the final

elements of the fabrication process will be completed and the system will be tested for effectiveness before being finally attached to the current frame of the thermosiphon mechanism.

After the lift is installed, the insulation modification will be completed and attached to the tank to provide a better method of removal for cooling the system than has previously been in use. These modifications are projected to take the least time out of those for the reservoir section and will interfere the least with the completion of the other sections, which is why they will be completed towards the end of the scheduled modifications time.

4.1.2.3 Tubing Modifications Status

As of the time of submission of this report, both the hot and cold legs have been fully assembled and fitted with insulation. Holes have been created adjacent to the inlet and outlet of the collector and at the inlet of the reservoir in preparation for the insertion of thermistors. The K-valve has been successfully fitted on the vinyl tubing to be placed between the active cooling system and collector inlet.

The assembled tubing is currently not connected to the reservoir or collector, as these components are being actively modified. After the new thermistors are calibrated and wired into the I/O device, they will be inserted into the holes in the tubing and sealed with non-permanent rubber spray sealant. Once the Rheotherm is returned from calibration at INTEK, the proper length of the parallel portion of the cold leg CPVC will be determined, and the cold leg will be fully assembled and attached.

4.1.2.4 Enclosure Modifications Status

As intended, the panel on the back of the enclosure was removed, sectioned, and reattached such that the folding wall design was implemented. This modification was crucial as the pump, tank, and collector can now be more readily accessed with a lesser risk to system components. This folding door will also assist greatly in cooling the system when desired, as it

removes insulation and increases ventilation. The exhaust fan for cooling the system was also installed in line with the initial design, and this is shown in figure 32.

Figure 32: Fan and exhaust opening

One new modification, added later in the design process, is a series of 3D-printed clamps that hold the hot-leg door to the enclosure closed more securely. Siemens NX 11.0 models of these clasps are shown in figure 33. Prior to this modification, Velcro strips held in place by duct tape were used to seal the door. Now, the flat clamp, shown in the figure, takes the place of the duct tape in securing the Velcro in place. The larger clamp shown is connected to carabiners and attached to the enclosure door to form a loop to which the Velcro strip attaches. Both are shown in figure 34. Excluding small adjustments to ease the installation of other subsection modifications, further enclosure modifications are unlikely.

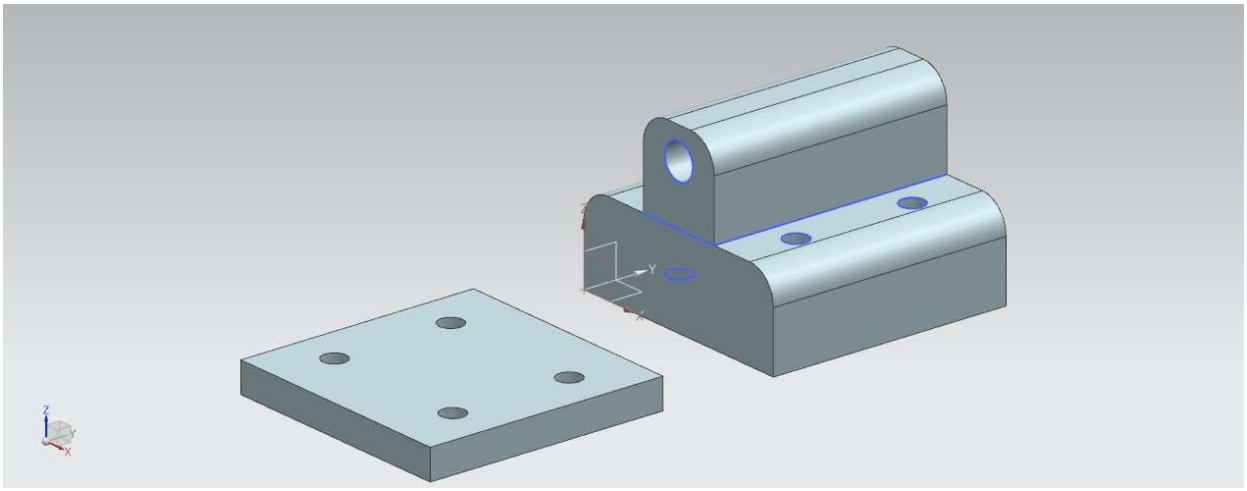

Figure 33: Model of clamping device

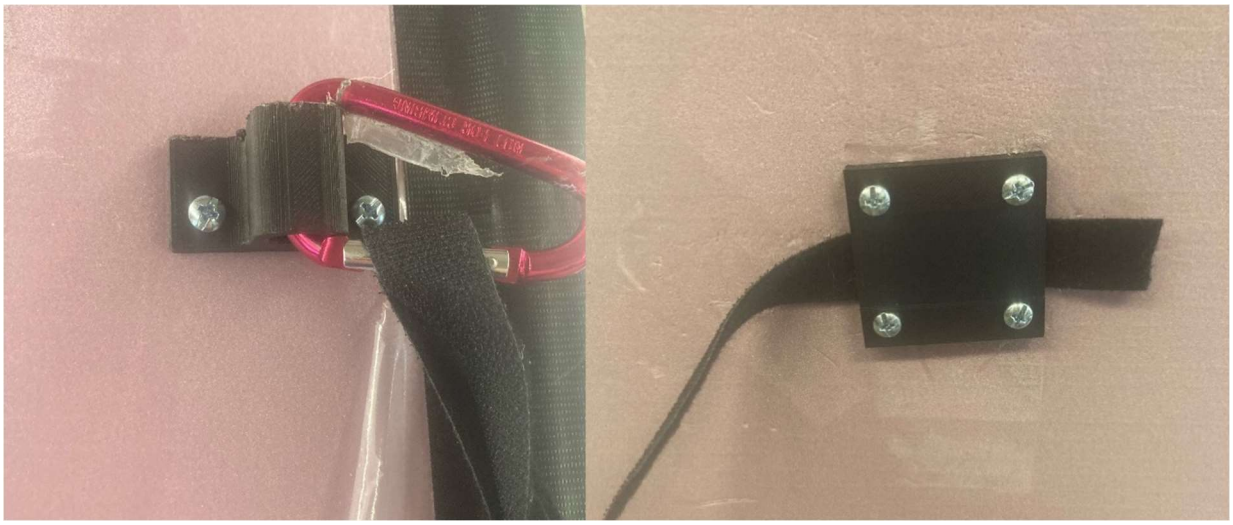

Figure 34: Clamps on enclosure and door

4.1.2.5 Active Cooling System Status

A ¾ inch inner diameter by ten foot CPVC tubing was cut into smaller sections following the 3D model and drawing prepared during the design process. The CPVC tubing sections, the CPVC elbow connectors, and the CPVC valve-connectors were assembled to form a circuit using solvent cement solution. The use of CPVC tubing resulted in significantly cheaper and easily modifiable circuit. Hence, the solvent cement was used to connect the tubing sections

instead of the traditional method of creating threads and then screwing. Furthermore, the use of cement also reduces the probability of air leakage from the tubing.

For the heat exchanger, a frame was fabricated using two three inch by twenty two inch wood studs and two three inch by twenty nine inch wood studs as seen in figure 35. Two holes were created on the side panel of the frame to accommodate the heat exchanger's inlet and outlet. The pipe network was connected to the heat exchanger using two high temperatures rated rubber tubing so that the heat exchanger could be rocked back and forth to remove trapped air molecules. In addition to the air vent on the heat exchanger, an air separator was installed in the pipe network to remove the remaining air bubbles and microbubbles present in the system as well as mitigate their development in future research. To expedite the convection process in the heat exchanger, the team will install the fan in the coming days.

Figure 35: Wooden frame built for the Heat Exchanger

As soon as the tubing section, the collector section, and the tank section is complete, the prepared cooling system will be connected to the system at the cold leg, across the flow meter. The cooling system will be separated by two valves so that it can be isolated when needed, as previously discussed in relation to its interface with the cold leg.

4.2 Experimental Results

The research performed is summarized in subsequent sections by testing phase and system parameter. A complete index of parameters settings, analysis ranges, and calculated efficiency for all tests that have been performed and reviewed is available in appendix H, and output instantaneous parameter data for analysis of a representative base case test is in appendix I.

4.2.1 Base Case Results

Before conducting research testing, the consistency of system performance was intended to be confirmed by a series of tests in which all parameters were held at base case values. Due to unforeseen complications in system performance and instrument failures which are subsequently described in detail, base case testing is best discussed in three distinct stages: a short initial set of tests which preceded all research testing and took place in early September, a slightly larger set of tests which interrupted research testing and began in late September before concluding in early October, and an extended period of tests which again interrupted research testing and continued from the end of January until the cessation of research testing in late March. A summary of all base case efficiency results is shown in figure 36 below, with the three distinct stages of testing clearly identified.

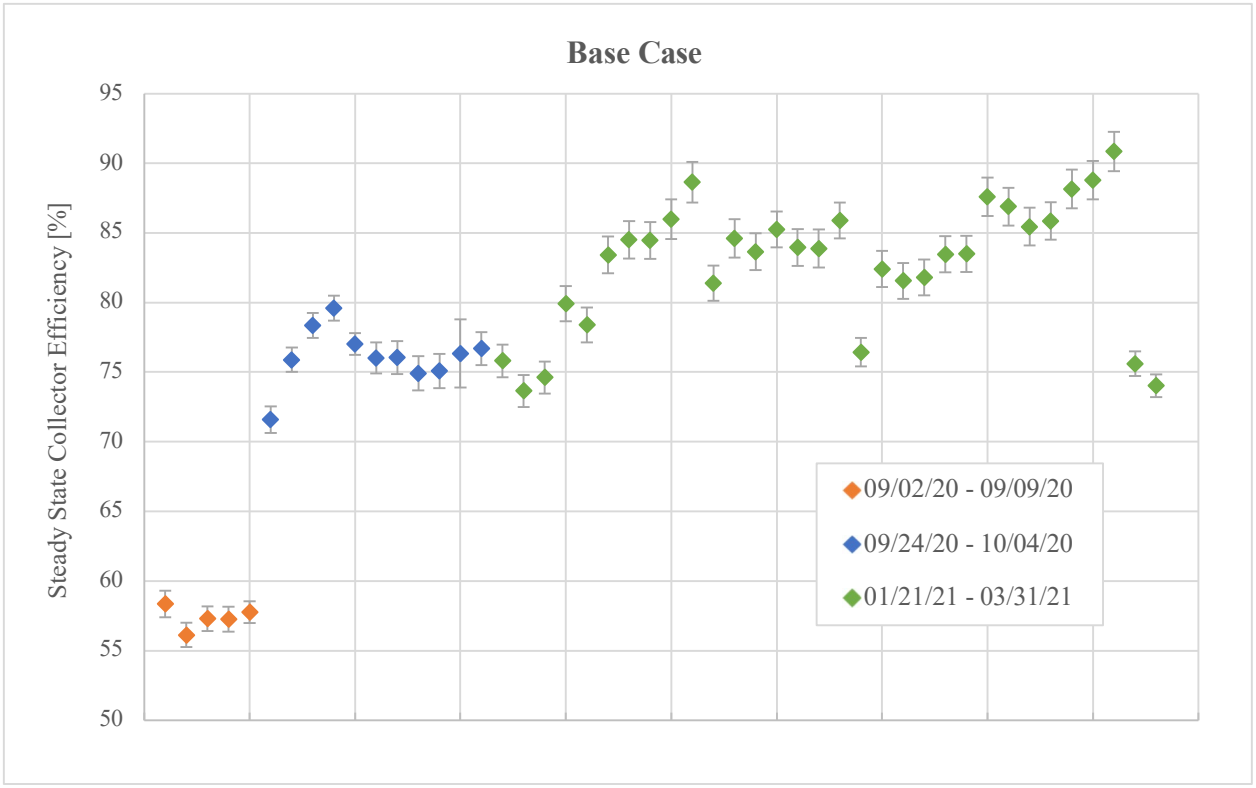

Figure 36: Base Case Efficiency Results, University of Evansville 2020-'21

Analysis of the first stage of base case tests performed between September 2 and September 9 produced average collector efficiencies which agreed completely with each other within their calculated uncertainties and indicated an even greater performance consistency than the base case testing performed by the 2019-2020 research team. The mean efficiency of this subset of tests was calculated to be 57.4 ± 0.4 %, a value slightly lower than base case testing performed under sufficiently identical conditions during the most recent previous year (in which system efficiencies varied in a range between approximately 62.5% and 70%). This inconsistency between previous and recent results invalidates direct comparison of current research data with data collected in the past, but this misalignment is anticipated. Research conducted at the university in recent years has not traditionally produced results which align precisely with tests conducted by other teams, making consistency of current results a higher priority than agreement with past values. Upon completion of five subsequent, consistent base

case tests, the reliability of system performance was considered proven and research testing commenced despite the disagreement with prior data.

A second set of base case tests was conducted from September 23 to October 4 in response to a dramatic change in system performance which occurred while conducting variable angle – constant high power testing. After the efficiency of the collector was observed to rise significantly and inexplicably during this set of research tests, the previously validated consistency of the system was in question and base case testing was reestablished to confirm the continued validity of results and identify a potential new baseline for system performance. This new baseline is clearly illustrated by the data in figure 36, in which the average efficiency of the collector is shown to rise until September 26, at which point it again levels off into a steady and self-consistent series of results which have a mean of 75.8 ± 0.7 %.

Because the stability of the reestablished system consistency was dubious after the unexpected change in results during research testing, the collector, tank, and tubing system components were repeatedly and vigorously adjusted to extreme angles, heights, and geometries in between the tests which make up the second stage of base case testing. The goal of these adjustments was to confirm that, even when exposed to indelicate testing procedures, extreme environmental conditions, or accidental impulses, the new base case result would remain consistent. As the data makes clear, this was proven to be the case, and so research testing commenced after this period.

The third and final stage of base case tests, which followed several months of successful research, was similarly initiated by a sudden and inexplicable increase in system efficiency results and the seeming loss of all correlation between calculated efficiency and system parameter settings. As in the previous case, research testing was immediately abandoned so that

the source of the inconsistency could be rectified, and stability reestablished. Despite exhaustive efforts to find the reason that the efficiency results were rapidly increasing in magnitude and randomness, the root of the issue was conclusively identified only after removal and shipping of the flowmeter, the details of which were discussed in previous sections along with their relevance to the anomalous data. Ultimately, the trouble-shooting efforts to resolve this problem which occurred over several months included, but were not limited to: confirmation of all electrical connections, confirmation of data collection software settings, removal of all air from system components, sealing of all tubing and piping interfaces, confirmation of fluid levels in all system components, confirmation of the accuracy of input power control and measurement techniques, and confirmation of a lack of obstruction in all tubing and piping.

In addition to experimental efforts to rectify the efficiency anomalies during both the second and third stage of base case testing, specific test parameter data sets were also investigated for further insights. Instantaneous flow rate data from three representative base case tests, one from each base case stage, were analyzed and are represented in figures 37, 38, and 39.

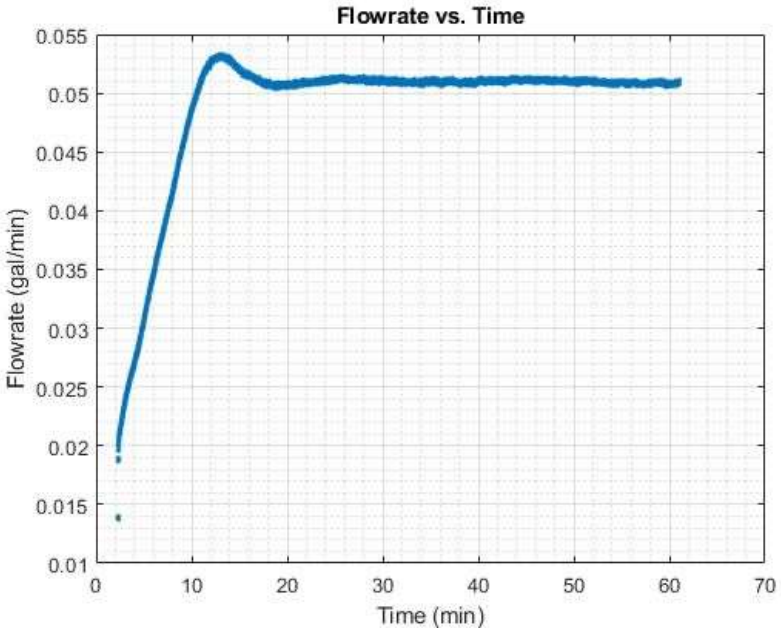

Figure 37: System Flow Data, University of Evansville 09/07/20

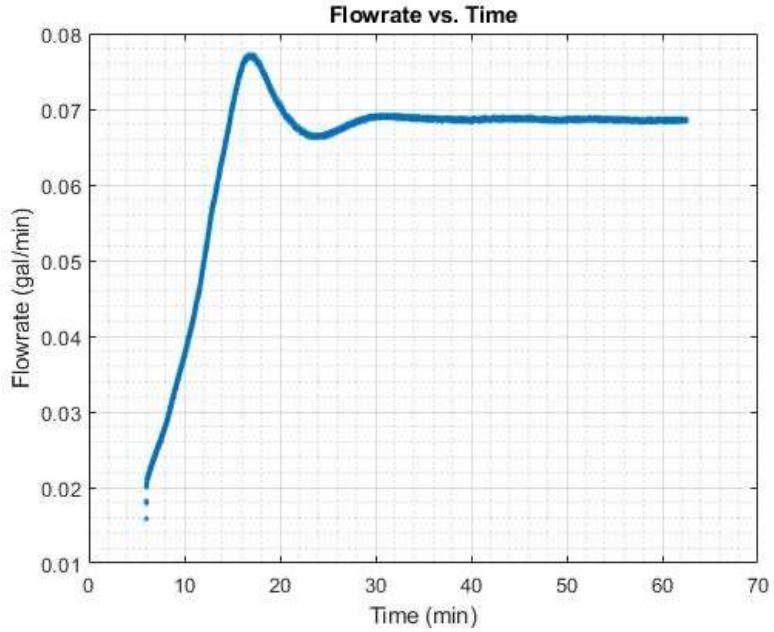

Figure 38: System Flow Data, University of Evansville 09/30/20

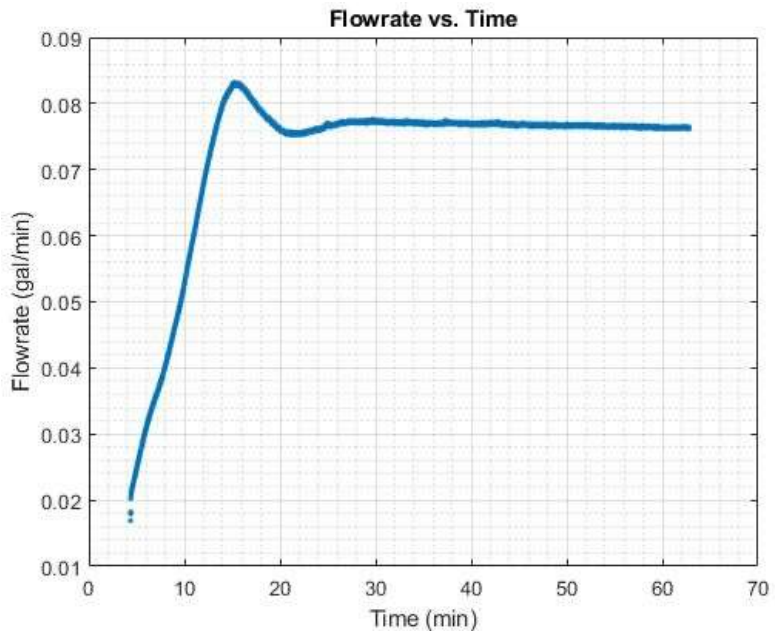

Figure 39: System Flow Data, University of Evansville 02/21/21

Contrasting the flow responses gives further insight into the nature of the efficiency change: the steady state flow rate for tests which took place in the second stage of tests is found to be significantly higher than the steady state flow rate recorded in previous tests. Similarly, the steady state flow rate from the third base case stage was found to generally increase but also vary in coordination with the efficiency changes. These changes in flow rate would lead to an associated increase in efficiency in accordance with equation 5. After the elimination of all other notable areas of risk and significant data analysis, this flow rate trend lead the team to the conclusion that the calibration of the flowmeter itself was the most likely source of sporadic efficiency changes and that the most effective solution was to cease research testing and proceed with the scheduled calibration of the instrument by the manufacturer. Ultimately this was proven correct when rusting inside a component upstream of the flowmeter was found to have impacted its readings.

Ultimately, a second set of base case tests will be performed after all system component and instrument modifications are completed in the coming days. Based on the seemingly unavoidable difference between base case efficiencies from tests conducted at significantly different times, the mean efficiency of this second set of tests is not expected to agree with either of the two mean efficiencies established by the completed testing, only to confirm a regained consistency of results after replacement of the flowmeter and upgrading of the system itself.

4.2.2 Power – Angle Research

4.2.2.1 Variable Angle – Constant Power Results

For the same reasons that base case testing was effectively segmented into three different performance levels, variable angle – constant high power testing is best interpreted as two distinct sets of results which include a sudden change in baseline system performance that interrupts them. The results of the first set of variable angle – constant high power tests, which took place from September 14 to September 20, are shown in figure 40 below and are annotated to distinguish between the first period of tests in which base case performance is stable and the second which are anomalous.

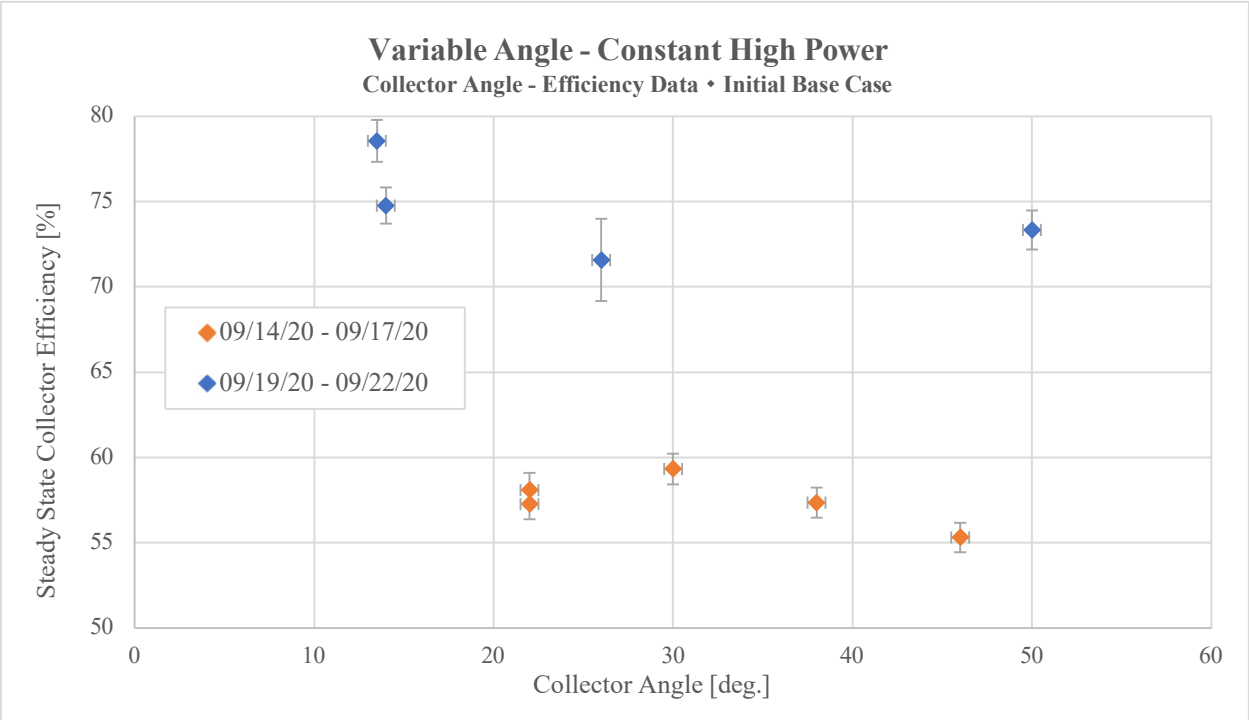

Figure 40: VACHP Initial Efficiency Results, University of Evansville 2020-'21

The average collector efficiencies for the four tests performed from September 14 to September 17 align with expected trends from years past and predictions based on previously described theories: a maximum efficiency is found to exist at a collector angle of approximately 30° under constant power conditions, with efficiency decreasing for angles which deviate from this central value. Admittedly, relatively few data points are available to determine general system behavior from this initial set of tests due to the sudden increase in calculated collector efficiency first noted in the test performed on September 19. The team's analysis of this anomaly is detailed in a previous section, and so will not be discussed further in relation to variable angle - constant power results.

After reestablishing consistency at the conclusion of the second stage of base case tests, a second set of variable angle – constant high power tests were conducted, the results of which are plotted in figure 41 below.

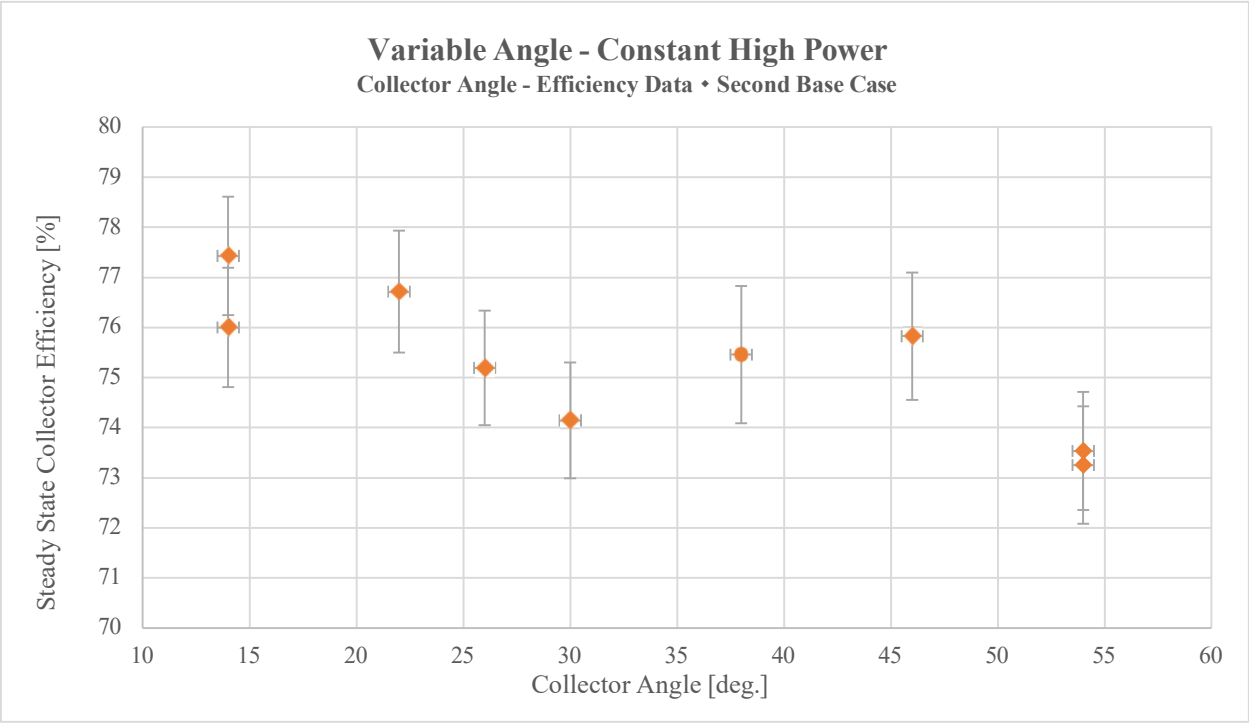

Figure 41: VACHP Second Efficiency Results, University of Evansville 2020-'21

This set of tests is notable for a trend which has been observed by some other institutions but has not been apparent in research testing at the University of Evansville in recent years: a general increase in efficiency associated with a decrease in collector angle, even for very low angles approaching 10°. In previous studies, this trend was observed at high angles but ceased after a local maximum efficiency at a relatively moderate collector angle between 25° and 45°, with lower collector angles then resulting in efficiency decreases as noted in figure 41. Though a local maximum can be observed in the variable angle - high power data set between 45° and 50°, the sparsity of points in that region make it difficult to ascertain the nature of the efficiency increase and validity of this feature. More notably, the general trend of increasing efficiencies with low angles even after the slight drop off associated with this local maximum causes the theory commonly associated with previous results to be questionable. This unexpected trend is

further confirmed by variable angle - constant low power testing results, which are summarized in figure 42 below.

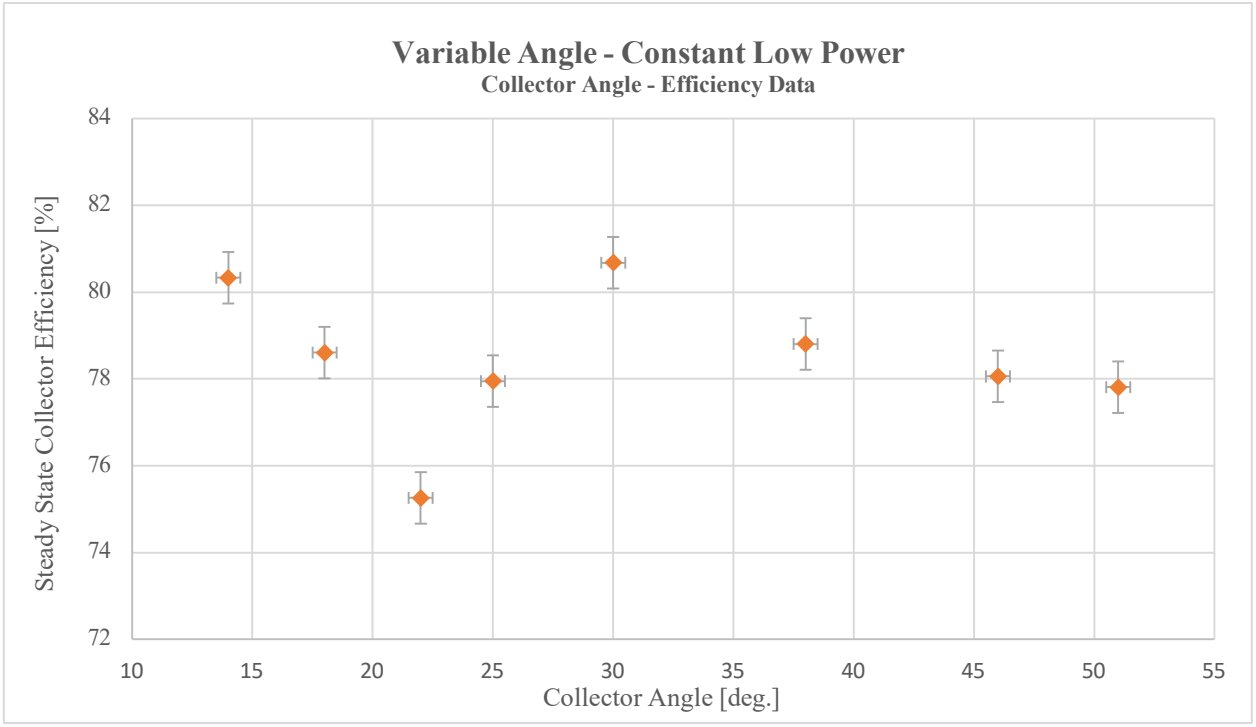

Figure 42: VACLP Efficiency Results, University of Evansville 2020-'21

The first thing of note in this set of results is the range of efficiencies observed, which is markedly lower than is the case for similar testing under high power input conditions. This observation aligns with expectations and is easily validated using simple theory involving convective heat transfer. Because low power input theoretically results in lower temperatures in the collector components, the associated temperature gradient between the collector and ambient temperature is reduced, thereby reducing the heat transferred to the ambient and improving system efficiency. As stated, this result is as anticipated based on theoretical knowledge and existing literature.

Also of interest in the low power data set is a seeming confirmation of the unexpected trend first noted in the high power results: decreasing collector angles are observed to be

associated with increasing efficiencies with the exception of a small region of interest around moderate collector angles, which produce a local efficiency maximum. In the low power case, this local maximum is more prominent and is more closely aligned with the 25° to 45° range in which it would be expected to exist based on previous findings.

The surprising nature of these efficiency results at low angles is based on their seemingly contradicting conventional wisdom about thermosiphon system operation. Traditionally, low angles are associated with low flow rates due to the directionality of the buoyant forces involved in fluid motion, as was briefly mentioned in discussion of the effect of increasing hot leg heights on system efficiency. Reduced volumetric flow at low angles under constant power conditions would then correspond to higher collector temperatures, due to the energy input to the collector and fluid being less rapidly carried into other system components. As previously discussed when relating low and high power results, one of the effects of this increased collector temperature would then theoretically be efficiency reduction as heat is lost to the ambient through convection. This theoretical connection between low angles and low efficiencies (low angles imply low flow, low flow implies high temperatures, high temperatures imply low efficiency) leaves little room for alternative interpretations, and yet is seemingly contradicted by recent experimental evidence of low flow rates producing not reduced, but increased efficiencies. Of course, it is also evident in equation 5 that high collector outlet temperatures are indicative of a high temperature gradient in the collector, which is unambiguously associated with increased efficiency as it implies greater energy absorption into the fluid. These two inherently contradictory effects on efficiency, both reasonably correlated with higher collector outlet temperatures, make analysis of this data an interesting opportunity to compare their relative

significances and the resulting expected net impact of high collector temperatures on system efficiency.

To confirm each of the relationships in the conventional argument relating low efficiency to low angles as well as investigate where the current data set may deviate from them, the primary efficiency data sets are cross-referenced with temperature and flow data. The concept of low angles being associated with low flow rates is illustrated by the results presented in figures 43 and 44, which are representative of high and low power input contexts respectively.

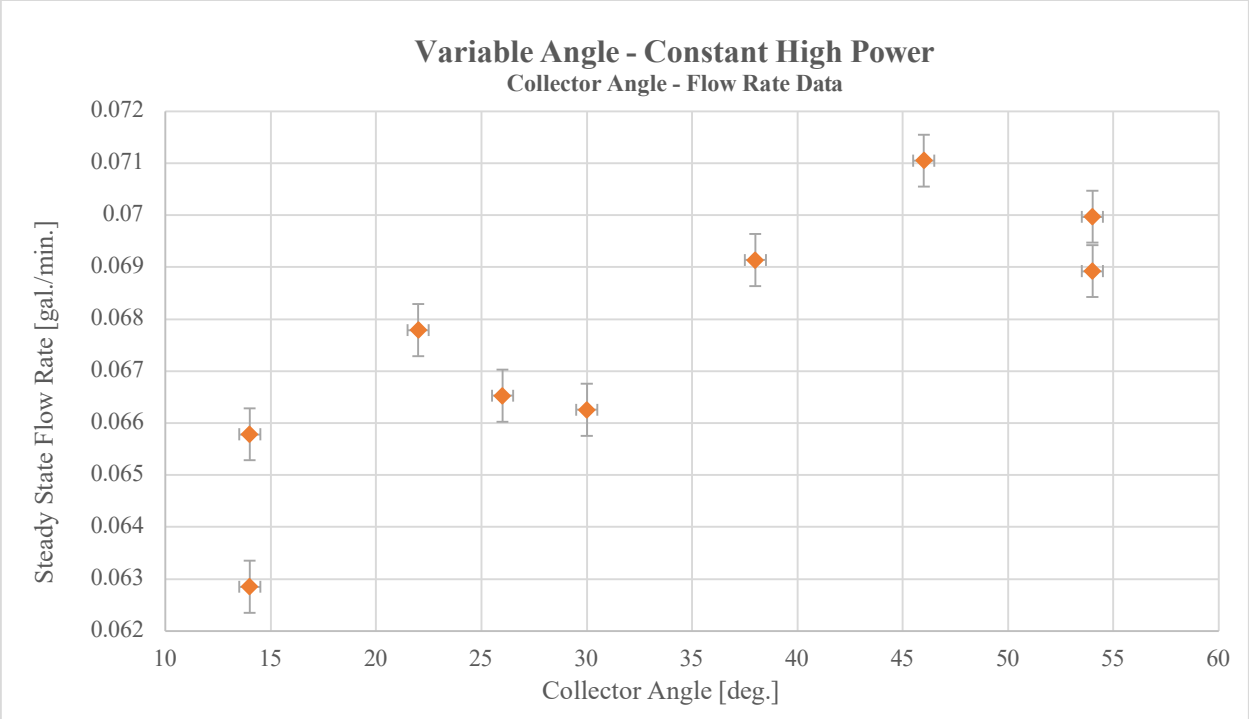

Figure 43: VACHP Flow Results, University of Evansville 2020-'21

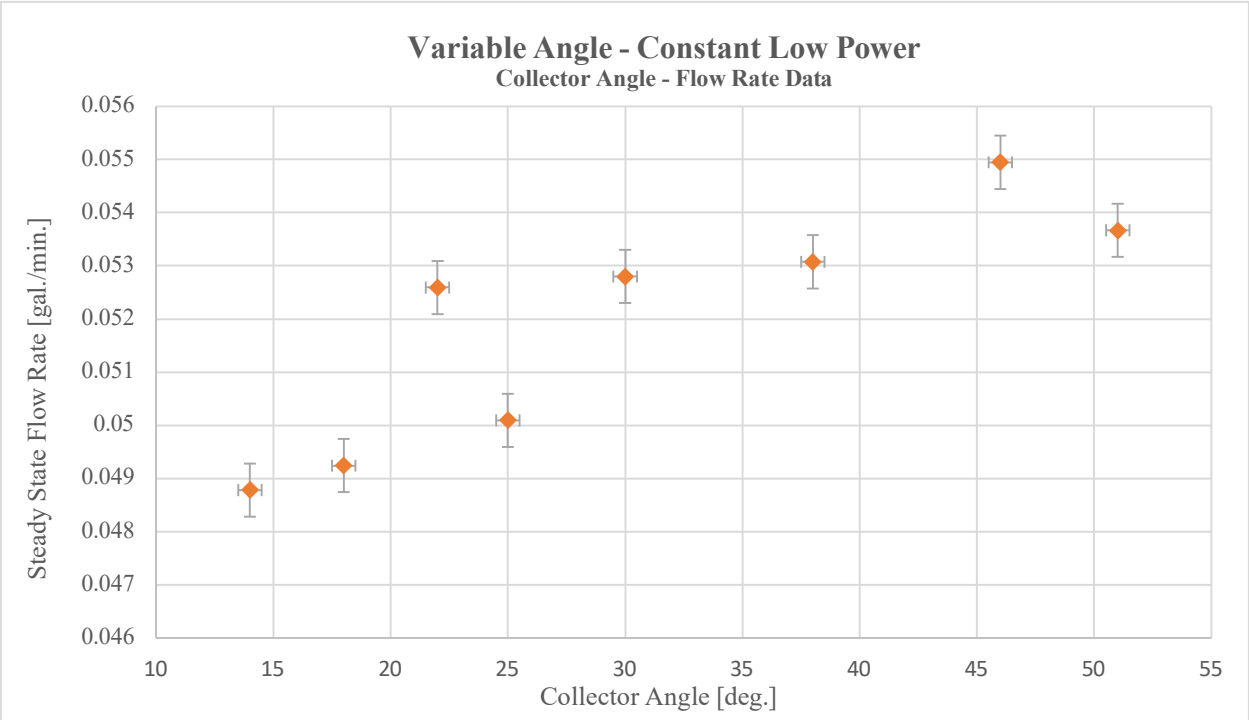

Figure 44: VACLP Flow Results, University of Evansville 2020-'21

As anticipated, these data sets both are demonstrative of a clear general relationship between increasing angles and increasing flow rates, confirming the stated theories. Figure As anticipated, these data sets both are demonstrative of a clear general relationship between increasing angles and increasing flow rates, confirming the stated theories. Figures 45 and 46 below are illustrative of a similar confirmation of the relationship between high angles and low collector outlet temperatures in high and low power contexts.

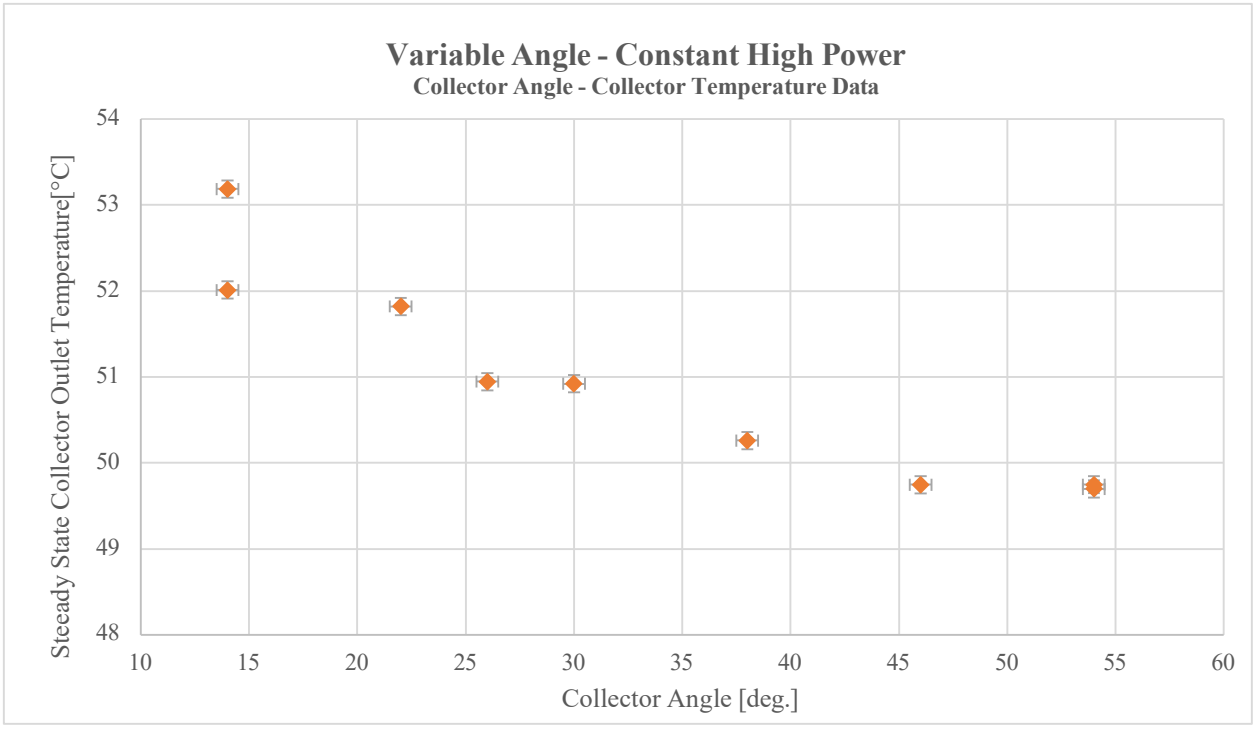

Figure 45: VACHP Collector Temperature Results, University of Evansville 2020-'21

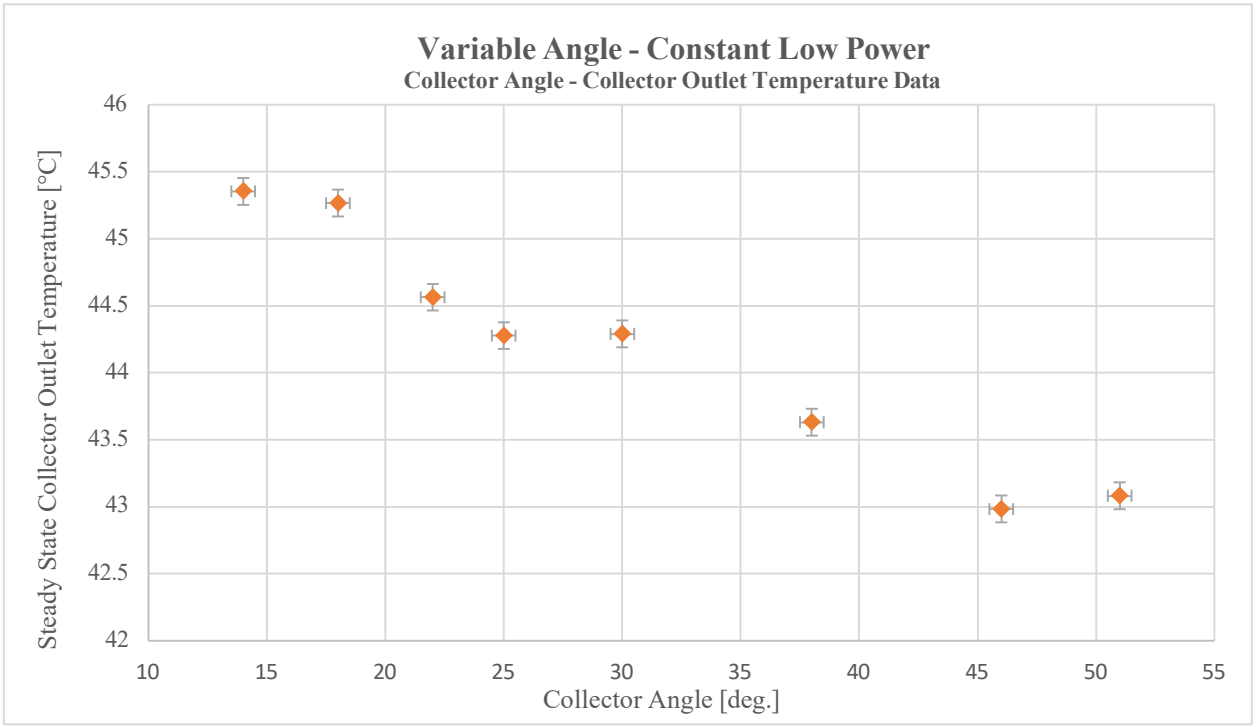

Figure 46: VACLP Collector Temperature Results, University of Evansville 2020-'21

Through comparison of these four data sets, each element of the logic traditionally used to associate low angles with a high potential for heat transfer are confirmed, implying that the causal effect of low angles reducing efficiency is reasonable and that the theory is sound. The fact that efficiency at low angles is shown to increase despite this very legitimate expectation leads to a clear conclusion: while the potential for heat loss to the ambient is greater at lower angles, the ultimate impact of this heat loss on efficiency is negligible relative to the effects of other parameter settings when the system is sufficiently insulated. To further confirm this theory and the trends associated with it, testing of uninsulated systems in varied environmental conditions is required. Through comparison of these four data sets, each element of the logic traditionally used to associate low angles with a high potential for heat transfer are confirmed, implying that the causal effect of low angles reducing efficiency is reasonable and that the theory is sound. The fact that efficiency at low angles is shown to increase despite this very legitimate expectation leads to a clear conclusion: while the potential for heat loss to the ambient is greater at lower angles, the ultimate impact of this heat loss on efficiency is negligible relative to the effects of other parameter settings when the system is sufficiently insulated. To further confirm this theory and the trends associated with it, testing of uninsulated systems in varied environmental conditions is required. Through comparison of these four data sets, each element of the logic traditionally used to associate low angles with a high potential for heat transfer are confirmed, implying that the causal effect of low angles reducing efficiency is reasonable and that the theory is sound. The fact that efficiency at low angles is shown to increase despite this very legitimate expectation leads to a clear conclusion: while the potential for heat loss to the ambient is greater at lower angles, the ultimate impact of this heat loss on efficiency is negligible relative to the effects of other parameter settings when the system is sufficiently insulated. To

further confirm this theory and the trends associated with it, testing of uninsulated systems in varied environmental conditions is required.

A summary and simplification of the experimentally determined trends between system parameters with reference to power angle and input power can be found in table A summary and simplification of the experimentally determined trends between system parameters with reference to power angle and input power can be found in table 11 below, with the most notable and applicable of these being a general increase in efficiency with decreased collector angles. Notably, this table does not incorporate the local maximum which has been noted in many data sets, but which is indicated by relatively few and sparse data points in the team's current research and therefore is not a feature which can be conclusively identified and related to existing theories.

Table 11: Summary of VACP Result Trends

	Magnitude Trend	
Parameter	Collector Angle, θ →	Power Input, P →
Collector Outlet Temperature, T_{out}	←	→
Flow Rate, ∀	→	→
Steady State Efficiency, η	←	←

4.2.2.2 Variable Angle – Variable Power Results .

To most effectively conduct research which relates deviation of the collector from the reference angle to the power input of the system, the power input must be controlled with extreme precision. In all other areas of research, the power input is monitored during testing with manual checks conducted once every ten minutes in which the three VARIACs voltages are measured and, if necessary, readjusted to values within 0.2 V of the goal output voltage. This

approach has proven sufficiently precise for research which involves no variation in power input between tests, but would be insufficiently precise for variable power tests in which the difference between power inputs may be as little as 0.3 V. To make trends clearer, testing procedures are revised for these phases to include VARIAC checks once every five minutes and the tolerance adjusted to be within 0.1 V of the goal voltage. This approach proves successful in maintaining consistent power input within significantly smaller tolerances, as shown in figure 47, which illustrates the recorded output voltage values of three VARIACs for two tests: the first with a goal voltage of 50 V monitored every ten minutes within a 0.2 V tolerance and the second with a goal voltage of 48.8 V monitored every five minutes within a 0.1 V tolerance.

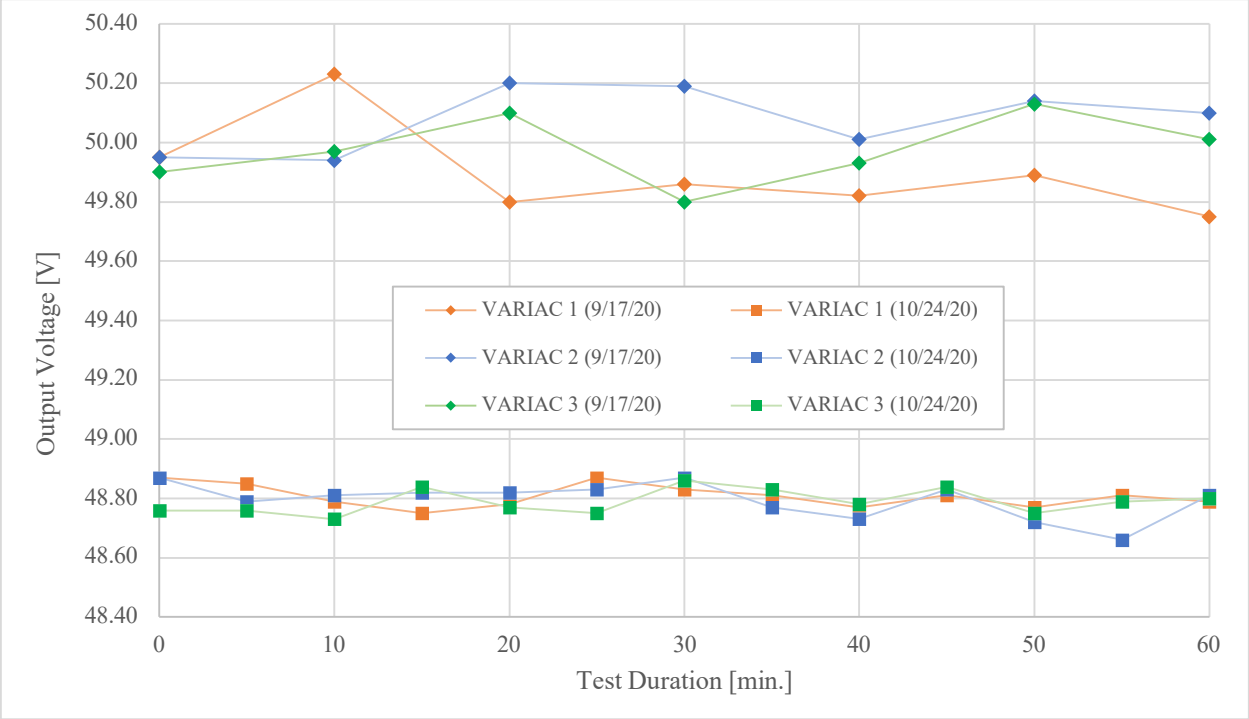

Figure 47: VARIAC Output for Varied Check Frequency and Tolerance

Having adjusted testing procedures to produce a high degree of precision in power input, variable angle – variable power testing is conducted at one of the two predetermined reference angles (14° and 62°) and with a presumed high power of 50 V input to the resistance heat tapes

at those angles. The results of the variable high angle – variable power tests, which are based on positive angular deviations from a reference angle of 14°, are shown in figure 48, in which both the collector angle and the angular deviation are noted for reference.

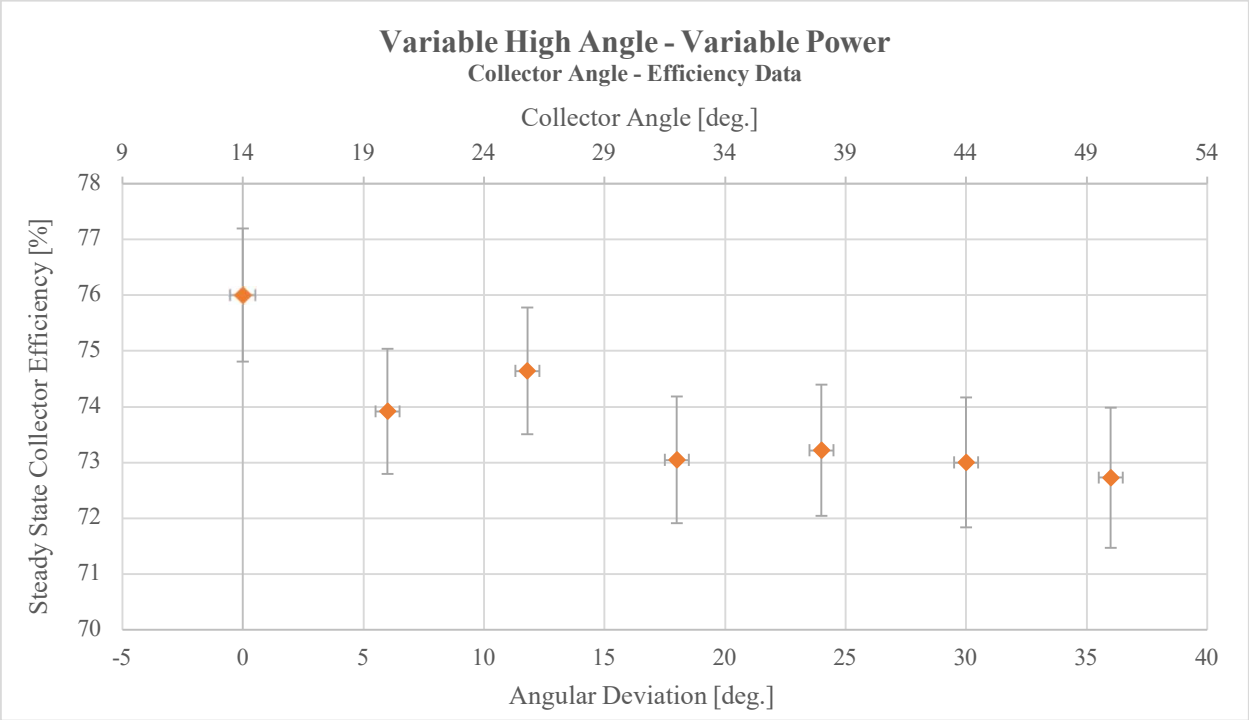

Figure 48: VHAVP Efficiency Results, University of Evansville 2020-'21

As in constant power testing, the single most notable trend in this data set is the general reduction in efficiency as the collector angle is increased, which in this case implies ever greater deviation from the relatively low reference angle. This is a particularly interesting relationship in this specific context because the choice of a low reference angle provides the opportunity to investigate two contradictory effects on efficiency and their relative significance: the trend established and investigated during constant power testing which indicates that low collector angles are associated with high efficiencies, and the trend of low power levels (which in this case are related to high collector angles because of their decreasing proximity to the reference angle) being associated with improved efficiencies.

Also of interest in this data is the local maximum at moderate collector angles which is suggested by the limited literature associated with this topic and which is experimentally observed to exist at between 24° and 29° in this case. While this was a feature of limited interest in variable angle constant power testing in that it obscured greater trends, it's nature and relative magnitude with the maximum efficiency found at extremely low collector angles is pivotal in the study of variable angle variable power system performance. Conventional wisdom indicates that optimal performance is achieved at reference angles and is guided by the impact of power flow being of greatest significance in system function. A local maximum at angles distant from the collector angle which is comparable to the maximum efficiency at the reference angle in low reference angle environments, however, would indicate that the second most optimal angle from the reference angle is not the one which is most proximal to it, as would traditionally be used, but a more distant angle which has improved efficiencies due to as yet unidentified effects. Of course, this would be especially relevant only at global positions in which the reference angle is both low enough to be below the moderate angles associated with local improved efficiencies and the high angles associated with reduced efficiencies due to other effects.

As was the case in constant power data analysis, isolation of individual temperature and flow parameters and their relationship with collector angle provides insight into the nature of both the general efficiency trend and the root of the local maximum. The efficiency data collected with a reference angle of 14° is related to collector outlet temperature in figure 49 below.

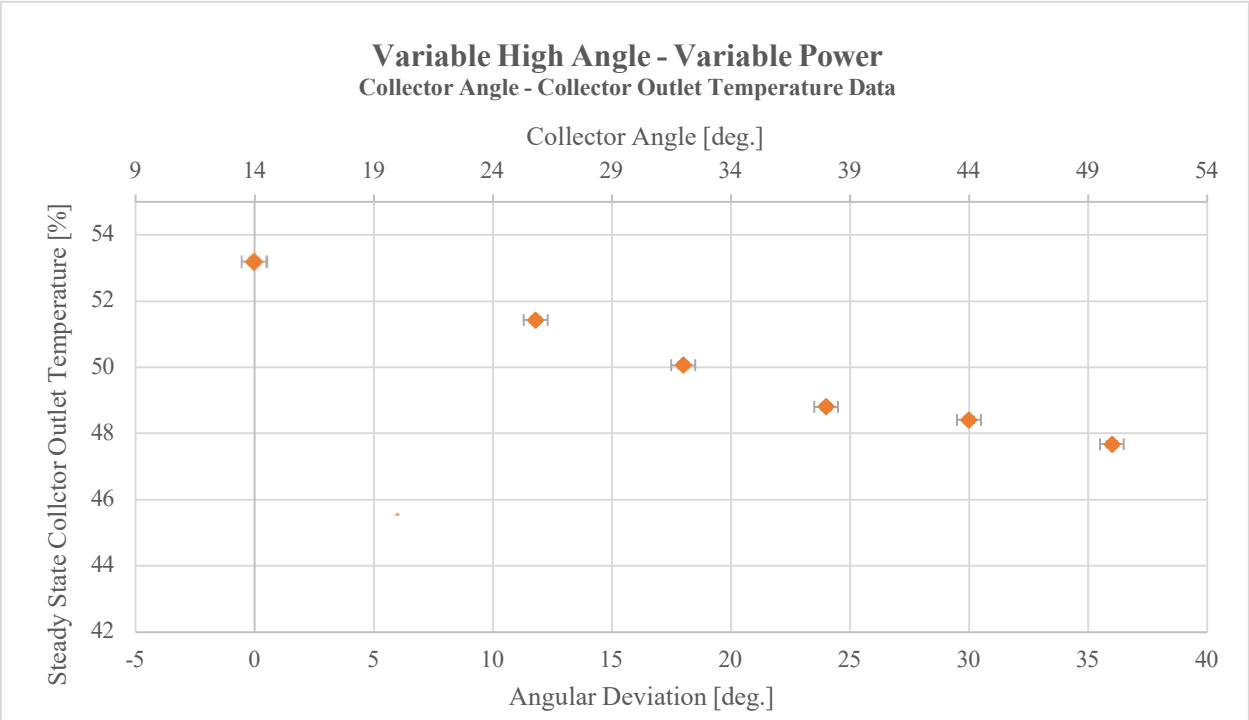

Figure 49: VHAVP Collector Outlet Temperature Results, University of Evansville 2020-'21

As was the case in constant power testing, increases in collector angle are found to be strongly associated with decreases in collector outlet temperature. The complex effects impacting the relationship between collector outlet temperature and system efficiency are discussed in detail in previous constant power analysis, and all conclusions appear to remain relevant in this case. This result aligns with literature and previous experimental results in two ways: high collector angles result in increased flow and thereby low temperatures, and high collector angles being in this case associated with reduced power inputs that have been strongly related to improved efficiencies. In this analysis, all previous theoreies are seemingly validated. Also notable is the lack of local maximum in this data set, which suggests that the observed local maximum efficiency is not the result of effects related to collector temperature. This is even more clear when angular deviations are cross referenced with flow rate data, as is the case in figure 50.

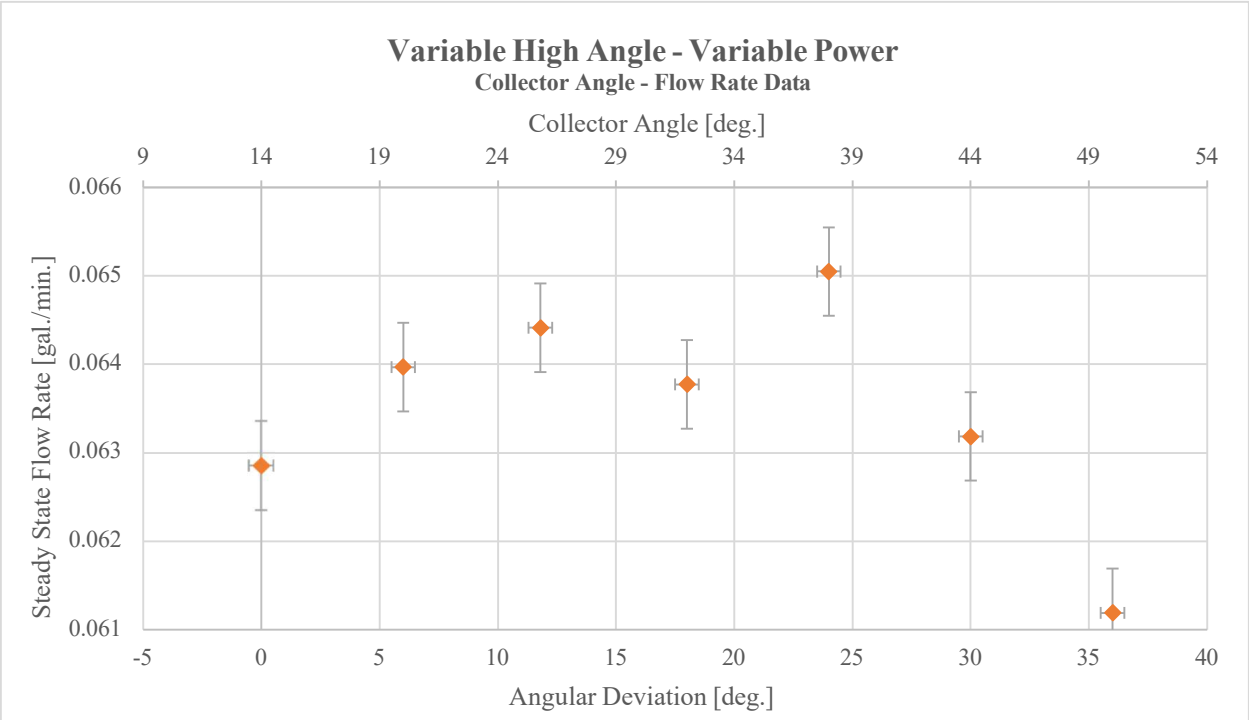

Figure 50: VHAVP Flow Results, University of Evansville 2020-'21

The single most significant feature of this flow rate data set is the way in which it deviates from similar plotting under constant power conditions: it does not linearly relate flow rate to collector outlet temperature and so to increasing angles. Instead, this data set features a prominent maximum flow at intermediate collector angles. In this way, it is seemingly confirmed that the local maximum observed in the primary efficiency data set is the result of variable power impacts on fluid forces, causing a disruption in the established relationship between collector outlet temperature and flow rate under other conditions. As expected, increases in collector angle in the low angle region cause an associated increase in flow rate. After moderate collector angles, however, system performance deviates from current theories. It is expected that high angles would cause further increases in flow in association with greater alignment of the collector piping with the direction of the buoyant force, continuing the upward trend and being in direct contradiction to the experimental results. Intriguingly, the parameter which differentiates

this data set from those previous that were thought to illustrate the validity of this theory (reduced input power at high angles) would also be expected to increase the efficiency in alignment with other effects and not further reduce it to the point of overwhelming other effects. This is suggestive of a missing component in the thermodynamic and fluid mechanical concepts used to explain thermosiphon behavior in variable power contexts, as analysis of the current data seemingly confirms the anticipated relationship between collector outlet temperature and collector angle while simultaneously invalidating the comprehensive nature of next logical connection: that between collector temperature and flow rate. Further testing involving greater density of data points and greater analysis of flow under different reference angle conditions would be necessary to investigate the perhaps unidentified system parameter which exerts this influence on flow rate, and therefore on efficiency, without an associated change in collector outlet temperature relationships.

Similar experiments carried out at a reference angle of 62° yield strikingly similar results, albeit indicative of a very different application context, as illustrated in figure 51.

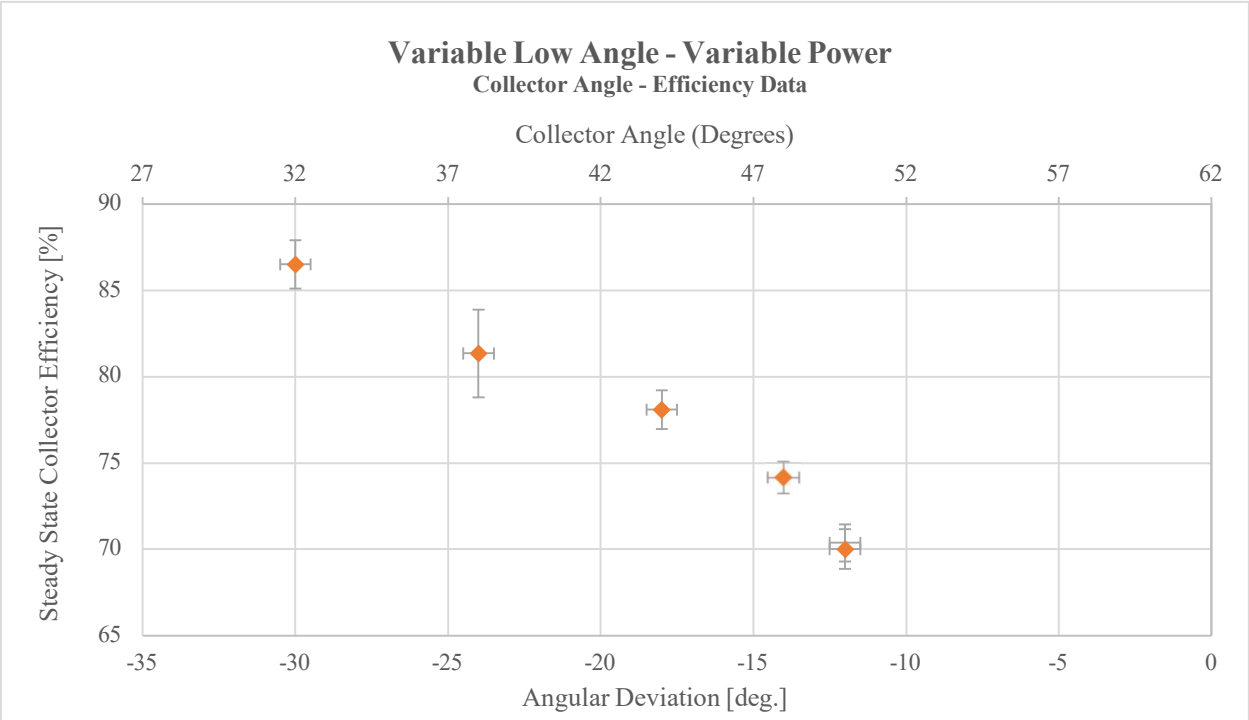

Figure 51: VLAVP Efficiency Results, University of Evansville 2020-'21

It is important to note the way in which a high reference angle context is differentiated from a low reference angle context: in this case, the effect of low collector angles theoretically being associated with high efficiencies and the effect of increasing deviation from the reference angle and the associated power reduction also being associated with high efficiencies are aligned. This was not the case for testing which used a reference angle of 14°, in which these effects were contradictory and so could be more clearly differentiated.

Due to limitations of the experimental apparatus, this data set does not include collector angles sufficiently low to determine whether the observed trend of increasing efficiency with decreasing collector angles would be expected to continue or similarly develop a local maximum at a moderate collector angle. As previously mentioned, however, this trend is in alignment with all expectations based on previous experiments and literature review.

The cross referencing of this collector angle data with both temperature and flow rate information is also of interest in this case, and the results of these analysis are presented in figures 52 and 53, respectively.

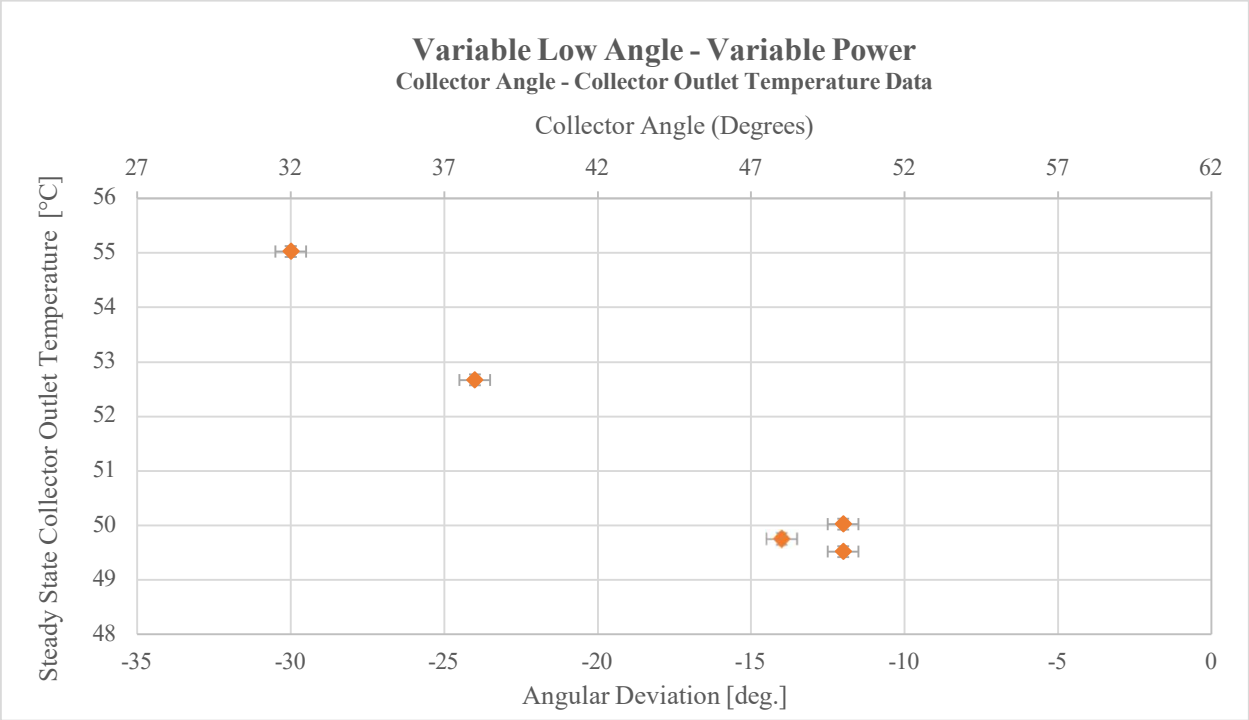

Figure 52: VLAVP Collector Outlet Temperature Results, University of Evansville 2020-'21

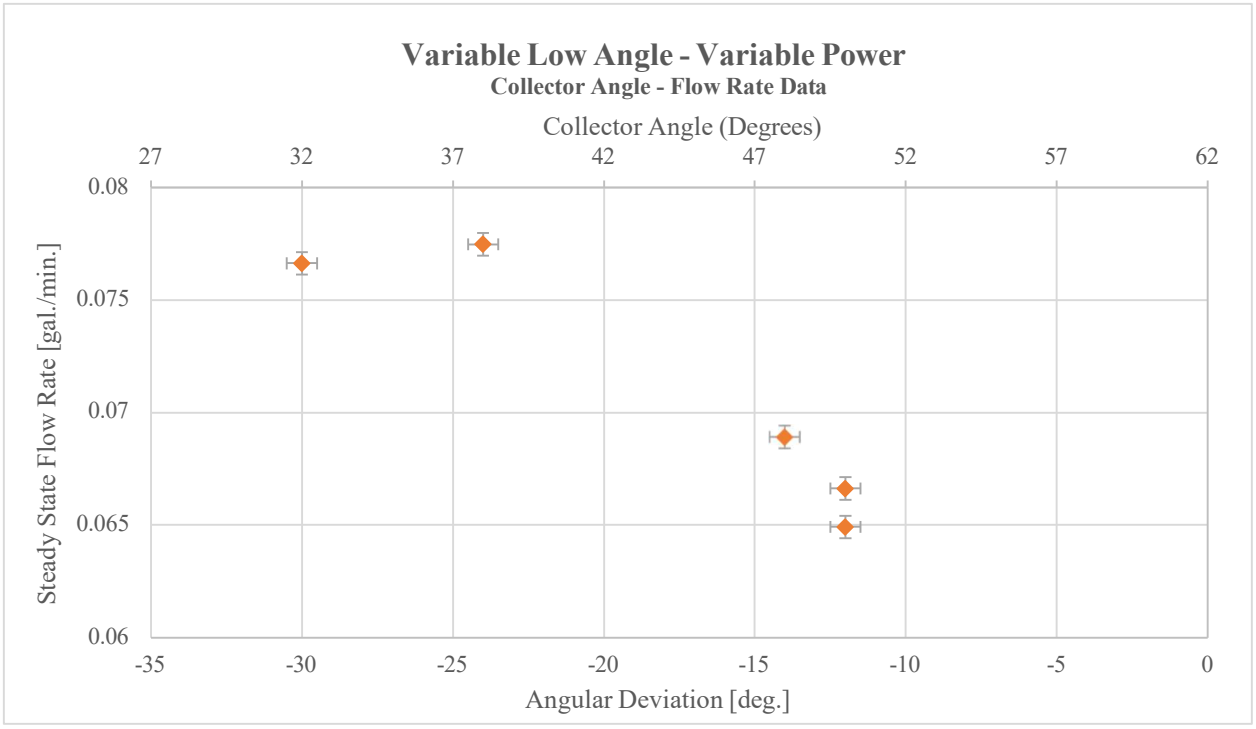

Figure 53: VLAVP Flow Results, University of Evansville 2020-'21

As in previous cases, the influence of variable power does not appear to significantly extend to collector outlet temperature effects: the collector outlet temperature is clearly associated with increasing collector angles. More intriguing in this case is the flow rate data, which features trends similar to previous analysis even including the potential for a local maximum in the 37° to 41° collector angle range. Without further testing at low angles it is impossible to conclusively identify this trend, but the data is at least in alignment with the findings of testing at a 14° reference angle.

A summary and simplification of the trends associated with variable angle - variable power testing is in table 12. While the location of the precise maximum is unclear, flow rate trends are denoted with opposing directions as an indication of the prominently observed tendency toward a maximum, while efficiency trends are noted as being more consistent in that the magnitude and location of the local maximum is subject to further experimentation. The

current data sets are suggestive of fascinating and potentially counterintuitive system behavior under these conditions, particularly the flow rate, and so further research at varying reference angle and with greater data sets is recommended to explain thermosiphon system performance more comprehensively that current theoretical models.

Table 12: Summary of VAVP Result Trends

	Magnitude Trend	
Parameter	Low Reference Angle Contexts, $\alpha = 14°$	High Reference Angle Contexts, $\alpha = 62°$
Collector Angle, θ	→	→
Angular Deviation, $\Delta\theta$	→	←
Input Power, P	←	→
Collector Outlet Temperature, T_{out}	←	←
Flow Rate, $\forall$	→ ←	→ ←
Steady State Efficiency, η	←	←

4.2.3 Other Research

4.2.3.1 Variable Hot-Leg Height Results

Though previously discussed instrument failures severely limited the scope of the variable hot leg height data set, the resulting trends are found to align with expectations based on literature and previous experiments and to provide insight into the soundness of the conceptual models conventionally used to relate this parameter to efficiency. Efficiency data for this parameter is summarized in figure 54.

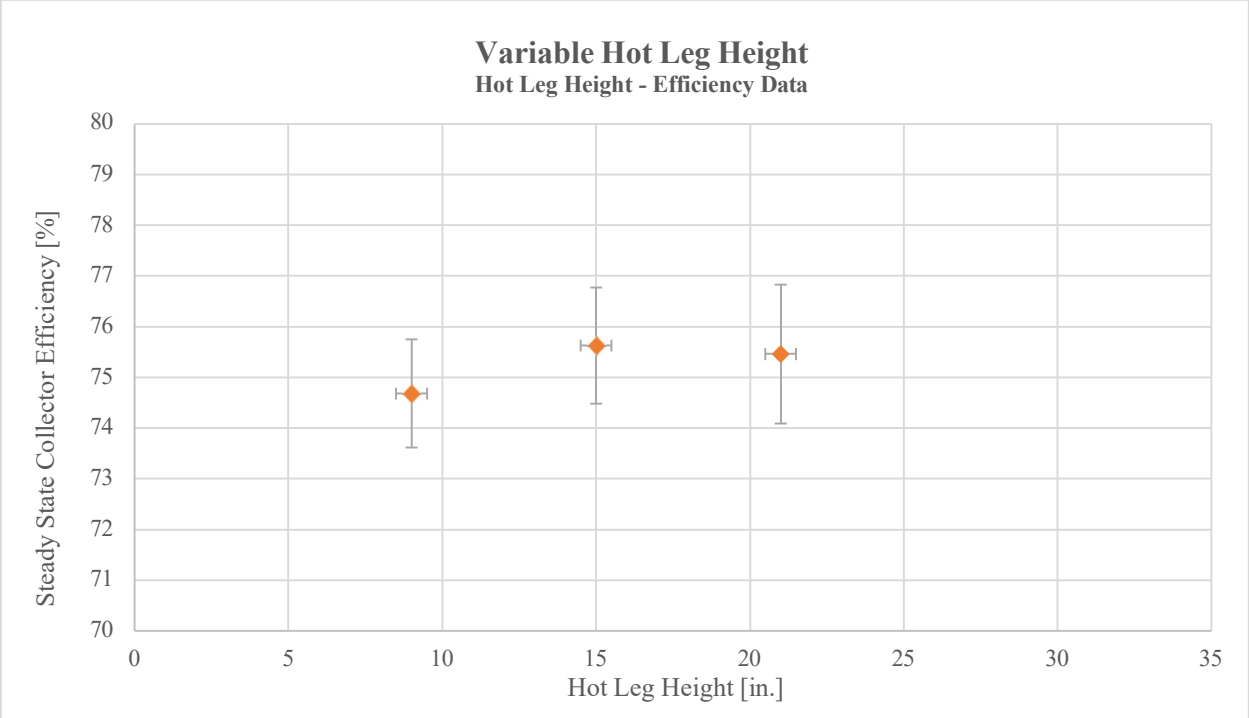

Figure 54: VH Efficiency Results, University of Evansville 2020-'21

Though the data points present in this data set are generally suggestive of increasing efficiency being associated with increasing hot leg height, as would be expected, the sparsity and limited scope make it difficult to conclusively identify a clear pattern. More focused investigation of the effect of hot leg height on temperature and flow data, which are presented in figures 55 and 56, produces more definitive trends.

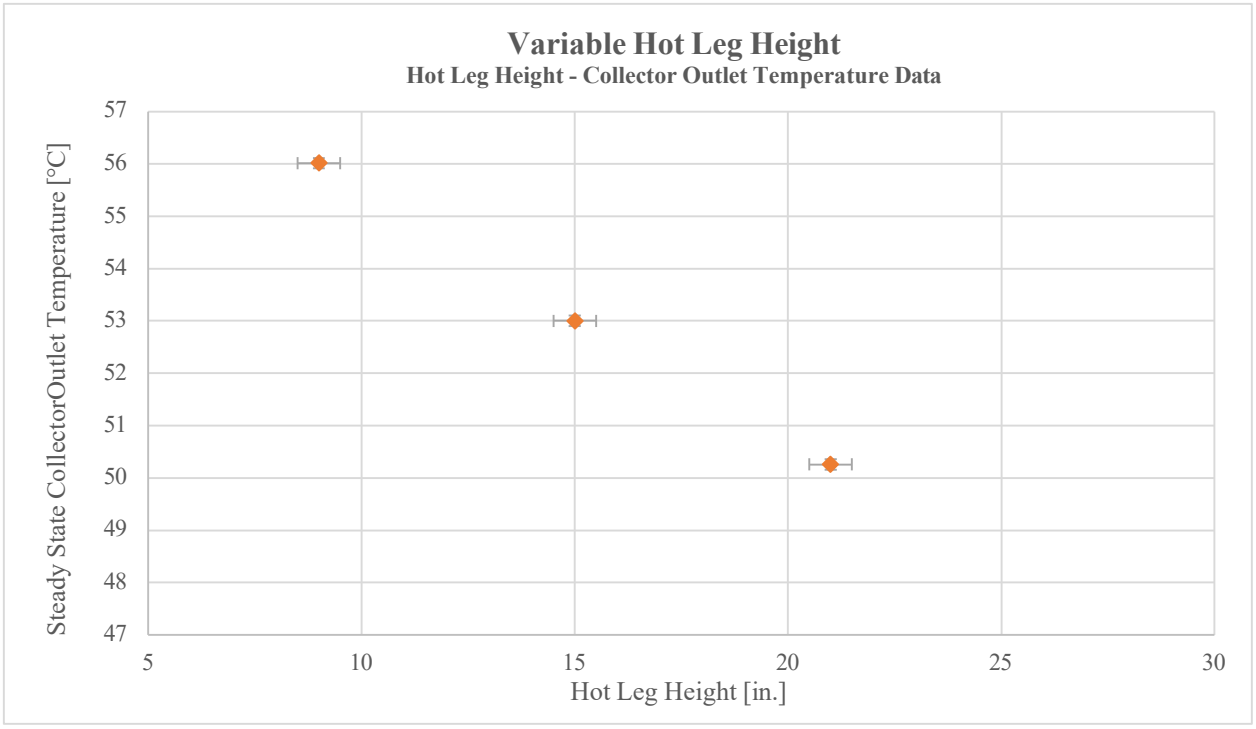

Figure 55: VH Collector Outlet Temperature Results, University of Evansville 2020-'21

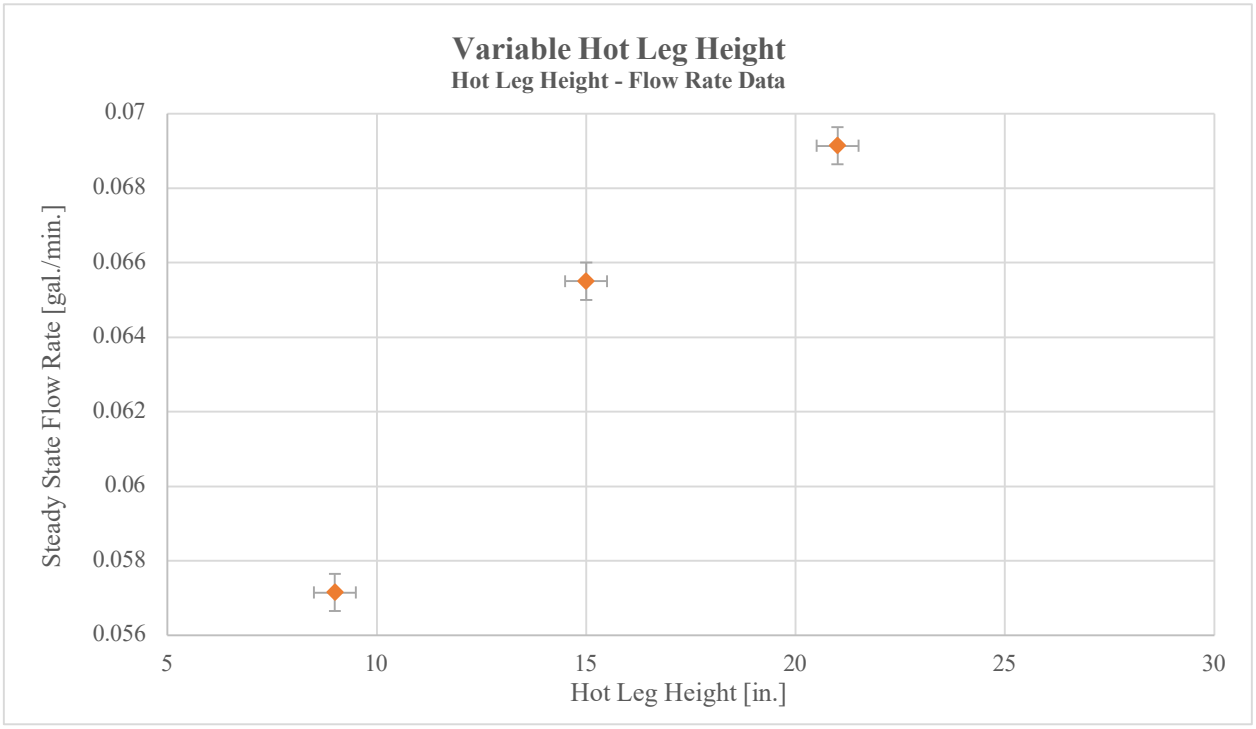

Figure 56: VH Flow Results, University of Evansville 2020-'21

When cross reference with flow rate and collector outlet temperature, the relationships associated with increasing hot leg heights are extremely clear: reduced collector outlet temperature and increased flow through the system. This result is in agreement with the explanations put forward by current literature to explain the relationship between increasing hot leg heights, which are related to increasingly vertical distances of tubing between system components, and an improved flow rate due to the previously discussed chimney effect. This increased flow rate, as has been well established, is shown to produce decreasing collector outlet temperatures as the input energy is more rapidly distributed to other system components. Increased collector temperature has been shown to have both positive and negative impacts on efficiency related to both greater energy absorption by the fluid and increased potential for heat loss, which is the subject of more detailed discussion in the analysis of power-angle effects. In this way, the experimental results of this testing phase, while not sufficiently comprehensive to be definitive, are unambiguously in agreement with the anticipated effects of increasing hot leg heights. These general results are summarized in the table below, though efficiency is omitted because the results are insufficiently clear to be presented in relation to the other parameters.

Table 13: Summary of VH Result Trends

Parameter	Magnitude Trend
Hot Leg Height, h	→
Collector Outlet Temperature, T_{out}	←
Flow Rate, ∀	→

A more comprehensive study of the hot leg height parameter to confirm the trends exhibited by this data and that of other institutions is recommended as a subject for further research in this field.

4.2.3.2 Variable Ambient Temperature Results

Like variable power testing, variable ambient temperature testing is a research object not frequently covered in thermosiphon literature and as such is of great interest to the current team, particularly in the comparison of results between institutions which may not have sufficiently controlled this parameter. The efficiency results associated with the variable ambient temperature testing phase are presented in figure 57, below.

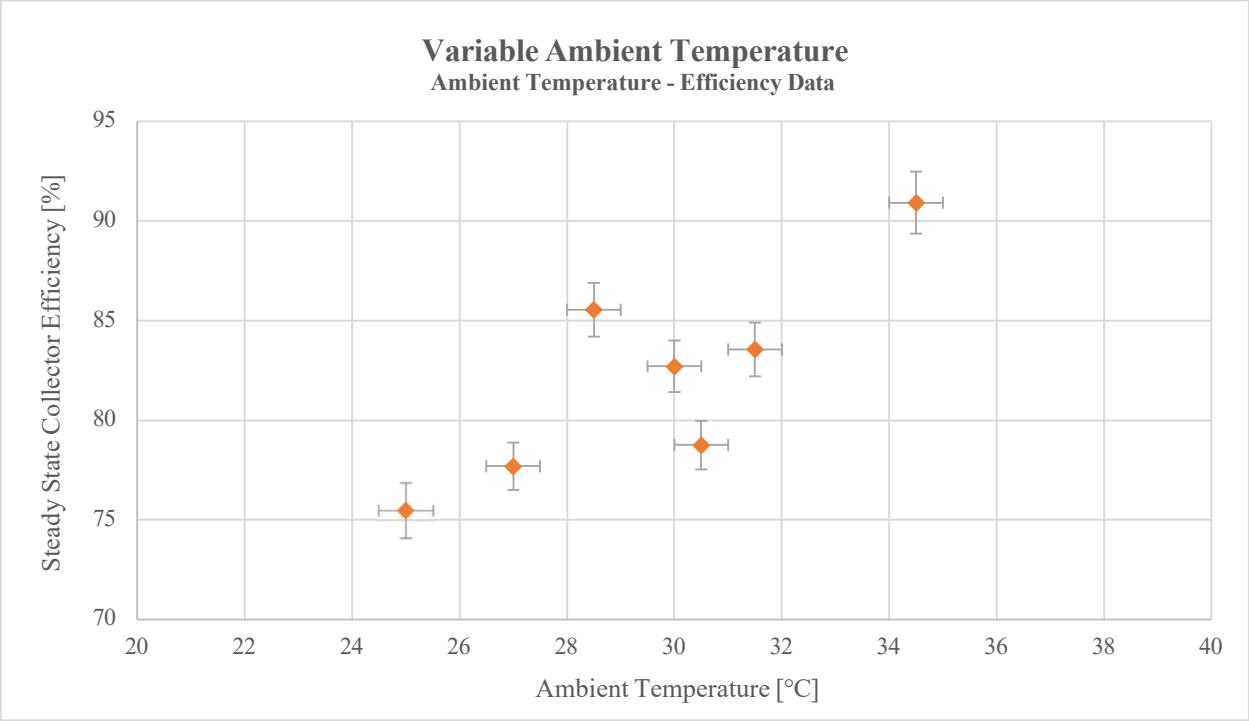

Figure 57: VT Efficiency Results, University of Evansville 2020-'21

The general trend in this data is evident and is in agreement with expectations discussed in previous sections: increasing ambient temperatures are unambiguously found to be associated with increased efficiency, theoretically due to reduced heat loss to the ambient as a result of a lower temperature difference between collector components and the environment. Though the linearity of the data set is mitigated by two outliers, it is expected that a more robust data set would confirm the linear relationship. Investigation into the efficiency results which are not

aligned revealed no significant source of error, leading to the conclusion that this anomaly is simply the result of the limitations of the current experimental apparatus to control and measure ambient temperature at a high sample frequency.

Analysis of this data set with respect to collector temperature and induced flow rate, the results of which are summarized in figures 58 and 59, seemingly confirms established theories.

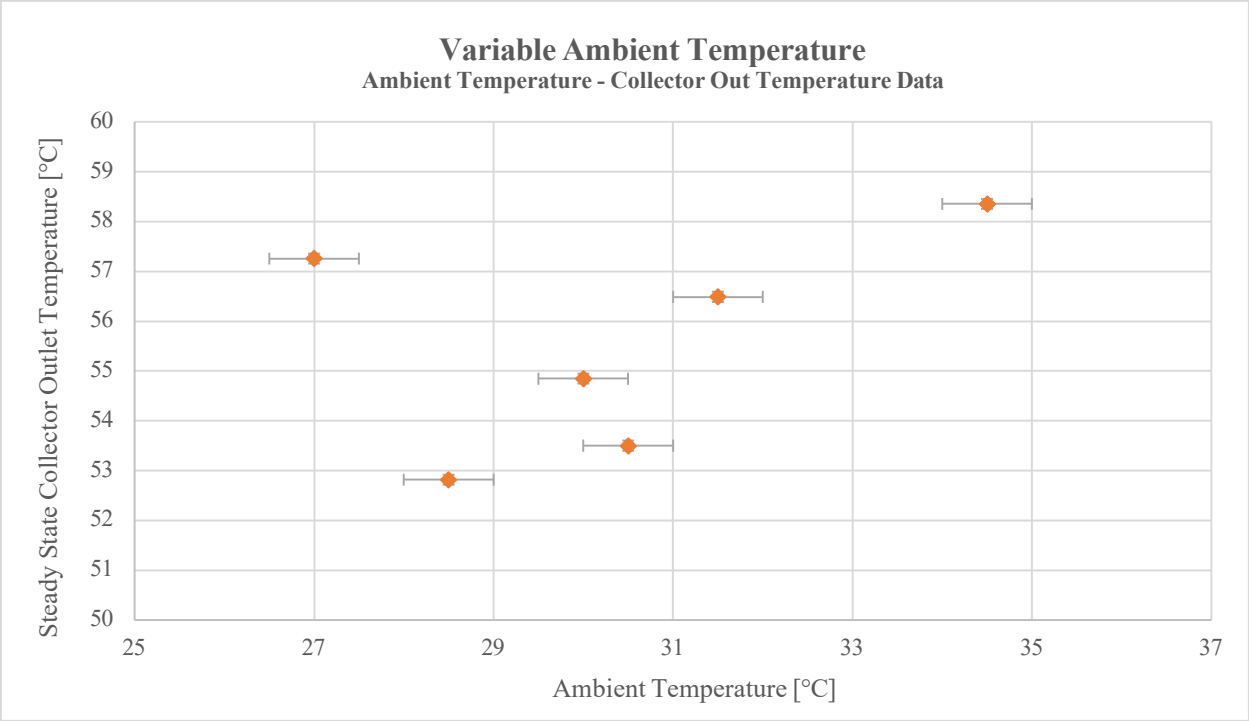

Figure 58: VT Collector Outlet Temperature Results, University of Evansville 2020-'21

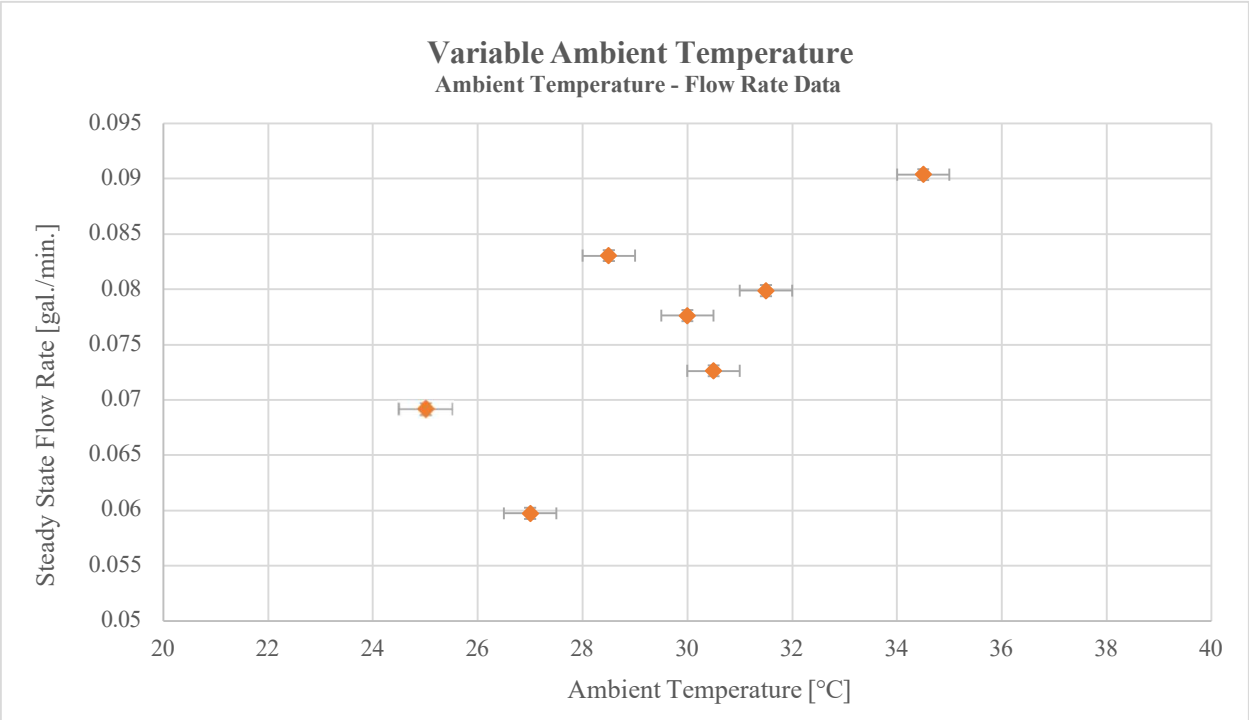

Figure 59: VT Flow Results, University of Evansville 2020-'21

As anticipated, the general trends in these results associate high ambient temperatures with increased flow rates, which is theoretically explained by the reduced heat loss causing greater transfer of applied energy into the fluid. In this case, the collector temperature data would similarly be expected to increase as greater energy absorption by the fluid would theoretically result in greater temperature gradients across the collector. This is observed to be the case, confirming both the significant impact of ambient temperature and the theoretical explanation for it. These resulting trends are summarized in the table below.

Table 14: Summary of VT Results Trends

Parameter	Magnitude Trend
Ambient Temperature, $T_{ambient}$	→
Collector Outlet Temperature, T_{out}	→
Flow Rate, ∀	→
Efficiency, η	→

Though the resulting data includes outliers and further research is warranted to more comprehensively identify the relationship between ambient temperature and efficiency, these results make clear the importance of controlling this parameter carefully while varying other system parameters if the consistency of results is to be maintained.

4.2.3.3 Variable Hydraulic Resistance Results

As a result of multiple instrument failures and the extended period of base case tests used to identify inexplicable anomalies in system performance, variable hydraulic resistance testing was demoted in priority and not performed to allow for more comprehensive testing of parameters which are of greater relevance to the current team. Hydraulic resistance, though extremely applicable in thermosiphon construction and design, was considered the parameter of lowest priority at the present time due to the abundance and extremely consistency of results from other institutions and previous years efforts at the University of Evansville and the importance of several other areas of novel research, including variable power and variable ambient temperature testing.

5 Project Deliverables

A weekly report that includes the progress made in the project and the time committed by each team member is submitted to the faculty advisor each week. At the end of the first of two semesters, a design report including a detailed experimental procedure, summary of tests conducted, and detailed plans for future facility upgrades was submitted to university faculty. A summary of all accomplished research and the associated results obtained during the academic year is submitted as a final report.

Every year, students from different universities present at the National Conference on undergraduate research (N.C.U.R.) with high quality mentored undergraduate research in different areas of interest in a wide range of current engineering research fields. Because the team obtained a sufficiently large and consistent data set, the team was able to publish the results at N.C.U.R. in the form of two presentations associated with power - angle research and variable ambient temperature results. As preparation for this presentation, each attending and presenting student completed and submitted an individual abstract to N.C.U.R. related to their area of research, and results were presented to conference attendees in mid-April. The team also hopes to work with university faculty (Dr. Douglas Stamps) to develop a formal publication of results in a scientific release of some type.

6 Project Resources

6.1 Project Schedule

Because of uncertainty surrounding the nature and duration of facility access in the early stages of this year, the proposed schedule placed emphasis on the immediate initiation and rapid completion of research testing. To accommodate this, many aspects of project planning, team formation, and initial documentation were accomplished by team leadership at the conclusion of the previous semester and all invasive facility modifications were scheduled to take place in the final stages of the project after testing has been completed. The result of these changes is a planned project timeline in which the majority of research tests and associated initial data analyses are carried out in the fall in addition to the conceptual design of facility modifications and, when necessary, instrument maintenance and replacement. This plan left the latter portion of the spring for significant facility modifications or instrumentation upgrades, general project data

review, and the formalization of project findings. Documentation deadlines are distributed throughout the year and are informed by provided submittal dates for coursework, university organizations, and the N.C.U.R. conference. The research portion of the schedule initially assumed a frequency of one test per 24-hour period and five of these tests per week, which experience has indicated is the maximum frequency which allows sufficient fluid cooling time between tests based on limited facility access. In their proposed state, research tests were generally ordered by priority, with the exception of variable ambient temperature testing, which was scheduled to take place during the period of lowest seasonal temperatures so that testing under the widest possible range of environmental conditions is made possible. Figure 60 summarizes the general task categories associated with these project areas and the timeline in which they were proposed to be completed in contrast to when they were actually completed. While this generalized representation is presented for clarity, each of the time steps and tasks in this figure is potentially the summation of a large grouping of subtasks associated with the full task breakdown and schedule, which is available in appendix J.

Notably, the detailed task timelines are presented both in terms of numbered weeks (Week 1, 2, 3…) and calendar dates. This was initially done so that, in the event of a fundamental change in the start, end, or duration of the semester, the week numbers associated with each task would remain applicable and need only be shifted to different dates without requiring significant reordering. This was significant because, in response to the COVID pandemic, the fall and spring semesters were both reduced. In the case of the fall semester, this change was from the traditional sixteen weeks which include breaks and holidays to a continuous thirteen weeks at the university, while the Spring semester similarly involved a reduction. The

traditional semester schedule is the basis for the included proposed Gantt chart, while the revised semester durations are indicated by a double line.

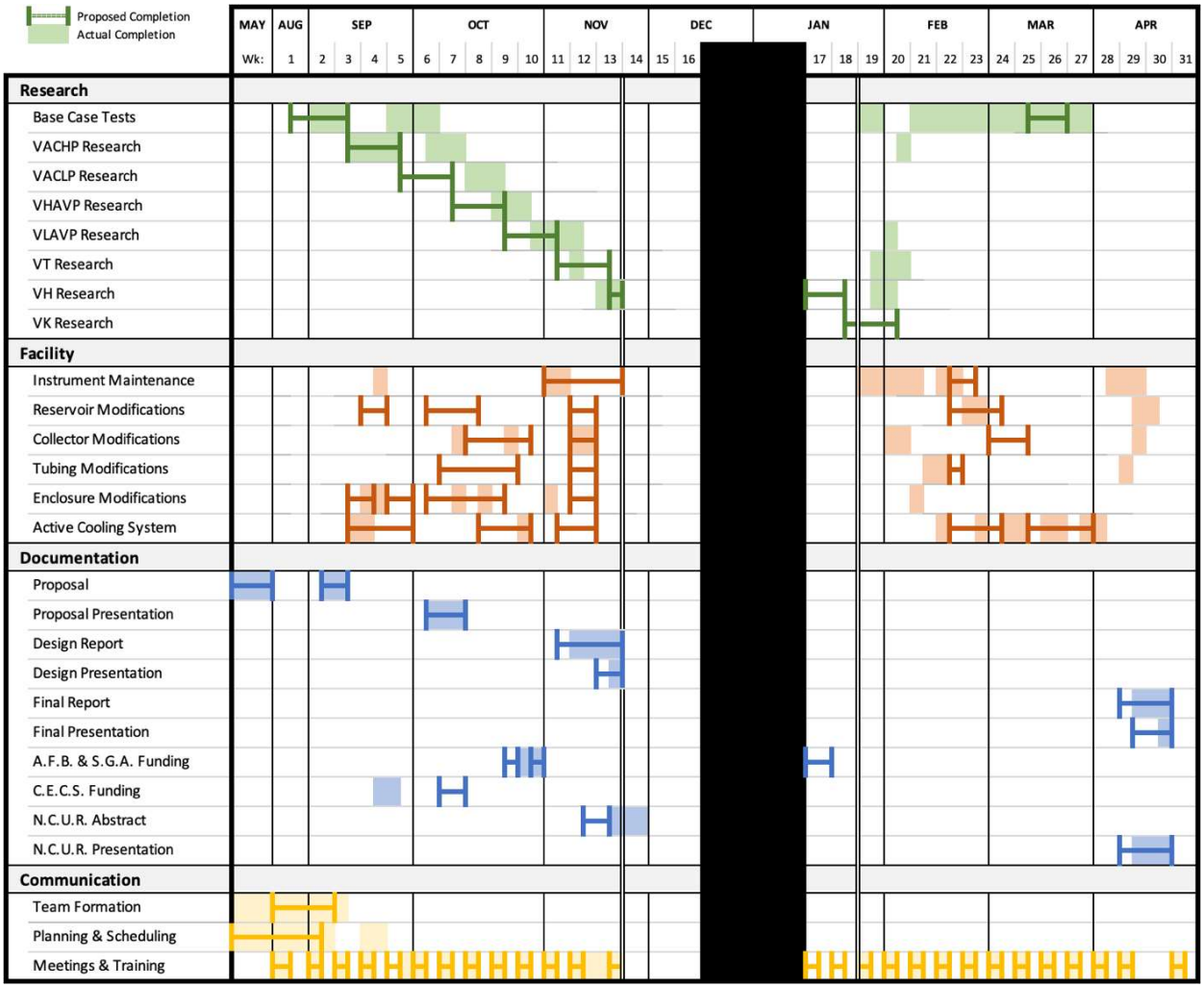

Figure 60: Generalized Project Schedule

As the timeline above makes clear, the proposed research plan was followed only for a limited time before circumstances caused testing to be delayed. The most significant of these delays during the fall semester was the unexpected change in calculated system performance which occurred during variable angle – constant high-power testing and is described in detail in previous sections. The necessary return to base case testing and subsequent redundant performance of this research phase caused testing to be offset from the proposed schedule for the

remainder of the semester fall. In addition to this delay, the distinct failures of both one VARIAC unit and of the pump in the fall, each of which required immediate acquisition of a new model and replacement, caused further unavoidable delays that were less impactful than the one caused by the inexplicable system results but nonetheless impacted the ability to regain the lost time.

Although testing was offset from the proposed schedule early in the project timeline, the rate at which tests were actually completed was greater than proposed in the fall, allowing some time to be regained. As previously noted, the proposed scheduled conservatively assumed facility access only during weekdays and business hours, a reality which was only accurate for the first several weeks of the semester before unlimited access was granted by the engineering department. After this point, testing frequency increased by almost 30%. While this gain was not sufficient to offset the three delays experienced by the team, it had the effect of mitigating their impact.

Notably, fall testing phases also took place in a different order than initial proposed, particularly at the end of the first semester. Unseasonably high environmental temperature limited the ability to conduct the scheduled variable angle testing, and in response variable ambient temperature tests were conducted during other research phases. The result of this decision is a testing schedule which is fairly sporadic during the final weeks of fall, but which nonetheless proceeded uninterrupted despite unexpected ambient conditions.

As indicated, similar and extremely significant delays in research testing also caused spring semester schedule to be notably divorced from the planned project timeline. The inexplicable efficiency increases first experienced to a lesser degree in the fall reappeared after only limited research testing in the spring and, as a result of the efforts previously discussed to rectify the issue, forced base testing to continue for the entire remainder of the project period.

This had an extreme effect on the project schedule for both research goals and the system modification timeline. One of the seven research phases, variable hydraulic resistance testing, was ultimately eliminated in response to the dramatically reduced ability to conduct legitimate tests. This extended base case period also resulted in a greater time spent on the redesign of and preparations for system modifications at the expense of installation time, the schedule for which was continually adjusted throughout the semester to allow all modifications sufficient time to by implemented while still permitting attempts to fix system performance and continue research for as long as possible. Ultimately, the demands of the modification schedule became dominant and research was forced to be abandoned before the system issues were conclusively identified, though subsequent removal of system components made the problems clear, as stated in previous sections.

It is also notable that in the early stages of project planning, the size and nature of the team was altered dramatically by the recruitment efforts of existing team member, which resulted in the increase of project leaders by 40% and of underclassmen team members by approximately 46%. In response to the greater number of team leaders and team members, facility modification tasks were delegated among team leaders, allowing them to be the sole focus of a distinct section leader as opposed to being organized by students who were also engaged in research work. This ability to delegate and categorize tasks had a dramatic impact on the way in which facility operations were undertaken, which is made clear in the project timeline. The critical nature of preliminary work during the fall semester was reduced due to the increase in available students to perform the work quickly and with focus in the spring. These changes ultimately resulted in facility modification tasks being accomplished based on rates and milestones produced by section leaders and not in accordance with the initially proposed timeline. Although the actual

completion dates are sporadic when compared with the initial proposal, this aspect of the project proceeded at or ahead of schedule in each section with respect to the evolving timelines produced by section leaders.

6.2 Project Budget

The team developed a detailed budget for the project to determine how much funding would be necessary in addition to deciding how much each section would be provided to spend on upgrades to the thermosiphon. As shown in table 15, the total amount from each section's required budget and spending equals $10,842.91. This included funds for a large variety of instruments, construction materials, and other project expenses as detailed in the expense summary below. Notably, this is significantly increased from original budgetary predictions, which totaled approximately $7,000.00. This increase is in response to significant additional funds becoming available for use in instrumentation purchases, freeing up existing funds for the use of higher quality materials for instrumentation, system component upgrades, and greater flexibility in the redesign of these components.

Table 15: Summary of Project Expenses

Item	Unit Cost	Quantity	Total Cost
Collector Modifications			***$ 2,520.00***
Winch	$ 110.00	1	$ 110.00
Pulleys	$ 20.00	4	$ 80.00
Cable	$ 30.00	1	$ 30.00
Lumber	$ 100.00	-	$ 100.00
Hardware & Fasteners	$ 20.00	-	$ 20.00
Cordless Hand Drill	$ 80.00	1	$ 80.00
VARIACs	$ 500.00	3	$ 1,500.00
Heat Tapes	$ 200.00	3	$ 600.00
Tubing Modifications			***$ 133.24***
FIP Brass Coupler	$ 7.18	1	$ 7.18

FIP Brass Reducer	$ 8.30	1	$ 8.30
MIP to Hose Brass Adapter	$ 4.39	1	$ 4.39
FIP Brass Reducer	$ 6.59	1	$ 6.59
Pipe Elbow Insulation	$ 3.28	4	$ 13.12
Pipe Tee Insulation	$ 3.68	2	$ 7.36
Pipe Insulation	$ 2.48	1	$ 2.48
Pipe Insulation	$ 2.98	3	$ 8.94
Pipe Insulation	$ 2.78	1	$ 2.78
CPVC to PEX Adapter	$ 7.61	2	$ 15.22
PEX Brass Elbow	$ 4.29	2	$ 8.58
Reinforced Vinyl Hose	$ 22.39	1	$ 22.39
Rubber Heater Hose	$ 25.91	1	$ 25.91
Reservoir Modifications			***$ 195.71***
Lead Screw	$ 24.25	1	$ 24.25
Treated Lumber	$ 10.57	8	$ 84.56
Grease	$ 10.00	1	$ 10.00
Set Screws	$ 3.07	1	$ 3.07
Rods	$ 6.48	4	$ 25.92
Bolts	$ 0.42	8	$ 3.36
Nuts	$ 0.13	8	$ 1.04
1/8 plate steel (4 inch by 5 inch)	$ 3.00	4	$ 12.00
1/8 plate steel (4 inch by 5 inch)	$ 2.10	4	$ 8.40
Rectangular Steel Bar	$ 11.49	2	$ 22.98
Nuts	$ 2.68	2	$ 5.36
Bottom Bearing	$ 4.88	1	$ 4.88
Bottom Bearing	$ 4.25	1	$ 4.25
Top Bearing	$ 5.78	2	$ 11.56
Enclosure Modifications & Active Cooling System			***$ 786.77***
Heat Exchanger	$ 209.00	1	$ 209.00
Fan	$ 100.00	1	$ 100.00
Pump	$ 139.00	1	$ 139.00
Rubber Tubing	$ 10.00	2	$ 20.00
Air Separator	$ 150.00	1	$ 150.00
Vent Fan	$ 15.35	1	$ 15.35
Wire	$ 25.00	1	$ 25.00
Switch	$ 3.97	2	$ 7.94

3 Wire Plug	$ 2.99	2	$ 5.98
CPVC Pipe	$ 5.12	2	$ 10.24
CPVC Pipe Fittings	$ 50.00	1	$ 50.00
CPVC Cutting Ratchet	$ 13.98	1	$ 13.98
CPVC Bond	$ 5.49	1	$ 5.49
Fender Washer	$ 3.84	3	$ 11.52
Screws	$ 3.59	3	$ 10.77
Hinge	$ 12.50	1	$ 12.50
Instrumentation			***$ 6,487.19***
DAQ Board	$ 1,500.00	1	$ 1,500.00
Additional Rheotherm	$ 4,100.00	1	$ 4,100.00
Rheotherm Calibration	$ 750.00	-	$ 750.00
Resistors	$ 7.00	2	$ 14.00
Capacitors	$ 8.00	1	$ 8.00
Screw Terminal Block	$ 8.00	1	$ 8.00
Threaded Thermistors	$ 11.51	3	$ 34.53
Straight Probe Thermistors	$ 12.11	6	$ 72.66
General Expenses			***$ 720.00***
NCUR Registration	$ 180.00	4	$ 720.00
Total Expenses			**$ 10,842.91**

As shown in table 16, the team received more than originally expected form multiple university sources. The proposal for the first of these, the CECS Dean's Office, was submitted on September 25, 2020. This proposal included a request for $3,000 dollars and, of the requested amount, $2,500 was provided. Another source of funding, the Student Government Association also awarded $4,050.00. The most significant funding impact on the project budget was the availability of additional funds from the CECS Dean's Office in the early spring specifically for use in purchasing instrumentation, which more than fulfilled the remaining budgetary requirements of the project and eliminated the need to request funds from the Student Government Association.

Table 16: Summary of Project Funding

Description	Amount Proposed	Amount Received
UE CECS Dean's Office, General	$3,000.00	$2,500.00
UE CECS Dean's Office, Instrumentation	$0.00	$6,350.00
UE Academic Fund Board (AFB)	$4,050.00	$4,050.00
UE Student Government Association (SGA)	$1,400.00	$0.00
Total Funding	**$8,450.00**	**$12,900.00**

Because the team was ultimately able to acquire more funding than originally expected, each modification section has plenty of funds to do the necessary updates. This helps provide a better working system for the future and a more optimal way of adjusting parameters.

7 Conclusion

As a result of the completed research, clear correlations were established between improved efficiency and reduced collector angles, reduced energy input, increased ambient temperatures, and increased hot leg heights. In the case of collector angle variations, this correlation was found to exist for both constant power and variable power contexts, indicating that the power loss effects associated with deviations from the reference angle are insignificant relative to the effects of collector angle as an isolated parameter. Through analysis of collector outlet temperatures, it was also found that heat loss to the ambient, which would traditionally be assumed to decrease efficiency and be associated with high collector temperatures, is similarly insignificant for a system which is sufficiently insulated. Both constant power and variable power testing produced seemingly local maximum efficiency at moderate angles, with these being more prominent in variable power testing and clearly associated with a local maximum in

flow rate in those cases. Further research into low and moderate collector angles at varying reference angles would be necessary to conclusively identify the relationship between this local maximum and the efficiencies associated with low collector angles. The stated trends variable ambient temperature and variable hot leg height testing confirm existing theories and are logically explained by conventional heat transfer and fluid mechanical concepts.

Due to schedule changes which resulted in extended base case testing, system modifications are currently underway and scheduled for completion in the near future. This includes designs which improved variability and ease of use for the collector frame and tank height, higher resilience in tubing components, and more rapid cooling capabilities for both ambient air and system fluid. The performed upgrades to data collection apparatus and the calibration of temperature and flow rate measurement instruments allows for greater data precision in future years and the potential expansion of the project scope into further research areas.

References

[1] L. A. Hoffman and T. T. Ngo, "Affordable Solar Thermal Water Heating Solution," *Renewable Energy,* vol. 115, pp. 1220-1230, 2018.

[2] K. S, "Thermal Performance, Economic and Environmental Life Cycle Analysis of Thermosiphon Solar Water Heaters," *Solar Energy,* pp. 39-48, 2009.

[3] T. Zhang, "Experimental Study on Forced Circulation Loop Thermosiphon Solar Water Heating System," *International Journal of Photoenergy,* no. May, pp. 1-12, 2018.

[4] K. S, "Solar Thermal Collectors and Applications," *Progress in Energy and Combustion Science,* pp. 231-295, 2004.

[5] Z. Wang, W. Yang, F. Qiu, X. Zhang and X. Zhao, "Solar Water Heating: From Theory, Application, Marketing and Research," *Renewable and Sustainable Energy Reviews,* pp. 68-84, 2015.

[6] K. Alsawaf, N. Gautam, R. Hendrix, P. Kirkey, E. Krouse, N. Regoli, T. Schulz and U. Shrestha, "Thermosiphon Research Project," University of Evansville, Evansville, 2019.

[7] R. Hendrix, U. Shrestha, T. Schulz, B. Key, J. Smith, N. Hemmersbach, N. Gibson, K. Herrin, B. Herrin, J. Hagler and S. Subhash, "Thermosiphon Research Project," University of Evansville, Evansville, 2020.

[8] Hamad, G. R. Saraf and F. A. Wahab, "Optimum Tilt Angle for a Flat Plate Solar Collector," in *Energy Conversion and Management*, 1988, pp. 185-191.

[9] J. Bracamonte, J. Parada, J. Dimas and M. Baritto, "Effect of the Collector Tilt Angle on Thermal Efficiency and Stratification," 2015.

[10] S. A. Kalogirou, "Flat-Plate Collector Construction and System Configuration to Optimize," 2013.

[11] H. A. Ekadewi, I. Djatmiko and Prabowo, "The Optimal Tilt Angle of a Solar Collector," *Elsevier BV,* vol. 32, 2013.

[12] Fluke, "8808A Digital Multimeter Users Manual," July 2007. [Online]. Available: https://www.fluke-direct.com/pdfs/cache/www.fluke-direct.com/fluke/multimeter/8808a/manual/fluke_8808a_multimeter_manual.pdf. [Accessed 15 April 2021].

[13] National Instruments, "Device Specifications: NI 6221 (37-Pin)," 16 June 2016. [Online]. Available: https://www.ni.com/pdf/manuals/375201c.pdf. [Accessed 15 April 2021].

[14] W. Riley, L. Sturges and D. Morris, Mechanics of Materials, 6th ed., Hoboken: John Wiley & Sons, 2007.

[15] D. G. R. William D. Callister Jr., Materials Science: An Introduction, 10th Edition ed., Hoboken, NJ: John Wiley & Sons, 2018.

[16] F. D. J. H. L. H. Erik Oberg, Machinery's Handbook: A Reference Book for the Mechanical Engineer, Draftsman, Toolmaker and Machinist, 20th Edition ed., P. B. Schubert, Ed., New York, NY: Industrial Press Inc., 1976.

[17] I. Standard, ISO 18265, 2003.

[18] ASTM, E18-15, West Conshohocken, PA: ASTM International, 2015.

[19] ASTM, E10-14, West Conshohocken, PA: ASTM International, 2014.

[20] ASME, *PTC 19.1 Test Uncertainty,* 2005.

[21] T. B. I. Eugene A. Avallone, Mark's Standard Handbook for Mechanical Engineers, 9th Edition ed., New York: McGraw-Hill Inc., 1987.

[22] J. W. Daniel A. Brandt, Metallurgy Fundamentals: Ferrous and Nonferrous, 6th Edition ed., Tilney Park, IL: The Goodheart-Willcox Company, Inc., 2021.

Appendix A

Procedure & Conceptual Training Confirmation Form

Thermosiphon Project 2020-'21

Training Check

Team leader conducting check: _____

Team member being checked: _____

Other testers: _____

Test Index: _____ Check Date: _____

Testing Procedure Check

Prepare Test

- ☐ Turn on computer & initiate LabView software
- ☐ Apply tank & collector insulation
- ☐ Set & record collector angle
- ☐ Set & record hot leg height
- ☐ Heat and/or cool & mix fluid to goal temperature
- ☐ Heat and/or cool ambient to goal temperature

Initiate Test

- ☐ Decide to start test when appropriate
- ☐ Set & record initial VARIAC voltages
- ☐ Record ambient & collector inlet temperatures
- ☐ Initiate LabView data collection
- ☐ Record test start time

Run Test

- ☐ Check & record VARIAC voltages & ambient temperatures every 10 minutes

Finish Test

- ☐ Decide to end test when appropriate
- ☐ Stop LabView data collection
- ☐ Rename, save, & upload data file
- ☐ Remove tank & collector insulation
- ☐ Converge fluid temperatures
- ☐ Record test end time & complete test data sheet
- ☐ Shut off computer & power sources
- ☐ Unplug all instruments

Data Analysis Check

- ☐ Access computer with MATLAB
- ☐ Download data analysis files (if not already downloaded)
- ☐ Download test data file
- ☐ Open data analysis file & run script
- ☐ Access data review spreadsheet
- ☐ Input results into data review spreadsheet

Concept Check

- ☐ How does the thermosiphon work?
- ☐ What is the purpose of a thermosiphon?
- ☐ What are the objectives of our research?

Other Questions

1. _____

   _____

2. _____

   _____

3. _____

   _____

Notes

_____

_____

_____

Appendix B

MATLAB Data Analysis Script

```
%************************************************************************
%
% PROGRAM FILE NAME:
% ThermosiphonResearchMK6MOD1.m
%
% Added from previous version:
% Uncertainty calculations updated. Spring 2018 calibration curves added.
%
% PREVIOUS MODS SHOULD NOT BE USED
%
% Created by:
% Philip Lax
% Justin Kahle
% Ryan DeHoff
%
% DATE REVISED: 25 March 2018
%
%************************************************************************

clear all
close all
clc
format long

R = {[11.708 11.699 11.702 11.776 11.775 11.794 11.803 11.858 11.838 ...
    11.762 11.778 11.956 12.068 11.802 11.727 11.709 11.700 11.698 ...
    11.760 11.703 11.686 11.663 11.660 11.658 11.703 11.695 11.685 ...
    11.681 11.681 11.829 11.645],[11.980 11.978 11.977 11.976 11.975 ...
    11.975 11.974 11.974 11.973 11.972 11.972 11.972 11.972 11.971 ...
    11.971 11.971 11.970 11.970 11.970 11.971 11.970 11.970 11.970 ...
    11.969 11.968 11.968 11.967 11.966 11.966 11.966 11.966],[12.549 ...
    12.883 12.845 12.834]};

    fprintf('--- INPUT #1 ----------------------------\n\n')
fprintf('What power level was used for this test?\n  "0" for LOW (37 V)\n  "1" for HIGH (50 V)\n  "2" for
        OTHER\n');
powerlevel = input('Power Level: ');
fprintf('\n');

if powerlevel == 0
    V = {[37.18 37.07 37.1 37.23 37.21 37.23 37.24 37.26 37.26 37.29 37.24 ...
    37.15 37.35 37.36 37.38 37.36 37.35 37.15 37.17 37.12 37.1 37.05 ...
    37.14 37.11 37.33 37.34 37.42], [37.68 37.45 37.66 37.69 37.44 37.38 ...
    37.32 37.65 37.71 37.41 37.84 37.35 37.38 37.27 37.21 37.24 37.32 ...
    37.23 37.5 37.38 37.35 37.36 37.27 37.3 37.37 37.42 37.4], [37.69 ...
    37.58 37.6 37.11 37.12 37.19 37.19 37.16 37.19 37.2 37.16 37.11 ...
    37.15 37.12 37.34 37.13 37.12 37.28 37.41 37.21 37.05 37.09 37.00 ...
```

```
    37.35 37.09 37.01 37.05]};
elseif powerlevel == 1
    V = {[50.04 50.10 50.05 50.14 49.96 49.99 50.07], [50.35 50.27 50.30 50.40 50.29 ...
    50.34 50.38], [50.04 50.10 50.15 50.00 49.95 49.91 50.13]};
elseif powerlevel == 2
    fprintf('--------------------------------------\n\n')
    for k = 1:3
            fprintf(['Input voltage checks for VARIAC #' num2str(k) '\n'])
        for j = 1:10
            V(k,j) = input(['   Check #' num2str(j) ': ']);
        end
            fprintf('\n')
    end
    V = {[V(1,:)], [V(2,:)], [V(3,:)]};
end

% V = {[51.429 51.427 51.409 51.417 51.501 51.438 51.422 51.425 51.43 ...
%       51.428 51.4 51.397 51.4 51.396 51.389 51.398 51.46 51.398 51.391 ...
%       51.404 51.551 51.421 51.395 51.404 51.406 51.375 51.395 51.403 ...
%       51.46 51.435],[49 49 49.1],[50 50 50.1]};
%
% V = {[49.86 49.88], [49.03 50], [50 50.10]};

% Heat Tape Voltage and Resistance Inputs

R1 = mean(R{1});
R2 = mean(R{2});
R3 = mean(R{3});

    fprintf('--- INPUT #2 -----------------------------\n\n')
fprintf('What were the VARIAC settings used for the test?\n');
V1 = input('VARIAC 1 (Volts): '); %37.24;
V2 = input('VARIAC 2 (Volts): '); %37.23;
V3 = input('VARIAC 3 (Volts): '); %37.46;
fprintf('\n');

% the power supplied is calculated
P = V1^2/R1+V2^2/R2+V3^2/R3;

filestart = 191;
fileend = 191;

% tempfunc undos the old thermistor calibration curve used in Labview that
% was solved for the wrong variable. tempfunc1 applies the new calibration
% curve solved for the correct variable
tempfunc = @(x) (x-0.7493)/0.9813;
% this line defines the correct collector outlet thermistor calibration
% formula
tempfunc1 = @(x) 1.0813*x -0.7262;

% Importing the LABVIEW files

% The number of %f's in this string corresponds to the number of columns of
% data in the LABVIEW files
```

```
formatSpec = '%f %f %f %f %f %f %f %f %f %f %f %f';
headers = 24;

labviewfiles = 1; % input('How many LabView files should be imported? ');

for n = 1:labviewfiles

    fprintf('--- INPUT #3 ----------\n\n')
        fprintf('What LabView file contains the test data?\n')
        labviewopened = fopen(input('File name: '));
        fprintf('\n')

        labviewtextscan = textscan(labviewopened,formatSpec,'Headerlines',headers,'Delimiter',' ');

        labviewopenedmat = cell2mat(labviewtextscan);

        sizemat = size(labviewopenedmat);

        % the offset is calculated based on the last time value of the most
        % recenctly imported file
        offset(n) = labviewopenedmat(sizemat(1),1);

        % this for loop calculates the increment between each time value of
        % the most recently entered file
    for m = 1:sizemat(1)-1

            deltat(m) = labviewopenedmat(m+1,1) - labviewopenedmat(m,1);

    end

        % this for loop adds the labview files together. It skips the first
        % file, and for all other files it adds the sum of the offsets (the last
        % time value recorded from each file) and the average difference of the
        % second most recent file (so the first time value of the current matrix
        % is not the same as the last time value of the previous matrix)
    if n == 1

    else
         for m = 1:sizemat(1)

                % for all labview files besides the first one, the previous
                % matrix final time and the average time increment is added to
                % each time value
                labviewopenedmat(m,1) = labviewopenedmat(m,1) + sum(offsetold) + diff(n-1);

         end
    end

        %The most recent file's matrix is compiled in the column of one cell
        labviewcell{n,1} = labviewopenedmat;

        %The previously calculated increments are averaged for use with the
        %next imported file
        diff(n)  =  sum(deltat(sizemat(1)-1)/(sizemat(1)-1));
```

```
        %offsetold is the last value of time for the current matrix and all
        %previous ones, which will be summed and added to the time values for
        %the next file entered
        offsetold(n) = offset(n);

end

%the labview files that were combiled in one large cell in the previous for
%loop are now converted to one large matrix
labviewmat = cell2mat(labviewcell);

sizelabview = size(labviewmat);

Time = 1;
CollectorIn = 2;
CollectorOut = 3;
Rheotherm = 4;
TankTop = 5;
TankMiddle = 6;
TankBottom = 7;
HotLegTop = 8;
Valve = 9;
Variac1 = 10;
Variac2 = 11;
Variac3 = 12;

for n = 1:sizelabview(1)

    if labviewmat(n,Rheotherm) <= 0.01

        labviewmat(n,Rheotherm) = NaN;

    else
    end

    labviewmat(n,Rheotherm) = labviewmat(n,Rheotherm)*((3.7854e-3)/60); %converts gpm to m^3/s

end

%this for loop finds the actual collector outlet temperature using the
%modified thermistor calibration curve formula
for n = 1:sizelabview(1)
    labviewmat(n,CollectorOut) = tempfunc1(tempfunc(labviewmat(n,CollectorOut)));
end

%%%% Spring 2018 Calibration Curves %%%%

labviewmat(:,CollectorIn) = 1.00133132127585*labviewmat(:,CollectorIn) - 0.0325448811333828;
labviewmat(:,HotLegTop) = 1.00077041602465*labviewmat(:,HotLegTop) + 0.0281972265023001;
labviewmat(:,CollectorOut) = 1.02802155626073*labviewmat(:,CollectorOut) - 0.642525079068641;
labviewmat(:,TankTop) = 0.987192289413568*labviewmat(:,TankTop) + 0.814619126700308;
labviewmat(:,TankMiddle) = 0.993945251644034*labviewmat(:,TankMiddle) - 0.175431267889266;
labviewmat(:,TankBottom) = 0.993945251644034*labviewmat(:,TankBottom) - 0.175431267889266;
```

```
%%%%%%%%%%%%%%%%%%%%%%%%%%%%%%%%%%%%%%%%

etafiltered = 0;
counteretafiltered = 0;
Thermistors = {[TankTop],[TankMiddle],[TankBottom],[CollectorOut],[CollectorIn]};
sizetherm = 5;

T_Cout_Set = labviewmat(:,CollectorOut);
T_Cout_Mean = mean(T_Cout_Set,'omitnan');
T_Cin_Set = labviewmat(:,CollectorIn);
T_Cin_Mean = mean(T_Cin_Set,'omitnan');
T_Cout_Rand_u = std((T_Cout_Set)/sqrt(size(T_Cout_Set,1)),'omitnan');
T_Cin_Rand_u = std((T_Cin_Set)/sqrt(size(T_Cin_Set,1)),'omitnan');

T_C_Rand_Avg =(T_Cout_Rand_u+T_Cin_Rand_u)/2;

rhoPlus_Rand = DensityMK1MOD3(T_Cin_Mean+T_C_Rand_Avg);
rhoMinus_Rand = DensityMK1MOD3(T_Cin_Mean-T_C_Rand_Avg);
rho_Rand_u = abs((rhoPlus_Rand-rhoMinus_Rand)/2);

cPlus_Rand = (SpecificHeatMK1MOD3(T_Cout_Mean+T_C_Rand_Avg) +
        SpecificHeatMK1MOD3(T_Cin_Mean+T_C_Rand_Avg))/2;
cMinus_Rand = (SpecificHeatMK1MOD3(T_Cout_Mean-T_C_Rand_Avg) + SpecificHeatMK1MOD3(T_Cin_Mean-
        T_C_Rand_Avg))/2;
c_Rand_u = abs((cPlus_Rand-cMinus_Rand)/2);

for n = 1:sizelabview(1)

    %Efficiency calculation are performed with use of the Density and
    %SpecificHeat  functions

    for m = 1:sizetherm

        if labviewmat(n,Thermistors{m}) > 100 || labviewmat(n,Thermistors{m}) < 0
            labviewmat(n,Thermistors{m}) = NaN;
        else
        end
    end

    %the instantaneous density through the collector is calculated
    rho(n,1) = DensityMK1MOD3(labviewmat(n,CollectorIn));

    rhoPlus_Sys = DensityMK1MOD3(labviewmat(n,CollectorIn)+0.1);
    rhoMinus_Sys = DensityMK1MOD3(labviewmat(n,CollectorIn)-0.1);
    rho_Sys_u_Set(n,1) = abs((rhoPlus_Sys-rhoMinus_Sys)/2);

    %the average specific heat of water through the collector is calculated
    c(n,1) = (SpecificHeatMK1MOD3(labviewmat(n,CollectorOut)) +
        SpecificHeatMK1MOD3(labviewmat(n,CollectorIn)))/2;

    cPlus_Sys = (SpecificHeatMK1MOD3(labviewmat(n,CollectorOut)+0.1) +
        SpecificHeatMK1MOD3(labviewmat(n,CollectorIn)+0.1))/2;
```

```
    cMinus_Sys = (SpecificHeatMK1MOD3(labviewmat(n,CollectorOut)-0.1) +
        SpecificHeatMK1MOD3(labviewmat(n,CollectorIn)-0.1))/2;
    c_Sys_u(n,1) = abs((cPlus_Sys-cMinus_Sys)/2);

    %the change in temp across the collector is calculated
    deltaT = labviewmat(n,CollectorOut) - labviewmat(n,CollectorIn);

    %the flowrate data point is extracted for convenience
    Vdot = labviewmat(n,Rheotherm);

    %the instantaneous efficiency is calculated
    eta(n,1) = (rho(n,1)*Vdot*c(n,1)*deltaT)/P;

end

rho_Mean = mean(rho,'omitnan');
rho_Sys_u_Mean = mean(rho_Sys_u_Set,'omitnan');
c_Mean = mean(c,'omitnan');
c_Sys_u_Mean = mean(c_Sys_u,'omitnan');

%The average collector efficiency is calculated

counterintegral = 1;

for n = 1:sizelabview(1)-1

    if isnan(eta(n+1,1)) == 0 && isnan(eta(n,1)) == 0

        trapezoideta(counterintegral) = (labviewmat(n+1,Time)-labviewmat(n,Time))*((eta(n+1,1)+eta(n,1))/2);
        counterintegral = counterintegral + 1;

    else
    end

end

etaave = sum(trapezoideta)/(labviewmat(sizelabview(1),Time)-labviewmat(1,Time));

%the average value of eta is printed to the command window
    fprintf('----- GENERAL RESULTS ---------------------- \n\n')
fprintf('Avg. collector efficiency = %f%%\n',etaave*100)

V_Flow_Set = labviewmat(:,Rheotherm);
V_Flow_Mean = mean(V_Flow_Set,'omitnan');

V_Flow_Rand_u = std((V_Flow_Set)/sqrt(size(V_Flow_Set,1)),'omitnan');
V_Flow_Sys_u = 0.01*V_Flow_Mean/2;
V_Flow_Sensitivity = (rho_Mean*c_Mean*(T_Cout_Mean-T_Cin_Mean))/(V1^2/R1+V2^2/R2+V3^2/R3);
V_Flow_Sys_Contribution = (V_Flow_Sys_u*V_Flow_Sensitivity)^2;
V_Flow_Rand_Contribution = (V_Flow_Rand_u*V_Flow_Sensitivity)^2;

T_Cout_Sys_u = 0.1;
T_Cout_Sensitivity = (V_Flow_Mean*rho_Mean*c_Mean)/(V1^2/R1+V2^2/R2+V3^2/R3);
T_Cout_Sys_Contribution = (T_Cout_Sys_u*T_Cout_Sensitivity)^2;
```

```
T_Cout_Rand_Contribution   =   (T_Cout_Rand_u*T_Cout_Sensitivity)^2;

T_Cin_Sys_u = 0.1;
T_Cin_Sensitivity = -(V_Flow_Mean*rho_Mean*c_Mean)/(V1^2/R1+V2^2/R2+V3^2/R3);
T_Cin_Sys_Contribution = (T_Cin_Sys_u*T_Cin_Sensitivity)^2;
T_Cin_Rand_Contribution   =   (T_Cin_Rand_u*T_Cin_Sensitivity)^2;

V1_Sys_u = ((0.002*mean(V{1}))+(0.0005*200))/2;
V1_Rand_u = std(V{1})/sqrt(length(V{1}));
V1_Sensitivity = -2*(V_Flow_Mean*rho_Mean*c_Mean*(T_Cout_Mean-
        T_Cin_Mean)*R1*V1*R2^2*R3^2)/((V1^2*R2*R3+V2^2*R1*R3+V3^2*R1*R2)^2);
V1_Sys_Contribution = (V1_Sys_u*V1_Sensitivity)^2;
V1_Rand_Contribution = (V1_Rand_u*V1_Sensitivity)^2;

V2_Sys_u = ((0.002*mean(V{2}))+(0.0005*200))/2;
V2_Rand_u = std(V{2})/sqrt(length(V{2}));
V2_Sensitivity = -2*(V_Flow_Mean*rho_Mean*c_Mean*(T_Cout_Mean-
        T_Cin_Mean)*R2*V2*R1^2*R3^2)/((V1^2*R2*R3+V2^2*R1*R3+V3^2*R1*R2)^2);
V2_Sys_Contribution = (V2_Sys_u*V2_Sensitivity)^2;
V2_Rand_Contribution = (V2_Rand_u*V2_Sensitivity)^2;

V3_Sys_u = ((0.002*mean(V{3}))+(0.0005*200))/2;
V3_Rand_u = std(V{3})/sqrt(length(V{3}));
V3_Sensitivity = -2*(V_Flow_Mean*rho_Mean*c_Mean*(T_Cout_Mean-
        T_Cin_Mean)*R3*V3*R1^2*R2^2)/((V1^2*R2*R3+V2^2*R1*R3+V3^2*R1*R2)^2);
V3_Sys_Contribution = (V3_Sys_u*V3_Sensitivity)^2;
V3_Rand_Contribution = (V3_Rand_u*V3_Sensitivity)^2;

R1_Sys_u = ((0.0003*mean(R{1}))+(0.00004*200))/2;
R1_Rand_u = std((R{1}))/sqrt(length((R{1})));
R1_Sensitivity = (V_Flow_Mean*rho_Mean*c_Mean*(T_Cout_Mean-
        T_Cin_Mean)*V1^2*R2^2*R3^2)/((V1^2*R2*R3+V2^2*R1*R3+V3^2*R1*R2)^2);
R1_Sys_Contribution = (R1_Sys_u*R1_Sensitivity)^2;
R1_Rand_Contribution   =   (R1_Rand_u*R1_Sensitivity)^2;

R2_Sys_u = ((0.0003*mean(R{2}))+(0.00004*200))/2;
R2_Rand_u = std(R{2})/sqrt(length(R{2}));
R2_Sensitivity = (V_Flow_Mean*rho_Mean*c_Mean*(T_Cout_Mean-
        T_Cin_Mean)*R1^2*V2^2*R3^2)/((V1^2*R2*R3+V2^2*R1*R3+V3^2*R1*R2)^2);
R2_Sys_Contribution = (R2_Sys_u*R2_Sensitivity)^2;
R2_Rand_Contribution   =   (R2_Rand_u*R2_Sensitivity)^2;

R3_Sys_u = ((0.0003*mean(R{3}))+(0.00004*200))/2;
R3_Rand_u = std(R{3})/sqrt(length(R{3}));
R3_Sensitivity = (V_Flow_Mean*rho_Mean*c_Mean*(T_Cout_Mean-
        T_Cin_Mean)*R1^2*R2^2*V3^2)/((V1^2*R2*R3+V2^2*R1*R3+V3^2*R1*R2)^2);
R3_Sys_Contribution = (R3_Sys_u*R3_Sensitivity)^2;
R3_Rand_Contribution = (R3_Rand_u*R3_Sensitivity)^2;

c_Sensitivity = (V_Flow_Mean*rho_Mean*(T_Cout_Mean-T_Cin_Mean))/(V1^2/R1+V2^2/R2+V3^2/R3);
c_Sys_Contribution = (c_Sys_u_Mean*c_Sensitivity)^2;
c_Rand_Contribution   =   (c_Rand_u*c_Sensitivity)^2;

rho_Sensitivity   =   (V_Flow_Mean*c_Mean*(T_Cout_Mean-T_Cin_Mean))/(V1^2/R1+V2^2/R2+V3^2/R3);
```

```
rho_Sys_Contribution = (rho_Sys_u_Mean*rho_Sensitivity)^2;
rho_Rand_Contribution = (rho_Rand_u*rho_Sensitivity)^2;

%Total Uncertainty Calculations
Efficiency_Calc = etaave; %(V_Flow_Mean*rho*c*(T_Cout_Mean-T_Cin_Mean))/(V1^2/R+V2^2/R+V3^2/R);
Sys_R = sqrt(V_Flow_Sys_Contribution + T_Cout_Sys_Contribution + T_Cin_Sys_Contribution +
        V1_Sys_Contribution + V2_Sys_Contribution + V3_Sys_Contribution + R1_Sys_Contribution +
        R2_Sys_Contribution + R3_Sys_Contribution + c_Sys_Contribution + rho_Sys_Contribution);
Rand_R = sqrt(V_Flow_Rand_Contribution + T_Cout_Rand_Contribution + T_Cin_Rand_Contribution +
        V1_Rand_Contribution + V2_Rand_Contribution + V3_Rand_Contribution + R1_Rand_Contribution +
        R2_Rand_Contribution + R3_Rand_Contribution + c_Rand_Contribution + rho_Rand_Contribution);

u_R = sqrt((Sys_R)^2+(Rand_R).^2);
U_R95 = 2*u_R*100;

xunc = [1:14];
yunc =
        100*[R1_Sys_Contribution+R2_Sys_Contribution+R3_Sys_Contribution,R1_Rand_Contribution+R2_Rand_Contri
        bution+R3_Rand_Contribution,rho_Sys_Contribution,rho_Rand_Contribution, ...
    V_Flow_Sys_Contribution,V_Flow_Rand_Contribution,c_Sys_Contribution, ...
    c_Rand_Contribution,T_Cin_Sys_Contribution,T_Cin_Rand_Contribution,T_Cout_Sys_Contribution, ...

        T_Cout_Rand_Contribution,V1_Sys_Contribution+V2_Sys_Contribution+V3_Sys_Contribution,V1_Rand_Contrib
        ution+V2_Rand_Contribution+V3_Rand_Contribution]*(1/(Sys_R^2+Rand_R^2));

fprintf('Uncertainty = %f%%\n\n',U_R95)

t = labviewmat(:,Time)/60; %sec to min
Cout = labviewmat(:,CollectorOut);
Cin = labviewmat(:,CollectorIn);
deltaTcollector = labviewmat(:,CollectorOut) - labviewmat(:,CollectorIn);
Flowrate = labviewmat(:,Rheotherm)*(60/(3.7854e-3)); %m^3/s to gal/min
Tbottom = labviewmat(:,TankBottom);
Tmiddle = labviewmat(:,TankMiddle);
Ttop = labviewmat(:,TankTop);
valveclosure = labviewmat(:,Valve);

%Plot of temperature difference across the collector as a function of time
figure(1)
plot(t,deltaTcollector,'.')
xlabel('Time (min)')
ylabel('Temperature Difference Across Collector (C)')
title('Temperature Difference vs. Time')
grid on
grid minor

%Plot of flowrate as a function of time
figure(2)
plot(t,Flowrate,'.')
xlabel('Time (min)')
ylabel('Flowrate (gal/min)')
title('Flowrate vs. Time')
grid on
grid minor
```

```
%Plot of flowrate and temperature difference across the collector as a
%function of time
figure(3)
yyaxis left
plot(t,Flowrate,'.')
xlabel('Time (min)')
ylabel('Flowrate (gal/min)')
yyaxis right
plot(t,deltaTcollector,'.')
ylabel('Temperature Difference Across Collector (C)')
legend('Flowrate','Temperature Difference Across Collector')
title('Flowrate and Temperature Difference vs. Time')
grid on
grid minor

%Plot of the tank temperatures as a function of time
figure(4)
plot(t,Ttop,'.',t,Tmiddle,'.',t,Tbottom,'.')
xlabel('Time (min)')
ylabel('Temperature (C)')
legend('Tank Top','Tank Middle','Tank Bottom')
title('Tank Temperatures vs. Time')
grid on
grid minor

figure(5)
yyaxis left
plot(t,valveclosure,'.b')
xlabel('Time (min)')
ylabel('Valve Closure (%)')
yyaxis right
plot(t,Flowrate,'.r')
ylabel('Flowrate (gal/min)')
legend('Valve Closure','Flowrate')
title('Valve Closure and Flowrate Vs. Time')
grid on
grid minor

%Plot of all temperatures as a function of time
figure(6)
plot(t,Ttop,'.',t,Tmiddle,'.',t,Tbottom,'.',t,Cin,'.',t,Cout,'.')
xlabel('Time (min)')
ylabel('Temperature  (C)')
legend('Tank Top','Tank Middle','Tank Bottom','Collector In','Collector Out')
title('System Temperatures vs. Time')
grid on
grid minor

%Plot of instantaneous efficiency as a function of time
figure(7)
plot(t,eta(:,1),'.')
xlabel('Time (min)')
ylabel('Instantaneous  Efficiency')
```

```
title('Instantaneous Efficiency vs. Time')
grid on
grid minor

%Plot of flowrate and efficiency vs time
figure(8)
yyaxis left
plot(t,eta,'.b')
xlabel('Time (min)')
ylabel('Efficiency')
yyaxis right
plot(t,Flowrate,'.r')
ylabel('Flowrate (gal/min)')
legend('Efficiency','Flowrate')
title('Efficiency and Flowrate Vs. Time')
grid on
grid minor

%Plot of temp diff across collector and efficiency vs time
figure(9)
yyaxis left
plot(t,eta,'.b')
xlabel('Time (min)')
ylabel('Efficiency')
yyaxis right
plot(t,deltaTcollector,'.r')
ylabel('Temperature Difference Across Collector (C)')
legend('Efficiency','Temperature Difference Across Collector')
title('Efficiency and Temperature Difference Across Collector Vs. Time')
grid on
grid minor

figure(10)
bar(xunc,yunc,'w','LineStyle','-','BarWidth',0.4,'Linewidth',4)
set(gca,'XTickLabel',{'R Sys', 'R Rand', ...
    'Rho Sys','Rho Rand','F Sys', ...
    'F Rand','Cp Sys','Cp Rand','Tin Sys', ...
    'Tin Rand','Tout Sys','Tout Rand','V Sys', ...
    'V Ran'},'FontSize',18)
xlabel('Components of Uncertainty')
xtickangle(90)
ylabel('Percent Contribution to Total Uncertainty')

graphcounter = 10;

    fprintf('----------------------------------------\n\n')
fprintf('Would you like to analyze specific time range?\n  "0" for NO, END\n  "1" for YES, CONTINUE\n')
tester1 = input('Answer: ');
fprintf('\n')

if tester1 == 0 || 1
else
    error('You have entered an invalid input. The options are 0 to end code or 1 to calculate system efficiency for
        a specific time range')
```

```
end

while tester1 == 1

    eta = 0;
    t = 0;
    Flowrate = 0;
    deltaTcollector = 0;
    etafilteredn = 0;
    counteretafilteredn = 0;
    fprintf('--- INPUT #4----------\n\n')
    fprintf('What time range do you want to analyze?\n')
    lowertime = input('Lower time value (min): ')*60; %min to sec
    uppertime = input('Upper time value (min): ')*60; %min to sec
    fprintf('\n')

    countereta = 1;

    V_Flow_Set = labviewmat(:,Rheotherm);
    T_Cout_Set = labviewmat(:,CollectorOut);
    T_Cin_Set = labviewmat(:,CollectorIn);
    T_Cout_Mean = mean(T_Cout_Set,'omitnan');
    T_Cin_Mean = mean(T_Cin_Set,'omitnan');

    T_Cout_Rand_u = std((T_Cout_Mean)/sqrt(size(T_Cout_Set,1)),'omitnan');
    T_Cin_Rand_u = std((T_Cin_Mean)/sqrt(size(T_Cin_Set,1)),'omitnan');
    T_C_Rand_Avg =(T_Cout_Rand_u+T_Cin_Rand_u)/2;

    rhoPlus_Rand = DensityMK1MOD3(T_Cin_Mean+T_C_Rand_Avg);
    rhoMinus_Rand = DensityMK1MOD3(T_Cin_Mean-T_C_Rand_Avg);
    rho_Rand_u = abs((rhoPlus_Rand-rhoMinus_Rand)/2);

    cPlus_Rand = (SpecificHeatMK1MOD3(T_Cout_Mean+T_C_Rand_Avg) +
        SpecificHeatMK1MOD3(T_Cin_Mean+T_C_Rand_Avg))/2;
    cMinus_Rand = (SpecificHeatMK1MOD3(T_Cout_Mean-T_C_Rand_Avg) + SpecificHeatMK1MOD3(T_Cin_Mean-
        T_C_Rand_Avg))/2;
    c_Rand_u = abs((cPlus_Rand-cMinus_Rand)/2);

    for n = 1:sizelabview(1)

        if labviewmat(n,Time) >= lowertime && labviewmat(n,Time) <= uppertime

            %the average specific heat of water through the collector is calculated
            cn = (SpecificHeatMK1MOD3(labviewmat(n,CollectorOut)) +
        SpecificHeatMK1MOD3(labviewmat(n,CollectorIn)))/2;

            %the change in temp across the collector is calculated
            deltaTn = labviewmat(n,CollectorOut) - labviewmat(n,CollectorIn);

            %the flowrate data point is extracted for convenience
            Vdot = labviewmat(n,Rheotherm);

            %Uncertainty Data Sets
            rho(countereta,1) = DensityMK1MOD3(labviewmat(n,CollectorIn));
```

```
        rhoPlus_Sys = DensityMK1MOD3(labviewmat(n,CollectorIn)+0.1);
        rhoMinus_Sys = DensityMK1MOD3(labviewmat(n,CollectorIn)-0.1);
        rho_Sys_u_Set(countereta,1) = abs((rhoPlus_Sys-rhoMinus_Sys)/2);

        c(countereta,1) = (SpecificHeatMK1MOD3(labviewmat(n,CollectorOut)) +
    SpecificHeatMK1MOD3(labviewmat(n,CollectorIn)))/2;

        cPlus_Sys = (SpecificHeatMK1MOD3(labviewmat(n,CollectorOut)+0.1) +
    SpecificHeatMK1MOD3(labviewmat(n,CollectorIn)+0.1))/2;
        cMinus_Sys = (SpecificHeatMK1MOD3(labviewmat(n,CollectorOut)-0.1) +
    SpecificHeatMK1MOD3(labviewmat(n,CollectorIn)-0.1))/2;
        c_Sys_u(countereta,1) = abs((cPlus_Sys-cMinus_Sys)/2);

        %the instantaneous efficiency is calculated
        eta(countereta,1) = labviewmat(n,Time);
        eta(countereta,2) = (rho(n,1)*Vdot*c(n,1)*deltaTn)/P;
        eta(countereta,3) = n;
        t(countereta) = labviewmat(n,Time)/60;
        Flowrate(countereta) = labviewmat(n,Rheotherm)*(60/(3.7854e-3)); %m^3/s to gal/min
        deltaTcollector(countereta) = labviewmat(n,CollectorOut) - labviewmat(n,CollectorIn);

        countereta = countereta + 1;

    else
    end

end

rho_Mean = mean(rho,'omitnan');
rho_Sys_u_Mean = mean(rho_Sys_u_Set,'omitnan');
c_Mean = mean(c,'omitnan');
c_Sys_u_Mean = mean(c_Sys_u,'omitnan');

%Uncertainty  Calculations

V_Flow_Mean = mean(V_Flow_Set,'omitnan');

V_Flow_Rand_u = std((V_Flow_Set)/sqrt(size(V_Flow_Set,1)),'omitnan');
V_Flow_Sys_u = 0.01*V_Flow_Mean/2;
V_Flow_Sensitivity = (rho_Mean*c_Mean*(T_Cout_Mean-T_Cin_Mean))/(V1^2/R1+V2^2/R2+V3^2/R3);
V_Flow_Sys_Contribution = (V_Flow_Sys_u*V_Flow_Sensitivity)^2;
V_Flow_Rand_Contribution  =  (V_Flow_Rand_u*V_Flow_Sensitivity)^2;

T_Cout_Sys_u = 0.1;
T_Cout_Sensitivity = (V_Flow_Mean*rho_Mean*c_Mean)/(V1^2/R1+V2^2/R2+V3^2/R3);
T_Cout_Sys_Contribution = (T_Cout_Sys_u*T_Cout_Sensitivity)^2;
T_Cout_Rand_Contribution = (T_Cout_Rand_u*T_Cout_Sensitivity)^2;

T_Cin_Sys_u = 0.1;
T_Cin_Sensitivity = -(V_Flow_Mean*rho_Mean*c_Mean)/(V1^2/R1+V2^2/R2+V3^2/R3);
T_Cin_Sys_Contribution = (T_Cin_Sys_u*T_Cin_Sensitivity)^2;
T_Cin_Rand_Contribution  =  (T_Cin_Rand_u*T_Cin_Sensitivity)^2;
```

```
V1_Sys_u = (0.002*mean(V{1}))+(0.0005*200)/2;
V1_Rand_u = std(V{1})/sqrt(length(V{1}));
V1_Sensitivity = -2*(V_Flow_Mean*rho_Mean*c_Mean*(T_Cout_Mean-
    T_Cin_Mean)*R1*V1*R2^2*R3^2)/((V1^2*R2*R3+V2^2*R1*R3+V3^2*R1*R2)^2);
V1_Sys_Contribution = (V1_Sys_u*V1_Sensitivity)^2;
V1_Rand_Contribution = (V1_Rand_u*V1_Sensitivity)^2;

V2_Sys_u = ((0.002*mean(V{2}))+(0.0005*200))/2;
V2_Rand_u = std(V{2})/sqrt(length(V{2}));
V2_Sensitivity = -2*(V_Flow_Mean*rho_Mean*c_Mean*(T_Cout_Mean-
    T_Cin_Mean)*R2*V2*R1^2*R3^2)/((V1^2*R2*R3+V2^2*R1*R3+V3^2*R1*R2)^2);
V2_Sys_Contribution = (V2_Sys_u*V2_Sensitivity)^2;
V2_Rand_Contribution = (V2_Rand_u*V2_Sensitivity)^2;

V3_Sys_u = ((0.002*mean(V{3}))+(0.0005*200))/2;
V3_Rand_u = std(V{3})/sqrt(length(V{3}));
V3_Sensitivity = -2*(V_Flow_Mean*rho_Mean*c_Mean*(T_Cout_Mean-
    T_Cin_Mean)*R3*V3*R2^2*R1^2)/((V1^2*R2*R3+V2^2*R1*R3+V3^2*R1*R2)^2);
V3_Sys_Contribution = (V3_Sys_u*V3_Sensitivity)^2;
V3_Rand_Contribution = (V3_Rand_u*V3_Sensitivity)^2;

R1_Sys_u = ((0.0003*mean(R{1}))+(0.00004*200))/2;
R1_Rand_u = std(R{1})/sqrt(length(R{1}));
R1_Sensitivity = (V_Flow_Mean*rho_Mean*c_Mean*(T_Cout_Mean-
    T_Cin_Mean)*V1^2*R2^2*R3^2)/((V1^2*R2*R3+V2^2*R1*R3+V3^2*R1*R2)^2);
R1_Sys_Contribution = (R1_Sys_u*R1_Sensitivity)^2;
R1_Rand_Contribution  =  (R1_Rand_u*R1_Sensitivity)^2;

R2_Sys_u = ((0.0003*mean(R{2}))+(0.00004*200))/2;
R2_Rand_u = std(R{2})/sqrt(length(R{2}));
R2_Sensitivity = (V_Flow_Mean*rho_Mean*c_Mean*(T_Cout_Mean-
    T_Cin_Mean)*R1^2*V2^2*R3^2)/((V1^2*R2*R3+V2^2*R1*R3+V3^2*R1*R2)^2);
R2_Sys_Contribution = (R2_Sys_u*R2_Sensitivity)^2;
R2_Rand_Contribution  =  (R2_Rand_u*R2_Sensitivity)^2;

R3_Sys_u = ((0.0003*mean(R{3}))+(0.00004*200))/2;
R3_Rand_u = std(R{3})/sqrt(length(R{3}));
R3_Sensitivity = (V_Flow_Mean*rho_Mean*c_Mean*(T_Cout_Mean-
    T_Cin_Mean)*R1^2*R2^2*V3^2)/((V1^2*R2*R3+V2^2*R1*R3+V3^2*R1*R2)^2);
R3_Sys_Contribution = (R3_Sys_u*R3_Sensitivity)^2;
R3_Rand_Contribution = (R3_Rand_u*R3_Sensitivity)^2;

c_Sensitivity = (V_Flow_Mean*rho_Mean*(T_Cout_Mean-T_Cin_Mean))/(V1^2/R1+V2^2/R2+V3^2/R3);
c_Sys_Contribution = (c_Sys_u_Mean*c_Sensitivity)^2;
c_Rand_Contribution  =  (c_Rand_u*c_Sensitivity)^2;

rho_Sensitivity = (V_Flow_Mean*c_Mean*(T_Cout_Mean-T_Cin_Mean))/(V1^2/R1+V2^2/R2+V3^2/R3);
rho_Sys_Contribution = (rho_Sys_u_Mean*rho_Sensitivity)^2;
rho_Rand_Contribution  =  (rho_Rand_u*rho_Sensitivity)^2;

%Total Uncertainty Calculations
Sys_R = sqrt(V_Flow_Sys_Contribution + T_Cout_Sys_Contribution + T_Cin_Sys_Contribution +
    V1_Sys_Contribution + V2_Sys_Contribution + V3_Sys_Contribution + R1_Sys_Contribution +
    R2_Sys_Contribution + R3_Sys_Contribution + c_Sys_Contribution + rho_Sys_Contribution);
```

```
Rand_R = sqrt(V_Flow_Rand_Contribution + T_Cout_Rand_Contribution + T_Cin_Rand_Contribution +
    V1_Sys_Contribution + V2_Sys_Contribution + V3_Sys_Contribution + R1_Rand_Contribution +
    R2_Rand_Contribution + R3_Rand_Contribution + c_Rand_Contribution + rho_Rand_Contribution);

u_R = sqrt((Sys_R)^2+(Rand_R)^2);
U_R95 = 2*u_R*100;

xunc = [1:14];
yunc =
    100*[R1_Sys_Contribution+R2_Sys_Contribution+R3_Sys_Contribution,R1_Rand_Contribution+R2_Rand_Contri
    bution+R3_Rand_Contribution,rho_Sys_Contribution,rho_Rand_Contribution, ...
    V_Flow_Sys_Contribution,V_Flow_Rand_Contribution,c_Sys_Contribution, ...
    c_Rand_Contribution,T_Cin_Sys_Contribution,T_Cin_Rand_Contribution,T_Cout_Sys_Contribution, ...

    T_Cout_Rand_Contribution,V1_Sys_Contribution+V2_Sys_Contribution+V3_Sys_Contribution,V1_Rand_Contrib
    ution+V2_Rand_Contribution+V3_Rand_Contribution]*(1/(Sys_R^2+Rand_R^2));


%the average value of eta is calculated
trapezoideta = 0;
counterintegral = 1;

for n = 1:countereta-2

    if isnan(eta(n+1,2)) == 0 && isnan(eta(n,2)) == 0

        trapezoideta(counterintegral) = (eta(n+1,1)-eta(n,1))*((eta(n+1,2)+eta(n,2))/2);
        counterintegral = counterintegral + 1;

    else
    end

end

etaave = sum(trapezoideta)/(eta(countereta-1,1)-eta(1,1));

fprintf('----- TIME RANGE RESULTS -------------------- \n\n')
fprintf('For Range: %1.0f min. to %1.0f min.\n', lowertime/60, uppertime/60)
fprintf('Avg. collector efficiency = %f%%\n',etaave*100)

%Plot of instantaneous efficiency as a function of time -Philip Lax
figure(graphcounter + 1)
plot(t,eta(:,2),'.')
xlabel('Time (min)')
ylabel('Instantaneous Efficiency')
title('Instantaneous Efficiency vs. Time')
grid on
grid minor

%Plot of flowrate and efficiency vs time
figure(graphcounter + 2)
yyaxis left
plot(t,eta(:,2),'.b')
xlabel('Time (min)')
```

```
    ylabel('Efficiency')
    yyaxis right
    plot(t,Flowrate,'.r')
    ylabel('Flowrate (gal/min)')
    legend('Efficiency','Flowrate')
    title('Efficiency and Flowrate Vs. Time')
    grid on
    grid minor

    %Plot of temp diff across collector and efficiency vs time
    figure(graphcounter + 3)
    yyaxis left
    plot(t,eta(:,2),'.b')
    xlabel('Time (min)')
    ylabel('Efficiency')
    yyaxis right
    plot(t,deltaTcollector,'.r')
    ylabel('Temperature Difference Across Collector (C)')
    legend('Efficiency','Temperature Difference Across Collector')
    title('Efficiency and Temperature Difference Across Collector Vs. Time')
    grid on
    grid minor

    figure(graphcounter + 4)
    bar(xunc,yunc,'w','LineStyle','-','BarWidth',0.4,'Linewidth',4)
    set(gca,'XTickLabel',{'R Sys', 'R Rand', ...
        'Rho Sys','Rho Rand','F Sys', ...
        'F Rand','Cp Sys','Cp Rand','Tin Sys', ...
        'Tin Rand','Tout Sys','Tout Rand','V Sys', ...
        'V Ran'},'FontSize',18)
    xlabel('Components of Uncertainty')
    xtickangle(90)
    ylabel('Percent Contribution to Total Uncertainty')

    graphcounter = graphcounter + 4;

    fprintf('Uncertainty = %f%%\n\n',U_R95)
    tester1 = 0; % input('Enter 0 to end code. Enter 1 to calculate system efficiency for another specific time
        range: ');

    if tester1 == 0 || 1
    else
        error('You have entered an invalid input. The options are 0 to end code or 1 to calculate system efficiency
        for a specific time range')
    end

end

close all

% END OF PROGRAM
```

Appendix C

Voltage Calibration Data Points

	Measurements					Uncertainty			
Nominal	**Actual**	**V1**	**V2**	**V3**	**Range**	**Actual**	**V1**	**V2**	**V3**
5.0	4.99	-0.000911	-0.000939	-0.000948	20	0.068003	0.00398	0.00398	0.00398
7.5	7.52	0.029668	0.027449	0.026454	20	0.069658	0.00398	0.00398	0.00398
10.0	9.98	0.14603	0.141603	0.140473	20	0.07157	0.00398	0.00398	0.00398
12.5	12.50	0.298366	0.292941	0.292001	20	0.073828	0.00398	0.00398	0.00398
15.0	14.97	0.460401	0.453653	0.452774	20	0.076292	0.00398	0.00398	0.00398
17.5	17.52	0.631755	0.624278	0.623558	20	0.079081	0.00398	0.00398	0.00398
20.0	20.00	0.802926	0.79445	0.793821	20	0.082007	0.00398	0.00398	0.00398
22.5	22.55	0.977807	0.96835	0.967767	200	0.159002	0.00398	0.00398	0.00398
25.0	25.04	1.153476	1.142836	1.142283	200	0.16355	0.00398	0.00398	0.00398
27.5	27.50	1.329626	1.317862	1.317335	200	0.168084	0.00398	0.00398	0.00398
30.0	29.94	1.499215	1.486234	1.485664	200	0.172585	0.00398	0.00398	0.00398
32.5	34.33	1.68511	1.671112	1.670422	200	0.180744	0.00398	0.00398	0.00398
35.0	34.91	1.8532	1.837747	1.837016	200	0.181829	0.00398	0.00398	0.00398
37.5	37.48	2.040826	2.024279	2.023394	200	0.186647	0.00398	0.00398	0.00398
40.0	39.98	2.219037	2.201291	2.200331	200	0.191344	0.00398	0.00398	0.00398
42.5	42.53	2.401548	2.382592	2.381518	200	0.196144	0.00398	0.00398	0.00398
45.0	45.00	2.578218	2.558134	2.556929	200	0.200818	0.00398	0.00398	0.00398
47.5	47.45	2.755693	2.734443	2.733188	200	0.205458	0.00398	0.00398	0.00398
50.0	50.01	2.940719	2.91824	2.916898	200	0.21032	0.00398	0.00398	0.00398
52.5	52.61	3.13064	3.106862	3.105564	200	0.215264	0.00398	0.00398	0.00398
55.0	54.99	3.301142	3.276313	3.275026	200	0.219818	0.00398	0.00398	0.00398
57.5	57.51	3.480119	3.454231	3.453027	200	0.224633	0.00398	0.00398	0.00398
60.0	59.92	3.653785	3.627003	3.625888	200	0.229244	0.00398	0.00398	0.00398
62.5	62.52	3.845322	3.817485	3.816463	200	0.234239	0.00398	0.00398	0.00398
65.0	65.11	4.027518	3.998702	3.99775	200	0.239215	0.00398	0.00398	0.00398
67.5	67.46	4.196673	4.167243	4.166452	200	0.243752	0.00398	0.00398	0.00398
70.0	69.94	4.373379	4.342679	4.341941	200	0.248532	0.00398	0.00398	0.00398
72.5	72.55	4.5636	4.532122	4.531432	200	0.253576	0.00398	0.00398	0.00398
75.0	74.93	4.735665	4.703229	4.702614	200	0.258183	0.00398	0.00398	0.00398
77.5	77.59	4.925513	4.892638	4.892354	200	0.263324	0.00398	0.00398	0.00398

Appendix D

Voltage Calibration Uncertainty Analysis

V_{supply} (multimeter)

Inputs: based on users manual [Systematic Uncertainty]

20V: 45Hz – 20kHz
- Uncertainty
  0.2 + 0.05

200V: 45Hz – 20kHz
- Uncertainty
  0.2 + 0.05

Uncertainties given as ± (% of reading + % of range)

Random Uncertainty
- Based upon the noise in the system

± 0.065 Volts

Total Uncertainty:

$$u_{V_{supply}} = \pm\left[(0.065V)^2 + \left(0.002(\text{Reading}) + 0.0005(\text{range})\right)^2\right]^{\frac{1}{2}}$$

V_{output} (LabVIEW)

Systematic Uncertainty: from data sheet

± 0.0031 V

Random Uncertainty: After filter added and determined visually

± 0.0025 V

Total Uncertainty:

$$u_{V_{output}} = \pm\left[(0.0031V)^2 + (0.0025V)^2\right]^{\frac{1}{2}}$$

$$= \pm 0.00398 \text{ Volts}$$

Regression Uncertainty

Slope:

$$u_{m_1} = \pm\frac{\text{upper 95\%} - \text{lower 95\%}}{2} = \pm\frac{14.3868535 - 13.9815529}{2} = \pm 0.2026503$$

Intercept:

$$u_{b_1} = \pm\frac{\text{upper 95\%} - \text{lower 95\%}}{2} = \pm\frac{8.76321552 - 7.63343247}{2} = \pm 0.56489152 \text{ Volts}$$

Equation:

$V_{supply} = m_1 V_{output} + b_1$

partials:

$$\frac{\partial U_s}{\partial m_1} = V_{output}$$

$$\frac{\partial U_s}{\partial V_o} = m_1 = 14.18420319$$

$$\frac{\partial U_s}{\partial b_1} = 1$$

uncertainty:

$$u_{U_s} = \pm\left[\left(\frac{\partial U_s}{\partial m_1} u_{m_1}\right)^2 + \left(\frac{\partial U_s}{\partial V_o} u_{V_o}\right)^2 + \left(\frac{\partial U_s}{\partial b_1} u_{b_1}\right)^2\right]$$

$$= \pm\left[\left(V_{output}(0.203)\right)^2 + \left(14.184\left(3.98\times10^{-3}V\right)\right)^2 + \left(1\,(0.565V)\right)^2\right]^{\frac{1}{2}}$$

Appendix E

Voltage Calibration Linear Regression

V1								
SUMMARY OUTPUT						Uncertainty		
						m	0.20265027	
Regression Statistics						b	0.56489152	
Multiple R	0.99931964					vo	0.00398	
R Square	0.99863975							
Adjusted R Sq	0.99859117							
Standard Erro	0.82538179							
Observations	30							
ANOVA								
	df	*SS*	*MS*	*F*	*Significance F*			
Regression	1	14004.185	14004.185	20556.448	1.1103E-41			
Residual	28	19.0751427	0.6812551					
Total	29	14023.2601						
	Coefficients	*Standard Error*	*t Stat*	*P-value*	*Lower 95%*	*Upper 95%*	*Lower 95.0%*	*Upper 95.0%*
Intercept	8.19832399	0.27577112	29.7287263	1.0056E-22	7.63343247	8.76321552	7.63343247	8.76321552
X Variable 1	14.1842032	0.09893066	143.3752	1.1103E-41	13.9815529	14.3868535	13.9815529	14.3868535

V2								
SUMMARY OUTPUT						Uncertainty		
						m	0.20616049	
Regression Statistics						b	0.5704723	
Multiple R	0.99930479					vo	0.00398	
R Square	0.99861005							
Adjusted R Sq	0.99856041							
Standard Erro	0.83434273							
Observations	30							
ANOVA								
	df	*SS*	*MS*	*F*	*Significance F*			
Regression	1	14003.7685	14003.7685	20116.6634	1.5022E-41			
Residual	28	19.4915782	0.69612779					
Total	29	14023.2601						
	Coefficients	*Standard Error*	*t Stat*	*P-value*	*Lower 95%*	*Upper 95%*	*Lower 95.0%*	*Upper 95.0%*
Intercept	8.24447018	0.27849556	29.603596	1.1277E-22	7.67399787	8.81494248	7.67399787	8.81494248
X Variable 1	14.2747044	0.10064429	141.833224	1.5022E-41	14.0685439	14.4808649	14.0685439	14.4808649

V3									
SUMMARY OUTPUT						Uncertainty			
						m	0.20649011		
Regression Statistics						b	0.5712302		
Multiple R	0.99930261					vo	0.00398		
R Square	0.99860571								
Adjusted R Sq	0.99855591								
Standard Erro	0.83564584								
Observations	30								
ANOVA									
	df	*SS*	*MS*	*F*	*Significance F*				
Regression	1	14003.7076	14003.7076	20053.8853	1.5693E-41				
Residual	28	19.552511	0.69830396						
Total	29	14023.2601							
	Coefficients	*Standard Error*	*t Stat*	*P-value*	*Lower 95%*	*Upper 95%*	*Lower 95.0%*	*Upper 95.0%*	
Intercept	8.25553331	0.27886556	29.6039906	1.1273E-22	7.68430311	8.8267635	7.68430311	8.8267635	
X Variable 1	14.2752014	0.10080521	141.611741	1.5693E-41	14.0687113	14.4816915	14.0687113	14.4816915	

Appendix F

Thermistor Calibration Data Analysis

Resistance			Dry Well Oven		Hg Thermometer		$T = \frac{1}{A + Bln(R) + Cln^3(R)}$
Range	B_R	S_R	B_T	S_T	B_T	S_T	
2000	0.02 + 0.003	0.5	0.2	0.05	0.5	0.1	
20000	0.02 + 0.003	0.5	% reading				$\frac{\partial T}{\partial R} = -\frac{3Cln^2(R) + B}{R[A + Bln(R) + Cln^3(R)]^2}$
% reading + % range							

Reference Temperatures		Collector In - 44007				Collector Out - 44007			
T (°C)	U_T	R1 (Ω)	U_{R1}	T (°C)	U_{T1}	R2 (Ω)	U_{R2}	T2 (°C)	U_{T2}
24.25	0.509901951	5096	1.694641	24.55708	0.00756	5175	1.709744	24.20772	0.007495
30	0.078102497	4050	1.496028	29.86162	0.008663	4055	1.496971	29.83269	0.008656
40	0.094339811	2731	1.25051	39.35886	0.011342	2706	1.245928	39.5868	0.01142
50	0.111803399	1821	0.655702	49.69415	0.009454	1827	0.656479	49.6078	0.009429
60	0.13	1276	0.591059	59.28121	0.01282	1283	0.591807	59.12986	0.012756
70	0.148660687	896	0.554271	69.33428	0.018073	909	0.555398	68.91392	0.01781

Tank Top - 44004				Tank Middle - 44004				Tank Bottom - 44006			
R4 (Ω)	U_{R4}	T4 (°C)	U_{T4}	R5 (Ω)	U_{R5}	T5 (°C)	U_{T5}	R5 (Ω)	U_{R6}	T6 (°C)	U_{T6}
2271	1.16676	24.8191302	0.011693	2187	1.151607	25.6791	0.012045	10065	2.660408	24.84478	0.006548
1811	0.65441	30.0502712	0.008481	1808	0.654023	30.08919	0.008492	8140	2.283415	30.17981	0.007153
1207	0.58382	39.8458552	0.012013	1209	0.584023	39.80474	0.011994	5592	1.789664	40.00719	0.008599
820	0.54788	49.7180589	0.017545	819	0.547801	49.7501	0.017567	3919	1.471361	49.80683	0.010618
573	0.52961	59.3840458	0.025601	571	0.529477	59.48092	0.025698	2791	1.261518	59.6511	0.013443
402	0.51934	69.4721428	0.037787	402	0.519338	69.47214	0.037787	2010	1.119823	69.66261	0.017424

Model	R25°C	A	B	C
44004	2252	1.468E-03	2.383E-04	1.007E-07
44005	3000	1.403E-03	2.373E-04	9.827E-08
44006	5000	1.032E-03	2.387E-04	1.580E-07
44007	10000	1.285E-03	2.362E-04	9.285E-08
44008	30000	9.376E-04	2.208E-04	1.276E-07

	A B C m b
Thermistor 1 Equation	-0.479444934477073+1.01852151659803*(1/((1.285E-3)+((2.362E-4)*ln((10000*V)/(IN-V))+((9.285E-8)*(ln((10000*V)/(IN-V)))**3))) - 273.15)
Thermistor 2 Equation	-0.534111809266257+1.02276576564882*(1/((1.285-3)+((2.362E-4)*ln((5100*V)/(IN-V))+((9.285E-8)*(ln((5100*V)/(IN-V)))**3))) - 273.15)
Thermistor 4 Equation	-0.884512575333467+1.02293381633847*(1/((1.468E-3)+((2.383E-4)*ln((10000*V)/(IN-V))+((1.007E-7)*(ln((10000*V)/(IN-V)))**3))) - 273.15)
Thermistor 5 Equation	-1.56625030426223+1.03416739392677*(1/((1.468E-3)+((2.383E-4)*ln((10000*V)/(IN-V))+((1.007E-7)*(ln((10000*V)/(IN-V)))**3))) - 273.15)
Thermistor 6 Equation	-0.870142423967955+1.01939996222434*(1/((1.032E-3)+((2.387E-4)*ln((10000*V)/(IN-V))+((1.580E-7)*(ln((10000*V)/(IN-V)))**3))) - 273.15)

	Therm 1	Therm 2	Therm 4	Therm 5	Therm 6
slope m	1.018521517	1.022765766	1.022933816	1.034167394	1.019399962
Uncertainty U_m	0.019157591	0.008097626	0.014128301	0.036542976	0.011080698
intercept b	-0.479444934	-0.534111809	-0.884512575	-1.566250304	-0.870142424
Uncertainty U_b	0.919926793	0.387637573	0.680788419	1.764476133	0.535640514

Steinhart Equation

$$T = \frac{1}{A + B\ln(R) + C\ln^3(R)} \qquad \frac{\delta T}{\delta R} = -\frac{3C\ln^2(R) + B}{R(A + B\ln(R) + C\ln^3(R))^2}$$

Collector In Temp 30°C

$R = 4050\,\Omega \quad A = 1.285\times10^{-3} \quad B = 2.362\times10^{-4} \quad C = 9.285\times10^{-8}$

$$T_{1\,(30°C)} = \frac{1}{(1.285\times10^{-3}) + (2.362\times10^{-4})\ln(4050) + (9.285\times10^{-8})\ln^3(4050)} = 303.01166\,K - 273.15°C$$

$T_{1\,(30°C)} = 29.86166\,32°C$

Resistance Uncertainty

$U_R = \sqrt{B_R^2 + S_R^2} \qquad B_R = 0.0002(R) + 0.00003(\text{range}) \qquad S_R = 0.5\,\Omega$

$R_{1\,30°C} = 4050\,\Omega \qquad B_R = 0.0002(4050\,\Omega) + 0.00003(20{,}000\,\Omega) = 1.41\,\Omega$

$$U_{R_1} = \sqrt{(1.41\,\Omega)^2 + (0.5\,\Omega)^2} = \pm 1.496028\,\Omega$$

Measured Temperature Uncertainty

$$\frac{\delta T}{\delta R}\ \text{for}\ {}^{T_1, R_1}_{(30°C)} = -\frac{3(9.285\times10^{-8})(\ln(4050))^2 + (2.362\times10^{-4})}{4050\left(1.285\times10^{-3} + 2.362\times10^{-4}(\ln(4050)) + 9.285\times10^{-8}(\ln^3(4050))\right)^2}$$

$$\frac{\delta T_1}{\delta R_1} = -0.005790511 \qquad U_{T_1} = \sqrt{\left[\frac{\delta T_1}{\delta R_1} U_{R_1}\right]^2} = \sqrt{\left[-0.005790511\,(1.496028)\right]^2}$$

$U_{T_{1\,30°C}} = \pm 0.008662767°C$

Regression Analysis's Uncertainty

Thermistor 1 slope sample (same method for intercept)

$$U_m = \frac{m_{\text{upper }95\%} - m_{\text{lower }95\%}}{2} = \frac{1.037679107 - 0.999363926}{2} = 0.019157591$$

Appendix G

Thermistor Calibration Linear Regression

THERMISTOR 1 (COLLECTOR IN) REGRESSION ANALYSIS

SUMMARY OUTPUT

Regression Statistics	
Multiple R	0.9999082
R Square	0.9998165
Adjusted R S	0.9997706
Standard Erro	0.26691
Observations	6

ANOVA

	df	SS	MS	F	Significance F
Regression	1	1552.2671	1552.2671	21788.976	1.263E-08
Residual	4	0.2849638	0.0712409		
Total	5	1552.5521			

	Coefficients	Standard Erro	t Stat	P-value	Lower 95%	Upper 95%	Lower 95.0%	Upper 95.0%
Intercept b	-0.479445	0.3313326	-1.44702	0.2214417	-1.399372	0.4404819	-1.399372	0.4404819
Slope m	1.0185215	0.0069	147.61089	1.263E-08	0.9993639	1.0376791	0.9993639	1.0376791

THERMISTOR 2 (COLLECTOR OUT) REGRESSION ANALYSIS

SUMMARY OUTPUT

Regression Statistics	
Multiple R	0.9999837
R Square	0.9999675
Adjusted R S	0.9999593
Standard Erro	0.1123592
Observations	6

ANOVA

	df	SS	MS	F	Significance F
Regression	1	1552.5016	1552.5016	122974.52	3.967E-10
Residual	4	0.0504983	0.0126246		
Total	5	1552.5521			

	Coefficients	Standard Erro	t Stat	P-value	Lower 95%	Upper 95%	Lower 95.0%	Upper 95.0%
Intercept b	-0.534112	0.1396165	-3.825563	0.018689	-0.921749	-0.146474	-0.921749	-0.146474
Slope m	1.0227658	0.0029165	350.67723	3.967E-10	1.0146681	1.0308634	1.0146681	1.0308634

THERMISTOR 4 (TANK TOP) REGRESSION ANALYSIS

SUMMARY OUTPUT

Regression Statistics	
Multiple R	0.9999505
R Square	0.999901
Adjusted R S	0.9998763
Standard Erro	0.1959995
Observations	6

ANOVA

	df	SS	MS	F	Significance F
Regression	1	1552.3984	1552.3984	40410.419	3.674E-09
Residual	4	0.1536632	0.0384158		
Total	5	1552.5521			

	Coefficients	Standard Erro	t Stat	P-value	Lower 95%	Upper 95%	Lower 95.0%	Upper 95.0%
Intercept b	-0.884513	0.2452015	-3.607289	0.022611	-1.565301	-0.203724	-1.565301	-0.203724
Slope m	1.0229338	0.0050886	201.02343	3.674E-09	1.0088055	1.0370621	1.0088055	1.0370621

THERMISTOR 5 (TANK MIDDLE) REGRESSION ANALYSIS

SUMMARY OUTPUT

Regression Statistics	
Multiple R	0.9996762
R Square	0.9993525
Adjusted R S	0.9991906
Standard Erro	0.5013101
Observations	6

ANOVA

	df	SS	MS	F	Significance F
Regression	1	1551.5468	1551.5468	6173.7927	1.572E-07
Residual	4	1.0052471	0.2513118		
Total	5	1552.5521			

	Coefficients	Standard Erro	t Stat	P-value	Lower 95%	Upper 95%	Lower 95.0%	Upper 95.0%
Intercept b	-1.56625	0.6355163	-2.464532	0.0693528	-3.330726	0.1982258	-3.330726	0.1982258
Slope m	1.0341674	0.0131618	78.573486	1.572E-07	0.9976244	1.0707104	0.9976244	1.0707104

THERMISTOR 6 (TANK BOTTOM) REGRESSION ANALYSIS

SUMMARY OUTPUT

Regression Statistics	
Multiple R	0.9999693
R Square	0.9999387
Adjusted R S	0.9999234
Standard Erro	0.1542564
Observations	6

ANOVA

	df	SS	MS	F	Significance F
Regression	1	1552.4569	1552.4569	65242.89	1.409E-09
Residual	4	0.0951801	0.023795		
Total	5	1552.5521			

	Coefficients	Standard Erro	t Stat	P-value	Lower 95%	Upper 95%	Lower 95.0%	Upper 95.0%
Intercept b	-0.870142	0.1929231	-4.510306	0.0107375	-1.405783	-0.334502	-1.405783	-0.334502
Slope m	1.0194	0.003991	255.42688	1.409E-09	1.0083193	1.0304807	1.0083193	1.0304807

Appendix H

Detailed Experimental Results

Phase 0: Base Case

Test Index	Test Date	Testers	Collector Angle (°)	Hot Leg Height (in.)	Ambient Temp. (°C)	VARIAC #1 (V_{RMS})	VARIAC #2 (V_{RMS})	VARIAC #3 (V_{RMS})	Analysis Start (min.)	Analysis End (min.)	Efficiency (%)	Uncertainty (%)
BC	9/2/20	Truman S, Sanjay M	38	21.5	26	49.86	50.03	49.97	45	55	58.348738	0.956492
BC	9/4/20	Truman S, Jesse H	38	20.25	24.5	50.08	50.15	49.88	45	55	56.12604	0.875921
BC	9/7/20	Truman S, Bastian K	38	20.5	26	49.90	50.24	49.99	40	50	57.296787	0.892647
BC	9/8/20	Sanjay M, Truman S	38	21.5	25	49.8	50.01	50.05	32	42	57.262228	0.893097
BC	9/9/20	Truman S, Jesse H	38	20	25.4	50.06	49.85	49.89	35	45	57.760638	0.788464
BC	9/23/20	Tyler C, Bradan B	38	21	26	49.92	50.1	49.82	70	80	71.585421	1.105162
BC	9/24/20	Jackson S, Bastian K	37	20	25	50.20	50.00	50.30	45	50	75.89076	1.175211
BC	9/25/20	Tyler C, Alek D	37	21.25	26	49.81	49.93	50.16	60	70	78.358325	1.222837
BC	9/26/20	Jesse H, Truman S, Justin F	38	20.75	24.5	49.80	49.99	50.10	45	55	79.595369	1.230092
BC	9/27/20	Sanjay M, Jackson S	38	20.75	25.5	49.95	49.91	50	45	55	77.018099	2.441935
BC	9/28/20	Jesse H, Truman S	38	20.25	25	50.20	50.12	50.09	45	55	76.021182	1.185167
BC	9/29/20	Jesse H, Truman S, Nicole H	38	21	24	49.9	50	49.93	45	55	76.04255	1.163882
BC	9/30/20	Tyler C, Truman S, Bradan B	38	21	24.5	49.83	50.10	50.17	45	55	74.92075	1.142535
BC	10/1/20	Sanjay M, Nick G	38	21	25	49.97	50.04	49.91	45	55	75.070736	3.07095
BC	10/2/20	Truman S, Tyler C, Justin F	38	20.75	25	49.91	50.16	49.87	45	55	76.343245	1.148356
BC	10/4/20	Truman S, Jackson S	38	21	25.5	50.08	50.13	49.8	45	55	76.681075	1.143259
BC	1/21/21	Truman S, Tyler C	38	21.5	25	50.00	50.10	50.00	40	50	75.80463	1.175797
BC	1/29/21	Sanjay M, Jackson S, Jackson S	38	21	25	49.98	50.03	50.09	45	55	73.647374	1.145738
BC	1/30/21	Sanjay M, Bradan B	38	21	28	49.99	49.98	50.08	35	45	74.606576	1.147169
BC	2/13/21	Truman S, Alek D, Sam K	38	21	25.5	50.11	49.9	50.13	45	55	79.920245	1.271108
BC	2/17/21	Jesse H, Nicole H, Jackson S	38	21	25	50.07	50.02	50.12	45	55	78.393313	1.249045
BC	2/20/21	Justin F, Sanjay M, Bradan B	38	21	25.5	50.04	50.07	50.16	40	50	83.422274	1.312837
BC	2/21/21	Bradan B, Jesse H, Edward F	38	21	25	50.14	49.91	50.18	30	40	84.5011	1.35011
BC	2/22/21	Tyler C, Alek D, Bradan B	38	21.5	26	49.9	49.92	49.91	45	55	84.457769	1.329444
BC	2/23/21	Tyler C, Edward F, Alek D	38	21	27	49.89	50.12	50.14	50	60	85.987672	1.419115
BC	2/24/21	Truman S, Justin F, Edward F	38	21	27.5	49.88	49.92	50.03	30	40	88.645042	1.459417
BC	2/26/21	Jesse H, Jackson S, Justin F	38	21	24.75	50.17	50.00	50.17	40	50	81.385387	1.259206
BC	2/27/21	Sanjay M, Alek D, Bradan B	38	21	25	50.1	49.94	50.04	50	60	84.604901	1.374824
BC	2/28/21	Tyler C, Nicole H, Bradan B	38	21	24	50.18	50.08	50.17	45	55	83.6509	1.329159

BC	3/4/21	Bastian K, Alek D, Bradan B	38	21	28	49.92	50.02	49.91	45	55	85.256576	1.289464
BC	3/5/21	Sam K, Jesse H, Justin F	38	21	25	50.00	50.03	50.05	45	55	83.946062	1.315027
BC	3/7/21	Bastian K, Nicole H, Edward F	38	21	27.9	49.85	50.15	50.15	40	50	85.889499	1.289868
BC	3/12/21	Tyler C, Alek D, Sam K	38	21	26	49.90	50.14	49.88	40	50	82.415101	1.294274
BC	3/14/21	Jesse H,Alek D, Braden B	38	21	25.75	50.16	49.99	50.15	45	55	81.795999	1.282503
BC	3/16/21	Tyler C, Jackson S, Justin F	38	21	25.5	50.17	50.11	50.89	45	55	83.50137	1.298687
BC	3/18/21	Sanjay M, Alek D, Nicole H	38	21	25.5	50.11	50.05	50.03	40	50	86.879995	1.350531
BC	3/20/21	Sanjay M, Bradan B	38	21	25	49.96	49.95	49.95	40	50	85.860915	1.342225
BC	3/22/21	Sanjay M, Alek D, Sam K	38	20.75	26	50.13	50.05	50.10	45	55	88.782513	1.376193
BC	3/30/21	Tyler C, Justin F, Jackson S	38	21	26	49.96	50.11	50.16	50	60	75.611807	0.888092
BC	3/31/21	Bradan B, Edward F, Jesse H	38	21	25	49.88	49.90	50.04	54	64	74.024586	0.809708

Phase 1: Variable Angle - Constant High Power

Test Index	Test Date	Testers	Collector Angle (°)	Hot Leg Height (in.)	Ambient Temp. (°C)	VARIAC #1 (V_{RMS})	VARIAC #2 (V_{RMS})	VARIAC #3 (V_{RMS})	Analysis Start (min.)	Analysis End (min.)	Efficiency (%)	Uncertainty (%)
1.2	9/14/20	Bastian K, Truman S, Jackson S	22	21	26	49.65	49.85	50.07	90	100	57.271895	0.88937
1.3	9/15/20	Jesse H, Truman S	30	21	25.5	49.89	49.9	49.96	45	55	59.324293	0.895373
1.4	9/16/20	Sanjay M, Truman S, Edward F	46	21.25	26.5	50.17	50.02	49.93	45	55	55.310802	0.867511
1.2	9/17/20	Tyler C, Truman S, Alek D	22	21	26	49.95	49.95	49.9	60	70	58.100321	0.995977
1.1	9/19/20	Truman S, Justin F	13.5	21.5	25.5	50.19	50.05	50.19	55	65	78.561972	1.232549
1.5	9/20/20	Truman S, Sanjay M	50	21	25.5	50.02	50.08	50.17	45	55	73.335219	1.138509
1.1	9/21/20	Jesse H, Truman S, Edward F	14	21	25	49.95	50.1	49.82	45	55	74.76747	1.059896
1.A	9/22/20	Sanjay M, Truman S, Nicole H	26	21	25	49.85	50.05	49.97	45	55	71.577444	2.413017
1.1	10/5/20	Jesse H, Truman S, Edward F	14	21	25.5	50.01	49.91	50.06	45	55	77.42822	1.183515
1.2	10/6/20	Sanjay M, Nick G	22	21	24.5	50.09	50.16	50.03	45	55	76.716776	1.216894

1.3	10/7/20	Tyler C, Bradan B, Truman S	30	20.75	25	49.91	50.1	50.06	45	55	74.147782	1.156147
1.4	10/8/20	Bastian K, Jackson S	46	21	25	49.92	50.1	49.9	30	40	75.82749	1.269622
1.5	10/9/20	Truman S, Sanjay M, Nicole H	54	20.75	25	50.12	49.95	50.09	45	55	73.25443	1.171839
1.1	10/10/20	Tyler C, Truman S, Alek D	14	21	25	49.98	49.9	50	45	55	76.002013	1.193351
1.A	10/11/20	Bastian K, Justin F, Truman S	26	21	25	50.08	49.96	50.05	45	55	75.192452	1.141918
1.5	10/12/20	Tyler C, Nicole H, Truman S	54	20.75	24.5	50	50	49.91	45	55	73.535121	1.179944
1.1	2/5/21	Jesse H, Jackson S, Sam K	14	21	26	49.98	49.98	49.9	45	55	85.084972	1.309681
1.B	2/6/21	Bastian K, Jackson S	10	21	25	49.9	50.05	50.12	45	55	81.647347	1.45385

Phase 2: Variable Angle - Constant Low Power

Test Index	Test Date	Testers	Collector Angle (°)	Hot Leg Height (in.)	Ambient Temp. (°C)	VARIAC #1 (V_{RMS})	VARIAC #2 (V_{RMS})	VARIAC #3 (V_{RMS})	Analysis Start (min.)	Analysis End (min.)	Efficiency (%)	Uncertainty (%)
2.2	9/18/20	Bastian K, Truman S, Bradan B	20	21	25	37.25	37.09	37.12	45	55	85.322267	1.671945
2.1	10/13/20	Bastian K, Truman S, Nick G	14	21.25	25	36.92	36.90	37.05	60	70	80.33359	1.50429
2.2	10/14/20	Sanjay M, Bradan B	22	21	24.5	36.83	37.10	37.13	47	57	75.25869	1.495822
2.3	10/15/20	Sanjay M, Truman S, Alek D	30	21	25	37.10	36.99	37.11	47	57	80.67955	1.483915
2.4	10/16/20	Tyler C, Truman S	38	20.75	24.5	37.15	37.16	36.97	45	55	78.805241	1.437235
2.5	10/17/20	Truman S, Justin F, Bastian K	46	21	25	36.90	37.07	37.14	45	55	78.059235	1.468752
2.6	10/18/20	Jesse H, Jackson S, Edward F	52	21	23	36.95	37.06	37.10	37	47	67.890259	5.946922
2.6	10/19/20	Sanjay M, Jackson S	51	21	24	36.83	37.08	36.84	40	50	77.810073	1.454279
2.A	10/20/20	Jesse H, Truman S, Alek D	25	21	25.5	37.00	37.07	37.04	48	58	77.949399	1.41869
2.B	10/21/20	Tyler C, Truman S, Bradan B	18	21	25.5	36.81	36.94	37.08	48	58	78.608992	1.431101

Phase 3: Variable High Angle - Variable Power

Test Index	Test Date	Testers	Collector Angle (°)	Angular Deviation (°)	Hot Leg Height (in.)	Ambient Temp. (°C)	VARIAC #1 (V_{RMS})	VARIAC #2 (V_{RMS})	VARIAC #3 (V_{RMS})	Analysis Start (min.)	Analysis End (min.)	Efficiency (%)	Uncertainty (%)
3.1	10/22/20	Sanjay M, Nick G	20	6	21	25	49.84	49.70	49.88	40	50	73.917588	1.120926
3.2	10/23/20	Edward F, Tyler C	25.8	11.8	21	25	49.44	49.53	49.56	53	63	74.642732	1.133893
3.3	10/24/20	Bastian K, Truman S, Justin F	32	18	21	24	48.84	48.81	48.76	45	55	73.047192	1.136723
3.4	10/25/20	Truman S, Nicole H, Bastian K	38	24	21	25	47.85	47.81	47.82	40	50	73.219938	1.177082
3.5	10/26/20	Sanjay M, Jackson S, Edward F	44	30	21	25	46.41	46.49	46.53	38	48	73.002401	1.165731
3.6	10/27/20	Nicole H, Justin F, Jesse H	50	36	21	24.5	45.06	45.00	45.00	55	65	72.728831	1.256367
3.6	10/31/20	Justin F, Bastian K	50	36	21	23.5	45.00	45.03	45.09	25	35	70.873385	1.200943

Phase 4: Variable Low Angle - Variable Power

Test Index	Test Date	Testers	Collector Angle (°)	Angular Deviation (°)	Hot-Leg Height (in.)	Ambient Temp. (°C)	VARIAC #1 (V_{RMS})	VARIAC #2 (V_{RMS})	VARIAC #3 (V_{RMS})	Analysis Start (min.)	Analysis End (min.)	Efficiency (%)	Uncertainty (%)
4.2	11/1/20	Jesse H, Jackson S	50	-12	21	24.5	49.45	49.55	49.50	45	55	70.015156	1.147376
4.2	11/5/20	Jackson S, Justin F, Sanjay M	50	-12	21	25.8	49.54	49.45	49.52	41	51	70.376385	1.078909
4.4	11/8/20	Jackson S, Edward F, Truman S	38	-24	21	29	47.80	47.80	47.87	45	55	81.348714	2.542932
4.3	11/9/20	Jesse H, Jackson S, Nicole H	44	-18	21	29	48.70	48.77	48.84	45	55	78.098238	1.121599
4.5	11/10/20	Alek D, Sanjay M, Nick G	32	-30	21	32	46.49	46.45	46.57	45	55	86.514165	1.40668
4.6	1/22/21	Bastian K, Sanjay M	26	-36	21	27	45.09	44.92	45.10	40	50	78.591366	1.27418
4.1	1/23/21	Sanjay M, Jesse H	52	-10	21	27	49.74	49.89	49.78	45	55	77.91549	1.220117
4.1	1/27/21	Tyler C, Alek D, Nicole H	48.5	-13.5	21	26	49.30	49.30	49.30	50	60	52.461324	0.902121
4.1	2/1/21	Truman S, Tyler C, Sam K	48	-14	21	25	49.34	49.26	49.17	35	45	74.143513	1.170732

Phase 5: Variable Hot Leg Height

Test Index	Test Date	Testers	Collector Angle (°)	Hot Leg Height (in.)	Ambient Temp. (°C)	VARIAC #1 (V_{RMS})	VARIAC #2 (V_{RMS})	VARIAC #3 (V_{RMS})	Analysis Start (min.)	Analysis End (min.)	Efficiency, Check #1 (%)	Uncertainty, Check #1 (%)
5.1	11/17/21	Nicole H, Edward F, Jesse H	38	9	25.4	50.17	50.11	49.98	45	55	74.681396	1.066737
5.2	11/19/21	Nick G, Alek D, Sanjay M	38	15	26	50.12	50.06	49.96	45	55	75.627423	1.146537
5.2	4/3/21	Sanjay M, Alek D, Nicole H	38	15	25	50.01	50.15	49.87	105	115	70.559825	0.826086
5.3	1/24/21	Jesse H, Tyler C	38	27	27	49.99	49.92	50.14	45	55	52.828391	0.992297
5.3	2/3/21	Sanjay M, Nicole H, Bradan B	38	27	28	50.01	50.08	50.11	45	55	87.657004	1.393909
5.A	2/4/21	Tyler C, Justin F, Nicole H	38	27.5	25.2	49.9	50.03	50.02	40	50	87.00509	1.387475
5.A	4/1/21	Tyler C, Justin F	38	27.5	25	49.85	49.90	49.96	50	60	75.114686	0.89031

Phase 6: Variable Ambient Temperature

Test Index	Test Date	Testers	Collector Angle (°)	Hot Leg Height (in.)	Ambient Temp. (°C)	VARIAC #1 (V_{RMS})	VARIAC #2 (V_{RMS})	VARIAC #3 (V_{RMS})	Analysis Start (min.)	Analysis End (min.)	Efficiency, Check #1 (%)	Uncertainty, Check #1 (%)
6.4	11/11/20	Truman S, Bradan B	38	21	30	50.11	50.16	49.82	45	55	82.711104	1.287915
6.5	11/12/20	Nick G, Tyler C, Alek D	37.5	21	31.5	49.83	49.99	50.14	50	60	83.554392	1.346284
6.4	11/13/20	Nicole H, Truman S	38	21	30.5	50.08	50.03	50.09	25	35	78.751495	1.225196
6.3	11/21/20	Bastian K, Jackson S, Justin F	38	21	27	50.01	49.96	49.96	60	70	77.690639	1.189293

6.6	1/25/21	Tyler C, Jackson S	38.5	21	35	50	50	50	40	50	56.605024	1.011123
6.6	2/2/21	Sanjay M, Alek D, Bradan B	38	21	34.5	49.93	50.16	50.09	50	60	90.922126	1.552649
6.B	2/9/21	Tyler C, Jackson S, Justin F	38	21	28.5	49.81	50.14	50.00	40	50	85.545008	1.353888

Appendix I

Detailed Instantaneous Test Results

Base Case Test Performed 09.24.20

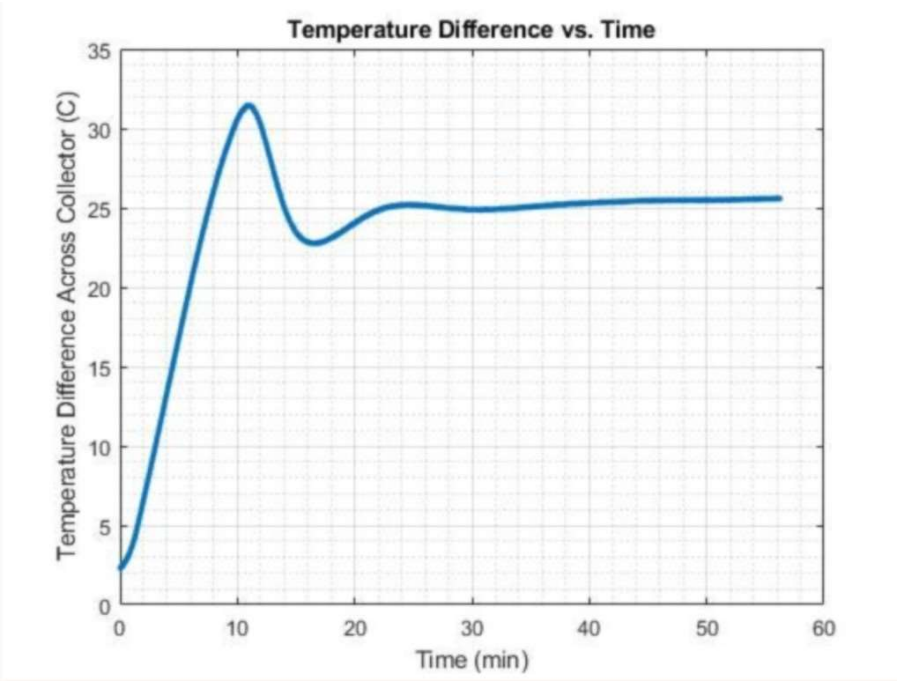

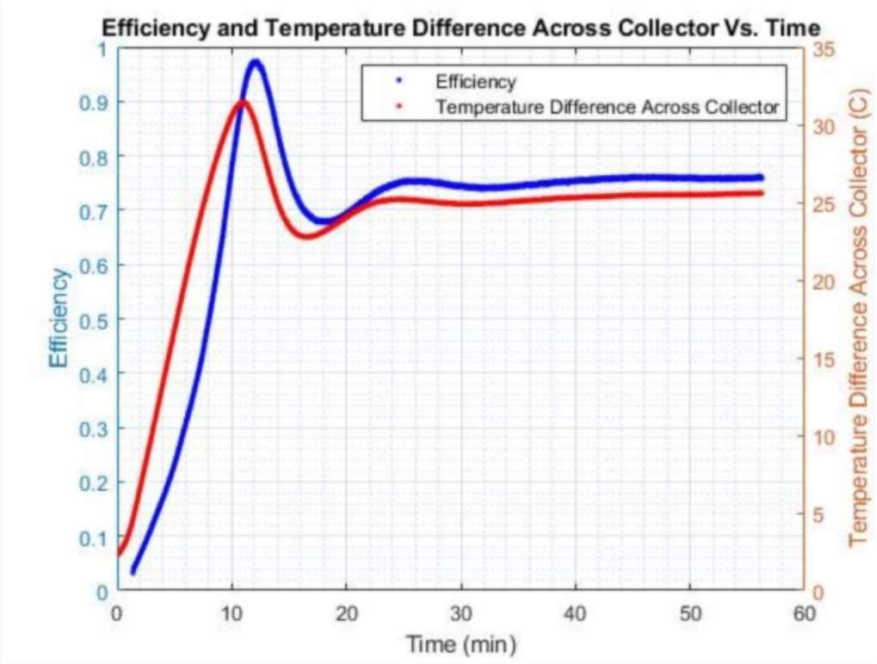

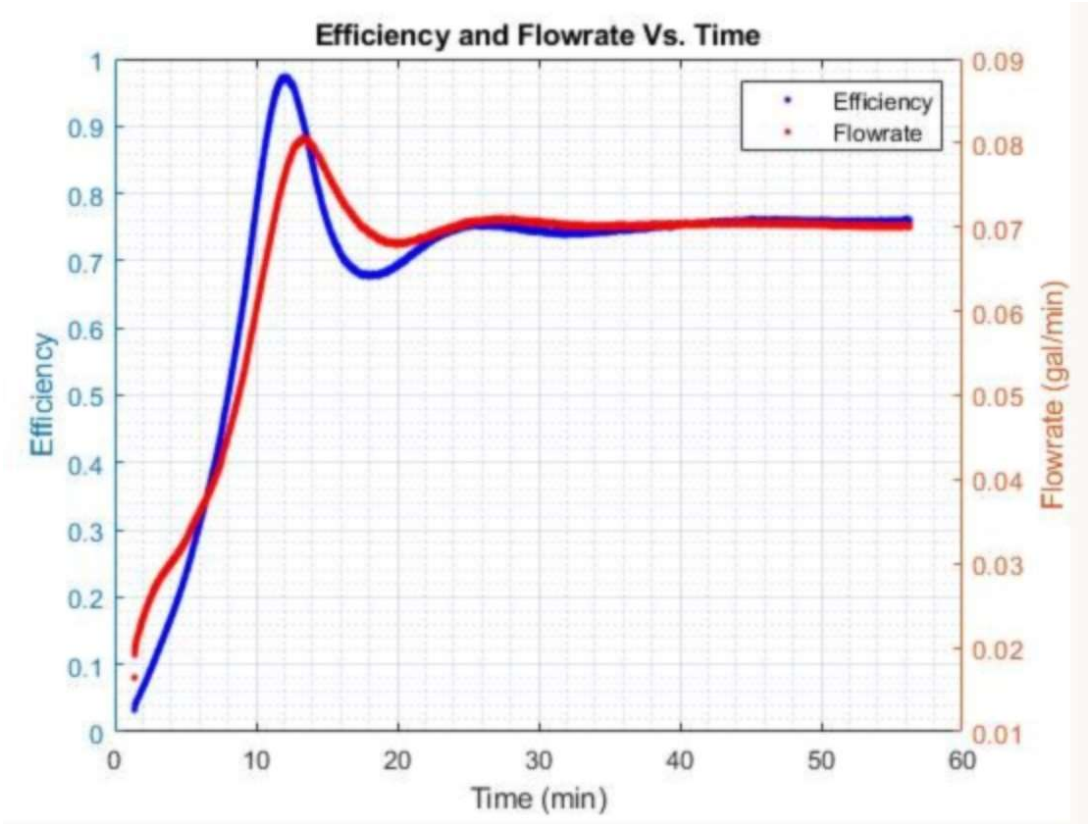
Efficiency and Flowrate Vs. Time
Efficiency
Flowrate
Efficiency
Flowrate (gal/min)
Time (min)
0
0.1
0.2
0.3
0.4
0.5
0.6
0.7
0.8
0.9
1
0.01
0.02
0.03
0.04
0.05
0.06
0.07
0.08
0.09
0
10
20
30
40
50
60

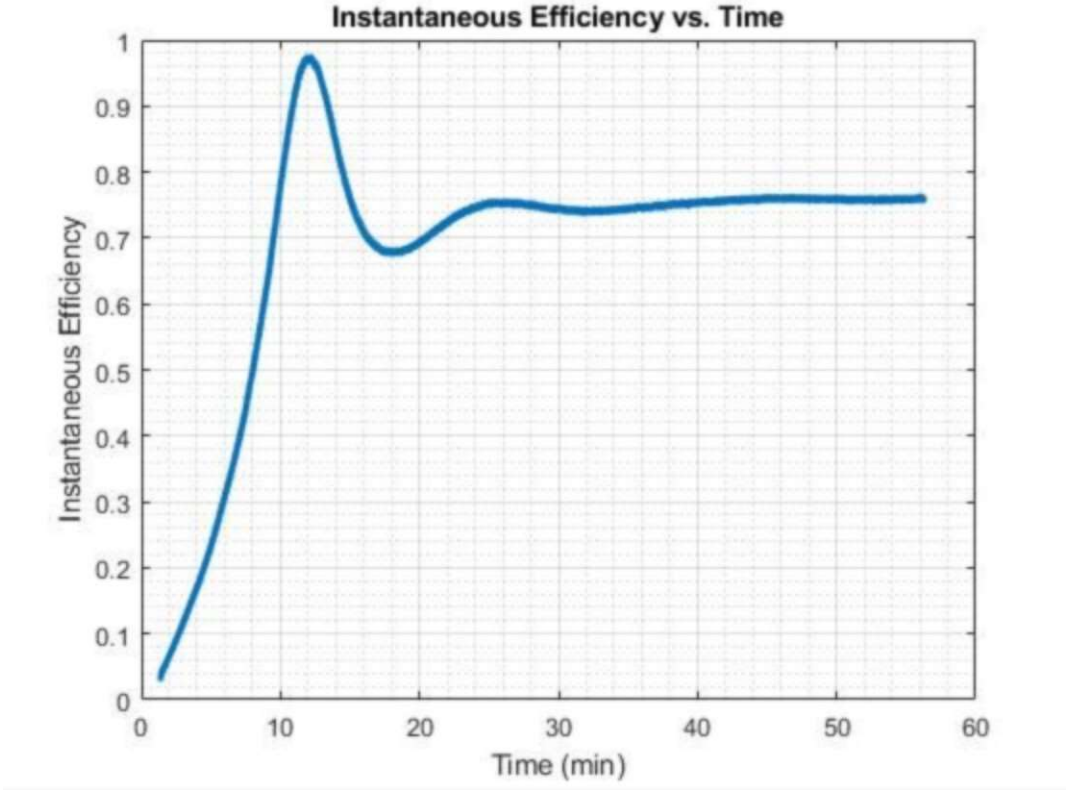
Instantaneous Efficiency vs. Time
Instantaneous Efficiency
Time (min)
0
0.1
0.2
0.3
0.4
0.5
0.6
0.7
0.8
0.9
1
0
10
20
30
40
50
60

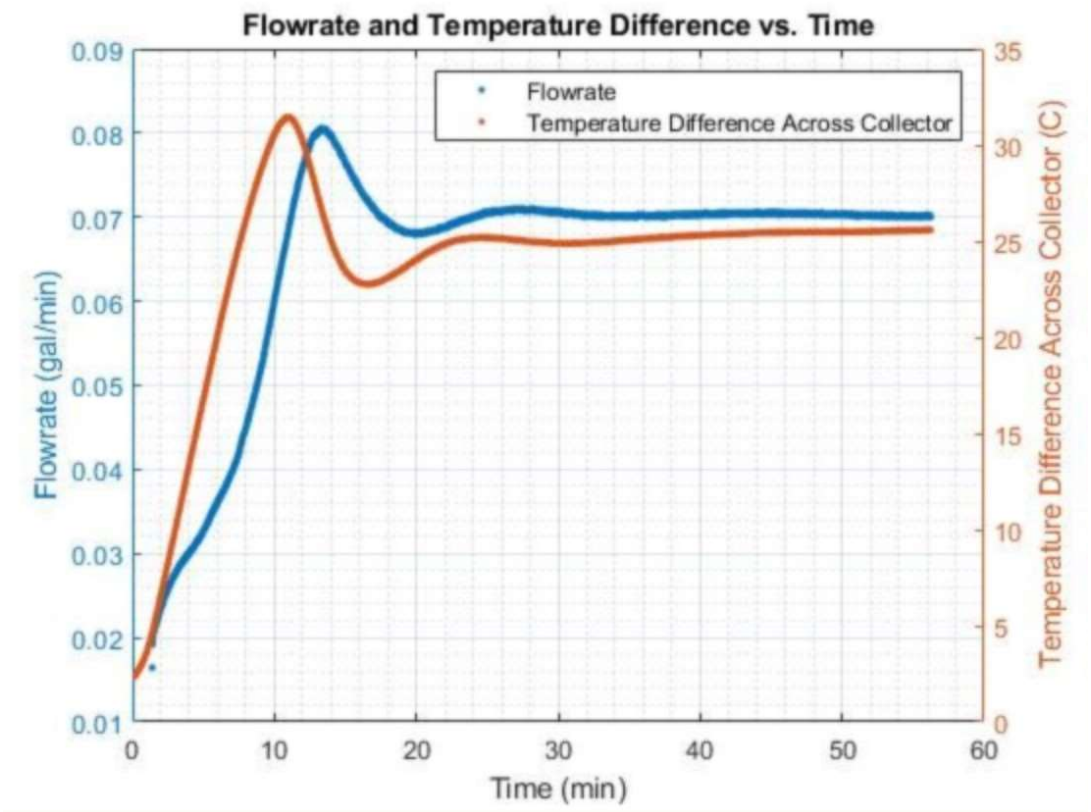
Flowrate and Temperature Difference vs. Time
Flowrate
Temperature Difference Across Collector
Flowrate (gal/min)
Temperature Difference Across Collector (C)
Time (min)
0.09
0.08
0.07
0.06
0.05
0.04
0.03
0.02
0.01
35
30
25
20
15
10
5
0
0
10
20
30
40
50
60

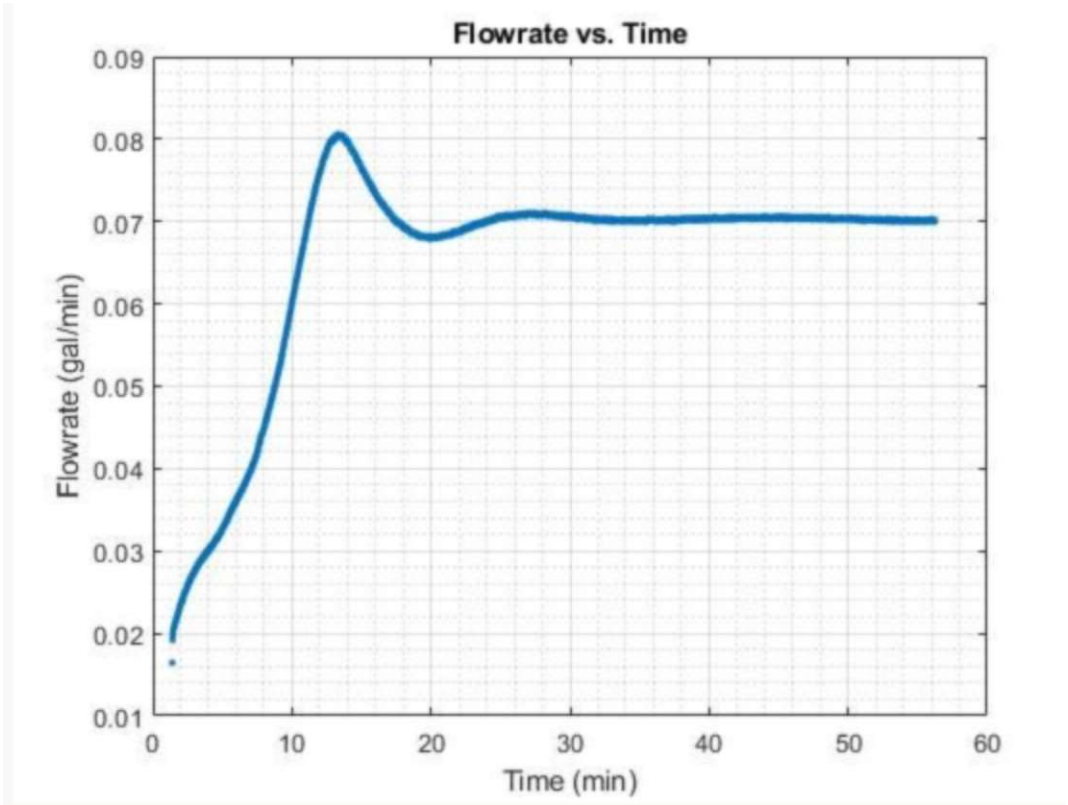
Flowrate vs. Time
Flowrate (gal/min)
Time (min)
0.09
0.08
0.07
0.06
0.05
0.04
0.03
0.02
0.01
0
10
20
30
40
50
60

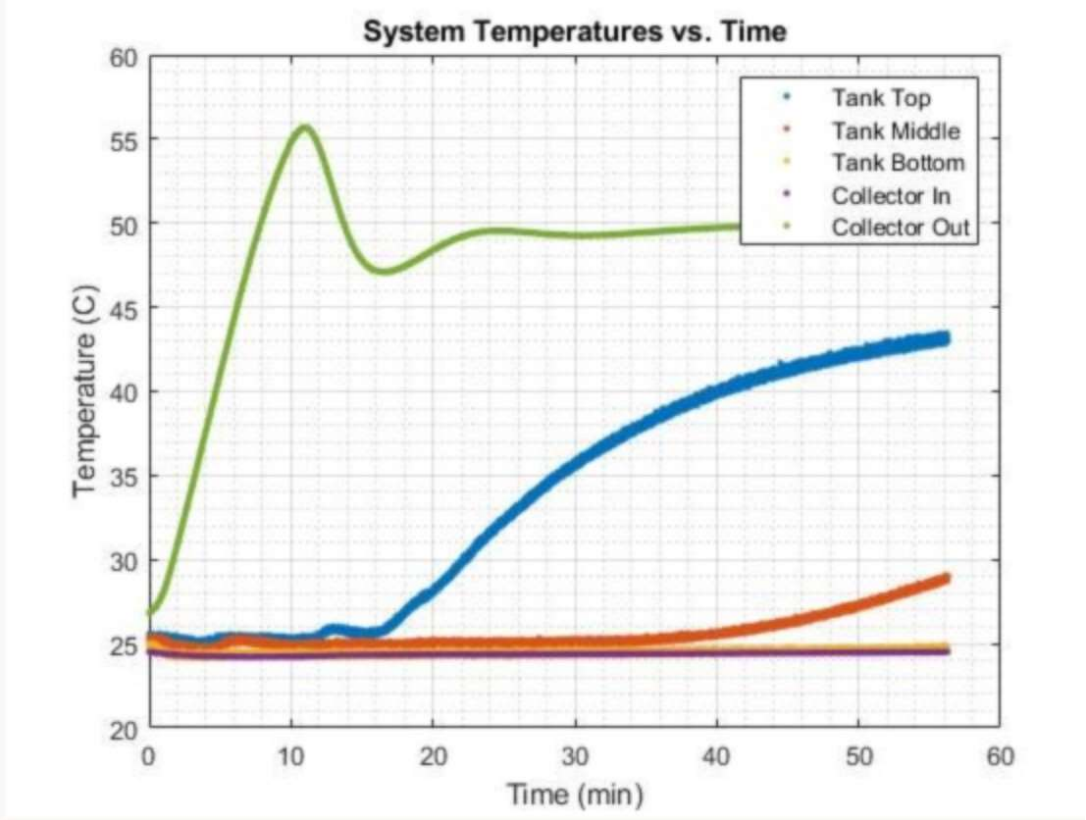
System Temperatures vs. Time
Tank Top
Tank Middle
Tank Bottom
Collector In
Collector Out
Temperature (C)
Time (min)
60
55
50
45
40
35
30
25
20
0
10
20
30
40
50
60

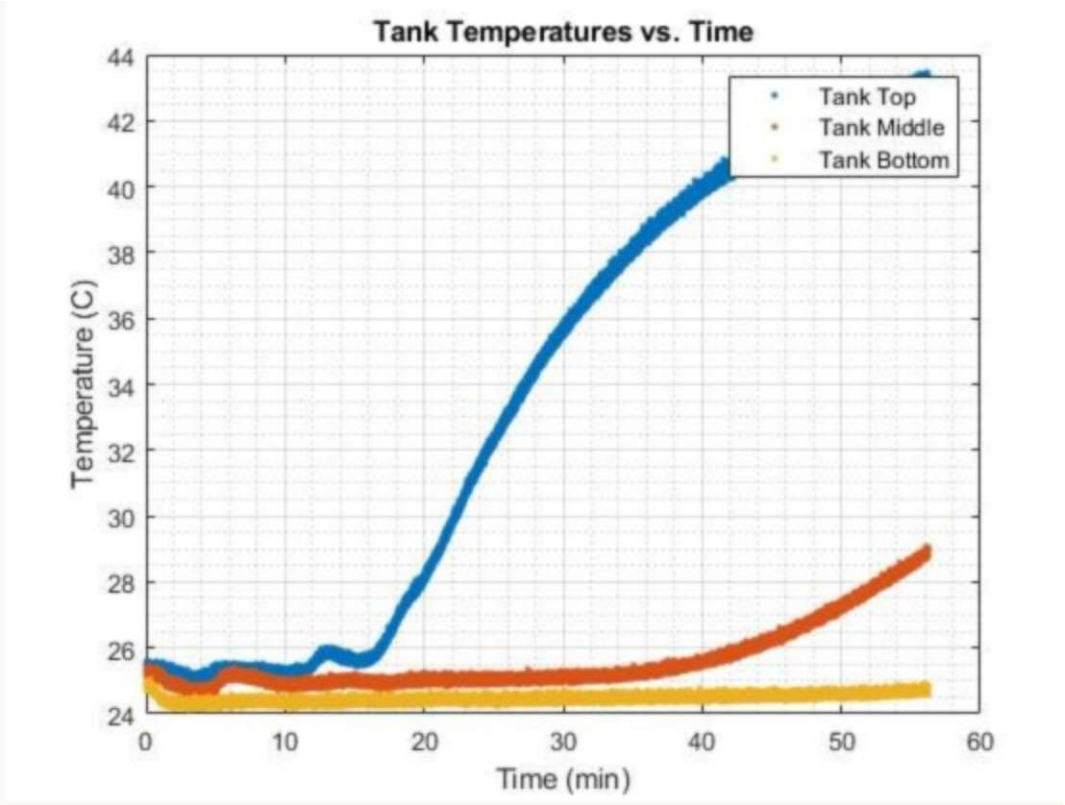
Tank Temperatures vs. Time
Tank Top
Tank Middle
Tank Bottom
Temperature (C)
Time (min)
44
42
40
38
36
34
32
30
28
26
24
0
10
20
30
40
50
60

Appendix J

Detailed Task Breakdown & Schedule

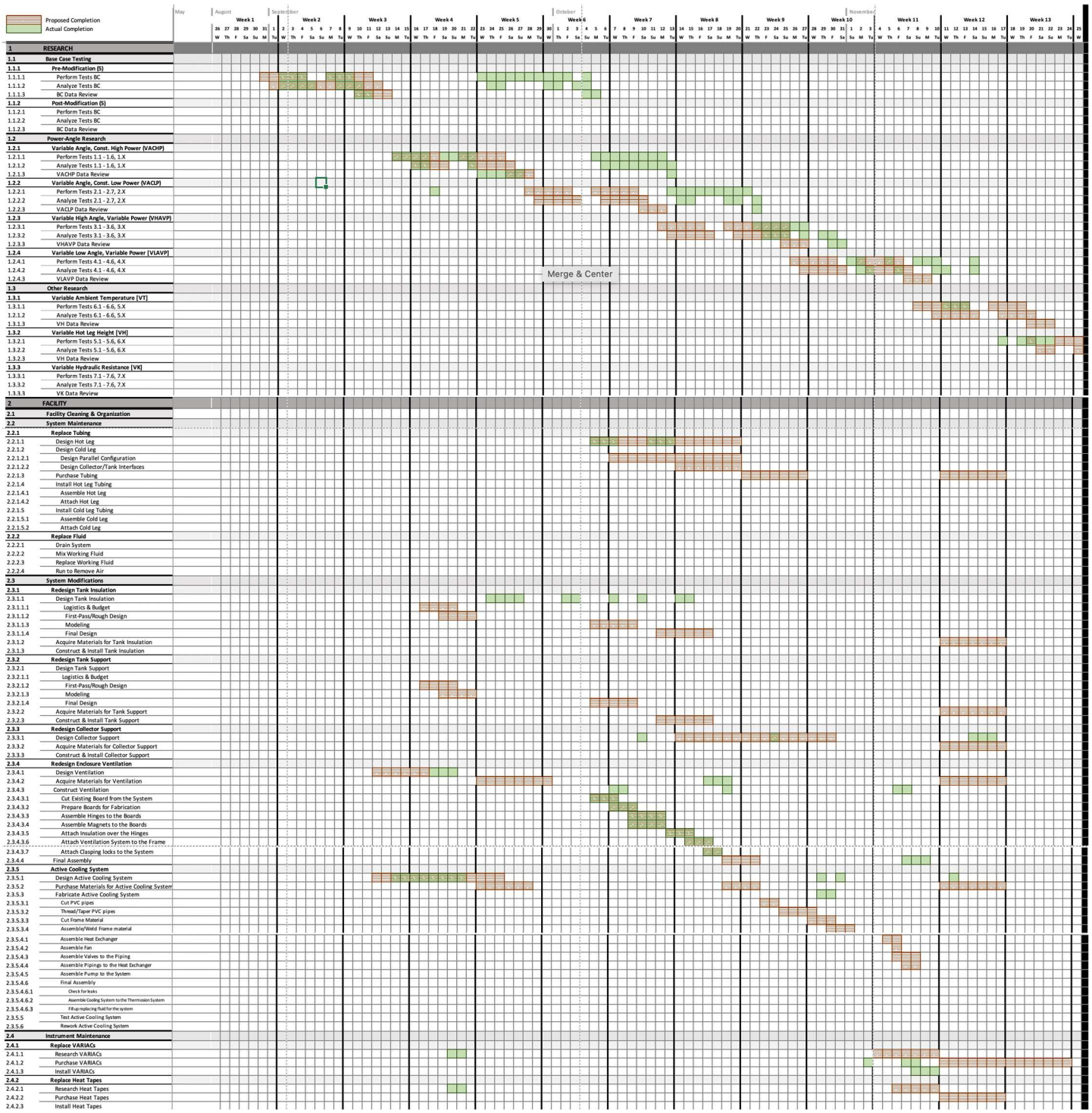

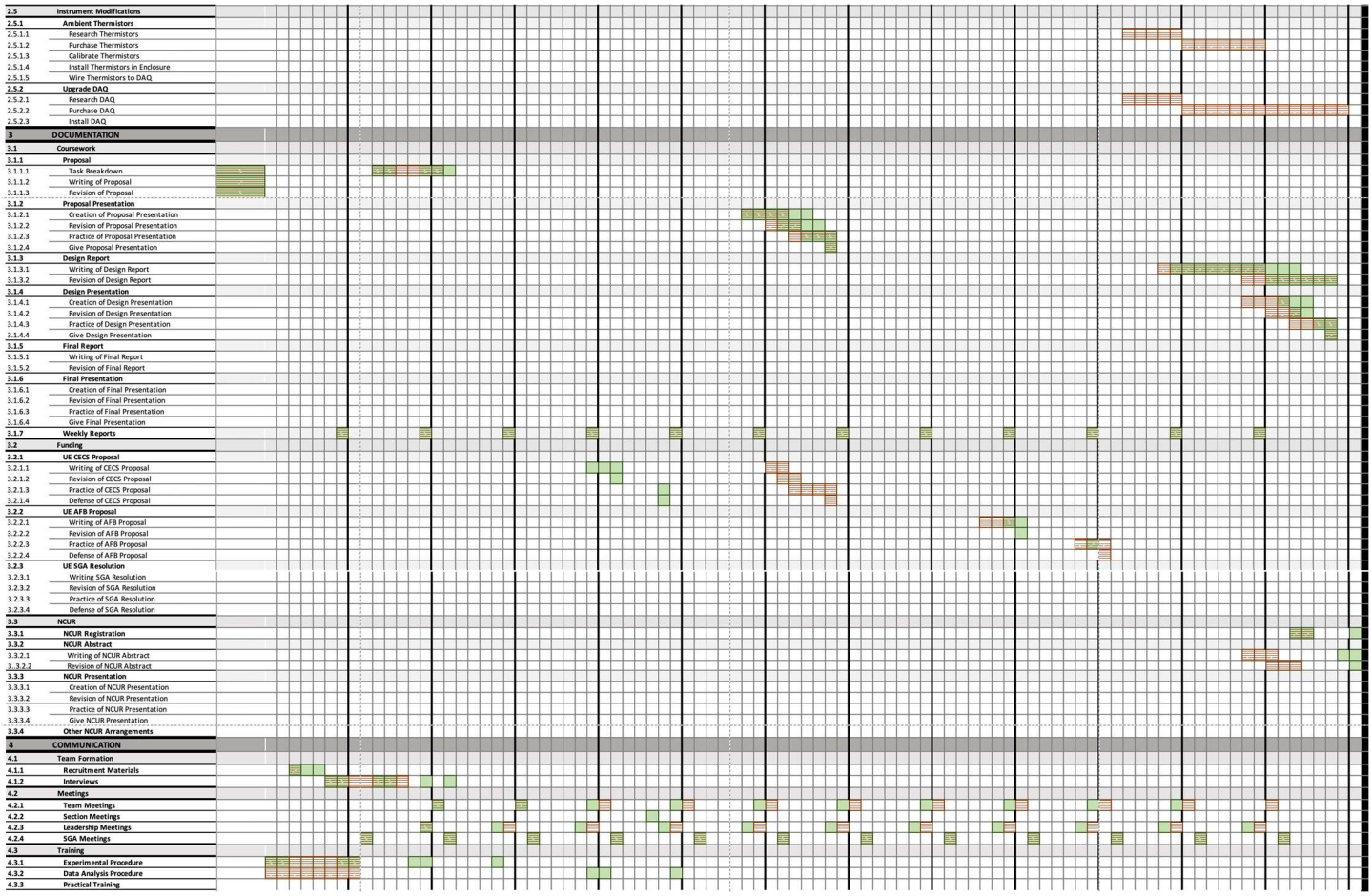
2.5 Instrument Modifications
2.5.1 Ambient Thermistors
2.5.1.1 Research Thermistors
2.5.1.2 Purchase Thermistors
2.5.1.3 Calibrate Thermistors
2.5.1.4 Install Thermistors in Enclosure
2.5.1.5 Wire Thermistors to DAQ
2.5.2 Upgrade DAQ
2.5.2.1 Research DAQ
2.5.2.2 Purchase DAQ
2.5.2.3 Install DAQ
3 DOCUMENTATION
3.1 Coursework
3.1.1 Proposal
3.1.1.1 Task Breakdown
3.1.1.2 Writing of Proposal
3.1.1.3 Revision of Proposal
3.1.2 Proposal Presentation
3.1.2.1 Creation of Proposal Presentation
3.1.2.2 Revision of Proposal Presentation
3.1.2.3 Practice of Proposal Presentation
3.1.2.4 Give Proposal Presentation
3.1.3 Design Report
3.1.3.1 Writing of Design Report
3.1.3.2 Revision of Design Report
3.1.4 Design Presentation
3.1.4.1 Creation of Design Presentation
3.1.4.2 Revision of Design Presentation
3.1.4.3 Practice of Design Presentation
3.1.4.4 Give Design Presentation
3.1.5 Final Report
3.1.5.1 Writing of Final Report
3.1.5.2 Revision of Final Report
3.1.6 Final Presentation
3.1.6.1 Creation of Final Presentation
3.1.6.2 Revision of Final Presentation
3.1.6.3 Practice of Final Presentation
3.1.6.4 Give Final Presentation
3.1.7 Weekly Reports
3.2 Funding
3.2.1 UE CECS Proposal
3.2.1.1 Writing of CECS Proposal
3.2.1.2 Revision of CECS Proposal
3.2.1.3 Practice of CECS Proposal
3.2.1.4 Defense of CECS Proposal
3.2.2 UE AFB Proposal
3.2.2.1 Writing of AFB Proposal
3.2.2.2 Revision of AFB Proposal
3.2.2.3 Practice of AFB Proposal
3.2.2.4 Defense of AFB Proposal
3.2.3 UE SGA Resolution
3.2.3.1 Writing SGA Resolution
3.2.3.2 Revision of SGA Resolution
3.2.3.3 Practice of SGA Resolution
3.2.3.4 Defense of SGA Resolution
3.3 NCUR
3.3.1 NCUR Registration
3.3.2 NCUR Abstract
3.3.2.1 Writing of NCUR Abstract
3.3.2.2 Revision of NCUR Abstract
3.3.3 NCUR Presentation
3.3.3.1 Creation of NCUR Presentation
3.3.3.2 Revision of NCUR Presentation
3.3.3.3 Practice of NCUR Presentation
3.3.3.4 Give NCUR Presentation
3.3.4 Other NCUR Arrangements
4 COMMUNICATION
4.1 Team Formation
4.1.1 Recruitment Materials
4.1.2 Interviews
4.2 Meetings
4.2.1 Team Meetings
4.2.2 Section Meetings
4.2.3 Leadership Meetings
4.2.4 SGA Meetings
4.3 Training
4.3.1 Experimental Procedure
4.3.2 Data Analysis Procedure
4.3.3 Practical Training

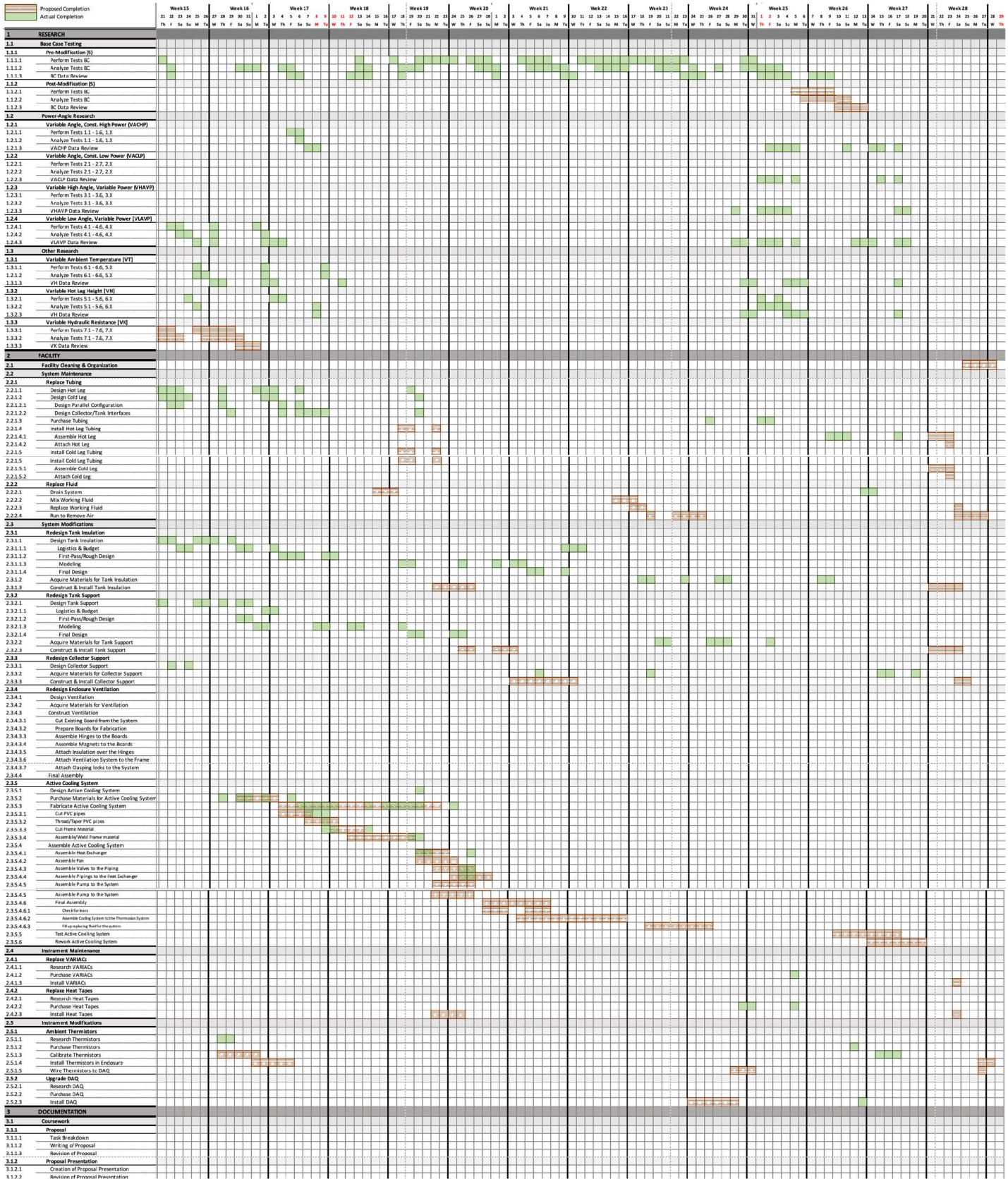
Proposed Completion
Actual Completion
Week 15
Week 16
Week 17
Week 18
Week 19
Week 20
Week 21
Week 22
Week 23
Week 24
Week 25
Week 26
Week 27
Week 28
1 RESEARCH
1.1 Base Case Testing
1.1.1 Pre-Modification (5)
1.1.1.1 Perform Tests BC
1.1.1.2 Analyze Tests BC
1.1.1.3 BC Data Review
1.1.2 Post-Modification (5)
1.1.2.1 Perform Tests BC
1.1.2.2 Analyze Tests BC
1.1.2.3 BC Data Review
1.2 Power-Angle Research
1.2.1 Variable Angle, Const. High Power (VACHP)
1.2.1.1 Perform Tests 1.1 - 1.6, 1.X
1.2.1.2 Analyze Tests 1.1 - 1.6, 1.X
1.2.1.3 VACHP Data Review
1.2.2 Variable Angle, Const. Low Power (VACLP)
1.2.2.1 Perform Tests 2.1 - 2.7, 2.X
1.2.2.2 Analyze Tests 2.1 - 2.7, 2.X
1.2.2.3 VACLP Data Review
1.2.3 Variable High Angle, Variable Power (VHAVP)
1.2.3.1 Perform Tests 3.1 - 3.6, 3.X
1.2.3.2 Analyze Tests 3.1 - 3.6, 3.X
1.2.3.3 VHAVP Data Review
1.2.4 Variable Low Angle, Variable Power [VLAVP]
1.2.4.1 Perform Tests 4.1 - 4.6, 4.X
1.2.4.2 Analyze Tests 4.1 - 4.6, 4.X
1.2.4.3 VLAVP Data Review
1.3 Other Research
1.3.1 Variable Ambient Temperature [VT]
1.3.1.1 Perform Tests 6.1 - 6.6, 5.X
1.2.1.2 Analyze Tests 6.1 - 6.6, 5.X
1.3.1.3 VH Data Review
1.3.2 Variable Hot Leg Height [VH]
1.3.2.1 Perform Tests 5.1 - 5.6, 6.X
1.3.2.2 Analyze Tests 5.1 - 5.6, 6.X
1.3.2.3 VH Data Review
1.3.3 Variable Hydraulic Resistance [VK]
1.3.3.1 Perform Tests 7.1 - 7.6, 7.X
1.3.3.2 Analyze Tests 7.1 - 7.6, 7.X
1.3.3.3 VK Data Review
2 FACILITY
2.1 Facility Cleaning & Organization
2.2 System Maintenance
2.2.1 Replace Tubing
2.2.1.1 Design Hot Leg
2.2.1.2 Design Cold Leg
2.2.1.2.1 Design Parallel Configuration
2.2.1.2.2 Design Collector/Tank Interfaces
2.2.1.3 Purchase Tubing
2.2.1.4 Install Hot Leg Tubing
2.2.1.4.1 Assemble Hot Leg
2.2.1.4.2 Attach Hot Leg
2.2.1.5 Install Cold Leg Tubing
2.2.1.5 Install Cold Leg Tubing
2.2.1.5.1 Assemble Cold Leg
2.2.1.5.2 Attach Cold Leg
2.2.2 Replace Fluid
2.2.2.1 Drain System
2.2.2.2 Mix Working Fluid
2.2.2.3 Replace Working Fluid
2.2.2.4 Run to Remove Air
2.3 System Modifications
2.3.1 Redesign Tank Insulation
2.3.1.1 Design Tank Insulation
2.3.1.1.1 Logistics & Budget
2.3.1.1.2 First-Pass/Rough Design
2.3.1.1.3 Modeling
2.3.1.1.4 Final Design
2.3.1.2 Acquire Materials for Tank Insulation
2.3.1.3 Construct & Install Tank Insulation
2.3.2 Redesign Tank Support
2.3.2.1 Design Tank Support
2.3.2.1.1 Logistics & Budget
2.3.2.1.2 First-Pass/Rough Design
2.3.2.1.3 Modeling
2.3.2.1.4 Final Design
2.3.2.2 Acquire Materials for Tank Support
2.3.2.3 Construct & Install Tank Support
2.3.3 Redesign Collector Support
2.3.3.1 Design Collector Support
2.3.3.2 Acquire Materials for Collector Support
2.3.3.3 Construct & Install Collector Support
2.3.4 Redesign Enclosure Ventilation
2.3.4.1 Design Ventilation
2.3.4.2 Acquire Materials for Ventilation
2.3.4.3 Construct Ventilation
2.3.4.3.1 Cut Existing Board from the System
2.3.4.3.2 Prepare Boards for Fabrication
2.3.4.3.3 Assemble Hinges to the Boards
2.3.4.3.4 Assemble Magnets to the Boards
2.3.4.3.5 Attach Insulation over the Hinges
2.3.4.3.6 Attach Ventilation System to the Frame
2.3.4.3.7 Attach Clasping locks to the System
2.3.4.4 Final Assembly
2.3.5 Active Cooling System
2.3.5.1 Design Active Cooling System
2.3.5.2 Purchase Materials for Active Cooling System
2.3.5.3 Fabricate Active Cooling System
2.3.5.3.1 Cut PVC pipes
2.3.5.3.2 Thread/Taper PVC pipes
2.3.5.3.3 Cut Frame Material
2.3.5.3.4 Assemble/Weld Frame material
2.3.5.4 Assemble Active Cooling System
2.3.5.4.1 Assemble Heat Exchanger
2.3.5.4.2 Assemble Fan
2.3.5.4.3 Assemble Valves to the Piping
2.3.5.4.4 Assemble Pipings to the Heat Exchanger
2.3.5.4.5 Assemble Pump to the System
2.3.5.4.5 Assemble Pump to the System
2.3.5.4.6 Final Assembly
2.3.5.4.6.1 Check for leaks
2.3.5.4.6.2 Assemble Cooling System to the Thermosiun System
2.3.5.4.6.3 Fill up replacing fluid for the system
2.3.5.5 Test Active Cooling System
2.3.5.6 Rework Active Cooling System
2.4 Instrument Maintenance
2.4.1 Replace VARIACs
2.4.1.1 Research VARIACs
2.4.1.2 Purchase VARIACs
2.4.1.3 Install VARIACs
2.4.2 Replace Heat Tapes
2.4.2.1 Research Heat Tapes
2.4.2.2 Purchase Heat Tapes
2.4.2.3 Install Heat Tapes
2.5 Instrument Modifications
2.5.1 Ambient Thermistors
2.5.1.1 Research Thermistors
2.5.1.2 Purchase Thermistors
2.5.1.3 Calibrate Thermistors
2.5.1.4 Install Thermistors in Enclosure
2.5.1.5 Wire Thermistors to DAQ
2.5.2 Upgrade DAQ
2.5.2.1 Research DAQ
2.5.2.2 Purchase DAQ
2.5.2.3 Install DAQ
3 DOCUMENTATION
3.1 Coursework
3.1.1 Proposal
3.1.1.1 Task Breakdown
3.1.1.2 Writing of Proposal
3.1.1.3 Revision of Proposal
3.1.2 Proposal Presentation
3.1.2.1 Creation of Proposal Presentation
3.1.2.2 Revision of Proposal Presentation

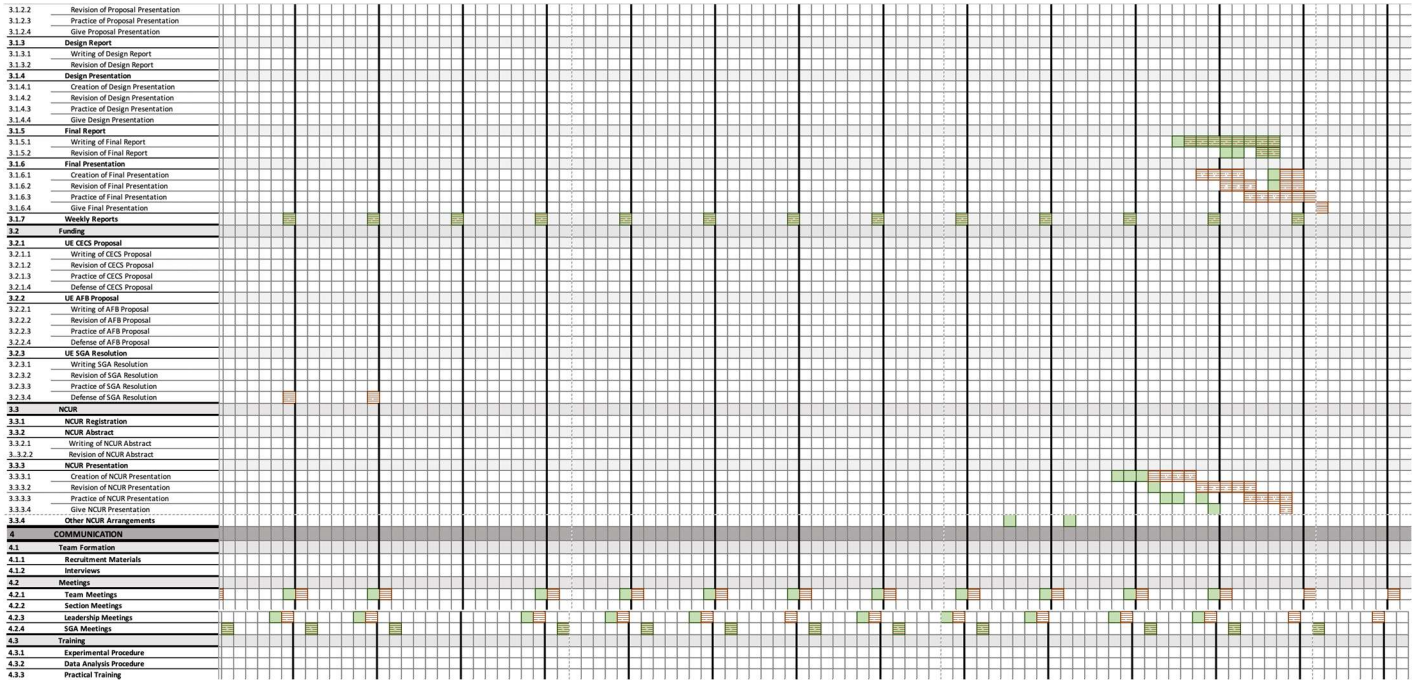
3.1.2.2 Revision of Proposal Presentation
3.1.2.3 Practice of Proposal Presentation
3.1.2.4 Give Proposal Presentation
3.1.3 Design Report
3.1.3.1 Writing of Design Report
3.1.3.2 Revision of Design Report
3.1.4 Design Presentation
3.1.4.1 Creation of Design Presentation
3.1.4.2 Revision of Design Presentation
3.1.4.3 Practice of Design Presentation
3.1.4.4 Give Design Presentation
3.1.5 Final Report
3.1.5.1 Writing of Final Report
3.1.5.2 Revision of Final Report
3.1.6 Final Presentation
3.1.6.1 Creation of Final Presentation
3.1.6.2 Revision of Final Presentation
3.1.6.3 Practice of Final Presentation
3.1.6.4 Give Final Presentation
3.1.7 Weekly Reports
3.2 Funding
3.2.1 UE CECS Proposal
3.2.1.1 Writing of CECS Proposal
3.2.1.2 Revision of CECS Proposal
3.2.1.3 Practice of CECS Proposal
3.2.1.4 Defense of CECS Proposal
3.2.2 UE AFB Proposal
3.2.2.1 Writing of AFB Proposal
3.2.2.2 Revision of AFB Proposal
3.2.2.3 Practice of AFB Proposal
3.2.2.4 Defense of AFB Proposal
3.2.3 UE SGA Resolution
3.2.3.1 Writing SGA Resolution
3.2.3.2 Revision of SGA Resolution
3.2.3.3 Practice of SGA Resolution
3.2.3.4 Defense of SGA Resolution
3.3 NCUR
3.3.1 NCUR Registration
3.3.2 NCUR Abstract
3.3.2.1 Writing of NCUR Abstract
3..3.2.2 Revision of NCUR Abstract
3.3.3 NCUR Presentation
3.3.3.1 Creation of NCUR Presentation
3.3.3.2 Revision of NCUR Presentation
3.3.3.3 Practice of NCUR Presentation
3.3.3.4 Give NCUR Presentation
3.3.4 Other NCUR Arrangements
4 COMMUNICATION
4.1 Team Formation
4.1.1 Recruitment Materials
4.1.2 Interviews
4.2 Meetings
4.2.1 Team Meetings
4.2.2 Section Meetings
4.2.3 Leadership Meetings
4.2.4 SGA Meetings
4.3 Training
4.3.1 Experimental Procedure
4.3.2 Data Analysis Procedure
4.3.3 Practical Training